

# Bending-Active Falsework For Tile Vaulting



Léopold Sepulchre

Master thesis in architectural engineering , June 2021  
under the supervision of Prof. Lars De Laet & Dr. Paula Fuentes Gonzalez







UNIVERSITÉ  
LIBRE  
DE BRUXELLES



VRIJE  
UNIVERSITEIT  
BRUSSEL

# Bending-active falsework for tile vaulting

**Léopold Sepulchre**

Master thesis submitted under the supervision of  
Prof. Lars De Laet

The co-supervision of  
Dr. Paula Fuentes Gonzalez


Academic year  
2020-2021

In order to be awarded the Master's Degree in  
Architectural Engineering

Exemplaire à apposer sur le mémoire ou travail de fin  
d'études,  
au verso de la première page de couverture.

Fait en deux exemplaires, Bruxelles, le 26/05/2021

Signature



Réservé au secrétariat : Mémoire réussi* NON	OUI
---	-----

**CONSULTATION DU MEMOIRE/TRAVAIL DE FIN  
D'ETUDES**

Je soussigné

NOM :  
Sepulchre.....  
.....

PRENOM :  
Léopold.....  
.....

TITRE du travail :  
Bending-active falsework for tile vaulting.....  
.....  
.....

**AUTORISE\***

~~**REFUSE\***~~

la consultation du présent mémoire/travail de fin  
d'études par les utilisateurs des bibliothèques de  
l'Université libre de Bruxelles.

Si la consultation est autorisée, le soussigné concède  
par la présente à l'Université libre de Bruxelles, pour  
toute la durée légale de protection de l'œuvre, une  
licence gratuite et non exclusive de reproduction et de  
communication au public de son œuvre précisée ci-  
dessus, sur supports graphiques ou électroniques, afin  
d'en permettre la consultation par les utilisateurs des  
bibliothèques de l'ULB et d'autres institutions dans les  
limites du prêt inter-bibliothèques.

\* Biffer la mention inutile

\* Biffer la mention inutile



## **Bending-Active Falsework For Tile Vaulting**





## Abstract

In this work we investigate the use of a bending-active gridshell to serve as a guidework for building tile-vaults, which are compression-only shells made of tiles that can cantilever during construction. The aim of this research is to reduce the waste and costs of the falsework for tile-vaults, but also to provide a kit-of-part and fool-proof system for local labors.

Bending active gridshells seem to be a promising solution for the falsework as they are constructed from initially linear elements that are bended in place. The challenge is then to get the final equilibrium shape to correspond to the compression shell, and to have a dense enough description of the shape for the mason.

In a first time, this work investigates computational modelling and design strategies of a bending active gridshell to serve as a falsework, and based on target geodesic curves drawn on the desired compression shell.

In a second time, a prototype model is built as a proof of concept, but also to gain feedback on the construction and detail design issues of such a gridshell. This prototype is based on the tile vault “drone port” of the 2016 Venice Biennale, at half scale.





## Acknowledgement

To my supervisors, Prof. Lars De Laet, and Dr. Paula Fuentes Gonzalez, thank you for your thrust, thank you for having let me do this master thesis, and for accompanying me regularly in this work with enthusiasm. It was a pleasure.

To the members of the computational geometry team, a.k.a the “jungle team”, Stijn Brancart, Aurélie Van Wylick, Arnaud De Coster, Maarten Van Craenenbroeck, and Arthur Winderickx, thank you for all your good advices during our discussion meetings.

To Svetlana Verbruggen and Daniel Debondt, thank you for your kind and effective help in the laboratory during the fabrication of the details.

To Arnaud, Aurélie et Maryllis, thank you for your precious help during the construction day of the gridshell. It was really fun.

To Maryllis, my fiancée and greatest source of happiness, I want to express you my deepest gratitude for your consistent loving support during this master.





# Table of content

<b>1</b>	<b>Introduction .....</b>	<b>1</b>
<b>2</b>	<b>State-of-the-art .....</b>	<b>3</b>
	2.1 Construction of tile vaults .....	3
	2.2 Bending-active structure as a falsework for tile-vaulting.....	5
<b>3</b>	<b>Research objectives.....</b>	<b>8</b>
	3.1 Problem statement and research goals .....	8
	3.2 Research questions .....	8
	3.3 Research methodology.....	8
<b>4</b>	<b>Choice of the target falsework.....</b>	<b>9</b>
	4.1 General scheme of the algorithm.....	9
	4.2 Curves on a surface .....	10
	4.3 Finding geodesic curves on a surface or a mesh.....	11
<b>5</b>	<b>Investigation on computational strategies for modelling a bending active gridshell .....</b>	<b>13</b>
	5.1 Bending active theory .....	13
	5.2 Numerical modelling of the rods .....	14
	5.3 Modelling of a 3D bending active gridshell.....	22
<b>6</b>	<b>Computational design of a bending active falsework based on geodesic curves for a simple compression only shell .....</b>	<b>27</b>
	6.1 The compression shell.....	27
	6.2 Choice of the target guidework .....	28
	6.3 Material choice and modelling of the rods .....	30
	6.4 Analysis of the structural behaviour of the guidework and adjustments to reduce deviation .....	31
	6.5 “Formwork behaviour” of the guidework for constructing the first arch .....	33
<b>7</b>	<b>Computational design of a falsework for a more complex shape : the drone port 36</b>	
	7.1 The drone port shell : using new technological advancements at the service of the poorest .....	36
	7.2 Choice of the target falsework .....	37
	7.3 Deviation of the bending active guidework .....	39
	7.4 Modelling of the brick load .....	41
	7.5 Displacement of the falsework under brick load .....	42
<b>8</b>	<b>Construction of a physical model of the falsework for the scaled drone port .....</b>	<b>44</b>
	8.1 Interview of a master mason : Carlos Martin .....	44

8.2	Rods .....	45
8.3	Investigation about nodes .....	48
8.4	Anchors .....	50
8.5	Construction steps of the gridshell .....	53
8.6	Construction issues, and feedback.....	56
<b>9</b>	<b>Conclusion.....</b>	<b>59</b>
<b>10</b>	<b>Annex : Form-finding of a compression only shell .....</b>	<b>63</b>
10.1	Force and form.....	63
10.2	Physical models for form finding.....	67
10.3	Thrust Network Analysis (TNA).....	70
10.4	Particle-Spring method.....	72
<b>11</b>	<b>Annex : Physical model : rods lengths and node position .....</b>	<b>74</b>
<b>12</b>	<b>References.....</b>	<b>77</b>
<b>13</b>	<b>Table of figures .....</b>	<b>79</b>







# 1 Introduction

We want our buildings to be efficient, economic and elegant, but also ecological by minimising pollution, resources and waste. A solution is to design our structures to achieve strength through geometry and material effectiveness. Shells and vaults are such efficient structural forms (Block et al. 2020).

For constructing shell structures, tile vaulting is advantageous because of its formal flexibility, material efficiency and reduction of formwork compared to other masonry techniques. Tile vault, also known as Catalan vaults or timbrel vaults, are unreinforced masonry structures made with thin bricks (tiles). The vault is composed of one or multiple layers. The tiles are chosen because of their lightness in order to build the first layer “in the air” without a formwork, and using quick fast-setting gypsum mortar also known as plaster of Paris. The bricks stick within few seconds. This first layer is constructed from a support element that can be a wall or arches<sup>1</sup>. Thanks to the quick adhesion bricks of the first layer can cantilever for some time avoiding the necessity of a formwork. The first layer serves as a permanent formwork for the other layer that can be built with Portland cement mortar or lime mortar (M. Ramage 2007).

Tile vaulting have origins in ancient constructions but experienced innovations in the late 19<sup>th</sup> century with Rafael Gustavino Moreno (1842-1908) who began his work in Spain then imported the technique to the United States. It gained in importance during the Catalan Art Nouveau with the works of Antoni Gaudi and Lluís Domènech i Montaner. However in the second part of the 20<sup>th</sup> century the technique was abandoned (López López, Van Mele, et Block 2016).

Nevertheless we observe a renaissance of tile vaulting as a way to build expressive free-form structures. It is possible thanks to a new form-finding software using an interactive equilibrium method called a Thrust Network Analysis (TNA) and based on the already well-known method of graphic statics. It enables the exploration of funicular forms and was developed by Philippe Block during his PhD at the MIT masonry research group. The TNA links in 3D the form diagram and the force diagram that represent respectively the force flow and the force equilibrium. Using this TNA, a plug-in for Rhino named RhinoVault was



Figure 1 : Mapungubwe National Park Interpretive Center (2008)<sup>2</sup>

---

<sup>1</sup> The arch is straight in plan and previously build on a formwork.

<sup>2</sup> <https://www.archdaily.com/57106/mapungubwe-interpretation-centre-peter-rich-architects>



developed, and enables thus to design free-form compression only structures. This translated in the construction of the Mapungubwe National Park Interpretive Center (2008) (Figure 1) by Michael Ramage, John Ochsendorf and Peter Rich, which is the first tile-vault building designed with these tools and that inspired then many other tile-vault construction (M. H. Ramage, Ochsendorf, et Rich 2010).

The traditional Catalan tile vaulting construction techniques enables to make the tiles cantilever, and thus for simple vault shapes, this enables to remove the need of a formwork or reduces it to some first supporting arches from which to rest of the tiles can cantilever, and only a guidework is sufficient to help the mason lays the bricks in the correct location. Nevertheless, free-form vaults rely on three-dimensional compression only equilibriums, thus it may be not possible to divide the vault into sections that are stable and could be built independently. Therefore we understand that the complexity of the form requires a guidework, that can sometimes help also to support some parts. The problem is that such a falsework generates extra costs and wastes and requires time to build. Therefore improving the formwork, i.e. reducing it, or making it reusable, is a subject of research.

Bending-actives gridshells are built from linear elements that are bended. This makes them easy to build manufacture and transport, but also linear elements can be more easily reused. Therefore the main goal of this research is to investigate the use of bending-active elements as a guidework for constructing tile vaults.

Firstly, we will look at the state of the art of the construction of tile vaults and the use of bending active elements for the falsework. Secondly, we will specify the research objectives. Thirdly we will discuss the choice of the target guidework on a given compression shape. Fourthly, we will investigate on computational strategies for modelling bending active gridshells. Fifthly, we will present the computational design of a bending active falsework, based on geodesic lines, for a simple compression shell. Sixthly, we will apply this computational design strategy to a more complex shape : the “Droneport” (Mairs 2016). Finally we will built a half scale physical model of the designed bending active falsework for the Droneport shell, as a proof of concept.

## 2 State-of-the-art

### 2.1 Construction of tile vaults

#### 2.1.1 Modern projects using the original Catalan tile vault technique

The historical tile vault can be made from local earth bricks with no formwork and minimal guidework. It thus offer a solution to the search of low-cost, formal exploration and sustainable construction. Because this construction technique has minimal environmental impact the project Crossway by Richard Hawks has been praised (López López et Domènech Rodríguez 2012) (Figure 2). Tile vaulting has also been seen as a response in a poverty context because that construction technique is sustainable, uses local material and employs many workers (Block et al. 2010). An example of this is the project for constructing sustainable urban dwelling units (SUDU) in Ethiopia in 2010 (Figure 3).



Figure 2: The Crossway, Hawks, 2009<sup>3</sup>



Figure 3: Sustainable urban dwelling unit (SUDU), Ethiopia 2010, (Block et al. 2020)

#### 2.1.2 Structurally improved tile-vaults

The Rwanda Cricket Stadium is made of tile-vaults constructed with a guidework. The supporting arches however needed a full formwork. Tile vaults were chosen because of their rapid construction and structural efficiency but also because it allowed to use local materials and employed local unskilled workers in a poverty relief program. However in that location it was necessary to consider the seismic risk that translated into dynamic lateral loads. Thus the vaults were reinforced by the incorporation of a triaxial geogrid that significantly improved its behaviour (M. Ramage et al. 2018).



Figure 4 : Rwanda Cricket Stadium, Kigali 2017, (M. Ramage et al. 2018)

---

<sup>3</sup> <https://www.hawkesarchitecture.co.uk/grand-designs/>

### 2.1.3 Formworks for free-form tile vaulting

To build free-form tile vaults that rely on a three-dimensional compression equilibrium, a formwork is usually needed and building just with a guidework requires this one to be much more complex than in traditional forms. When constructing a shell the formwork is usually one of the most challenging parts. It is often expensive and time consuming and is a limitation to the construction of shells today. Thus it is a challenge to come up with better solution in terms of costs, schedule sustainability, ease of implementation, versatility, etc.

In 2011 the Block Research Group (BRG) built in Zurich an innovative formwork for building a prototype of the first free-form tile vault. The formwork formed of a CNC-cut cardboard. The cardboard forms boxes that are placed on shipping pallets which allows reducing the cardboard needed and serves as a platform to stand for builders (López López, Van Mele, et Block 2016).

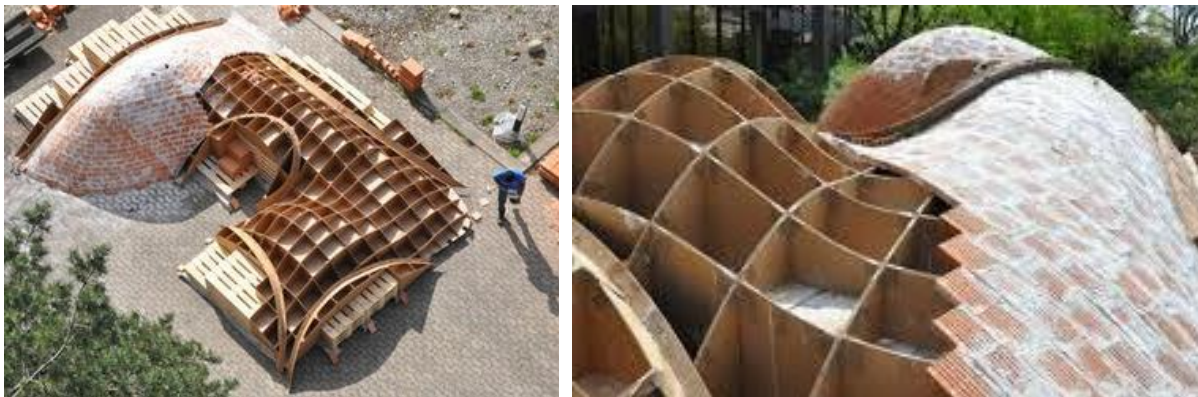


Figure 5 : Prototype free-form tile vault, BRG, 2011, (López López, Van Mele, et Block 2016)

In 2013 the “Brick-topia” pavilion was built in Barcelona (López López, Domènech Rodríguez, et Fernández 2014). Another formwork system was used that had three elements : scaffolding, cardboard and steel rods. The scaffolding was used like the pallets in the prototype to reduce the cardboard needed. The cardboard were cut on site following the shape of the sections. Then a net of steel rebars was placed on the upper edges of the cardboard. The bars where bend in situ and attached together with steel wires to form a gridshell. Then the cardboard and the scaffoldings were taken out and only the grid shell remained to serve as the formwork. The advantage with the gridshell is that the masons can reach and check the underside of the brick layer during construction.

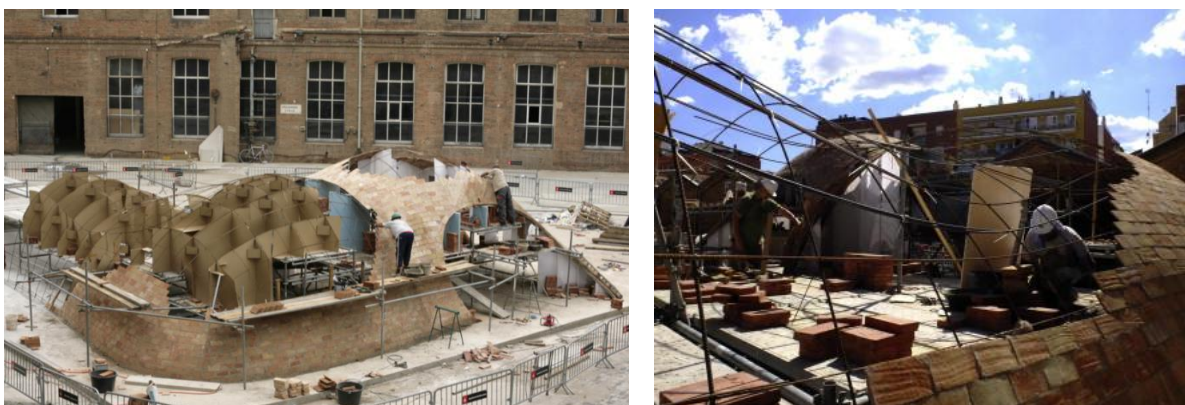


Figure 6 : Brick-topia, Barcelona, 2013, (López López, Domènech Rodríguez, et Fernández 2014)



Ribbed tile vault were investigated during two workshops in Australia in 2012 and 2013 (Block et al. 2014). A formwork was only created to support the ribs (centering). The infill surface was then build using the cantilevering characteristic of the tiles with the fast setting mortar. The vault of the first workshop required a complex formwork because the ribs were curved both in plan and in section. However the vault of the second workshop (Figure 7) had ribs that were straight in plan and that required only a simple formwork. Thus the introduction of ribs allows to reduce the size and so the cost and waste, of the formwork. The resulting vault is the result of a compromise between the possibilities of free-form tile vault and the efficiency of the traditional Catalan technique.



Figure 7 : Workshop at MADA Melbourne, 2013 (López López, Van Mele, et Block 2016)

## 2.2 Bending-active structure as a falsework for tile-vaulting

### 2.2.1 Bending active guidework

When using the traditional tile vault technique a guidework is needed to help the mason lay the bricks at the correct location. When the vault has a simple single curvature then straight ropes can be used (Figure 3). However for double curvature shapes new guideworks are experimented.

In 2016 the Norman Foster Foundation and BRG built a drone port (Figure 8) at the Venice biennale (Mairs 2016). The objective was to enable Rwanda to create this structure themselves with local workers and with local materials such as non-fired soil bricks. Thus the guidework had to be designed as a fool-proof and low cost system. The supporting arches need a formwork but the vault was constructed following a guidework made of bent wires. These wires were attached to a light scaffolding. This is a first example of using bent materials for the guidework.



Figure 8 : Drone port, Venice Biennale 2016, (Mairs 2016)



The MIT worked also on a bending-active formwork made of fiberglass splines (Dessi-Olive et al. 2018). The brick used are Autoclaved-aerated concrete (AAC) bricks which are light and have good porosity for cohesion with gypsum mortar. A first central steel arch is created as a load bearing formwork. There is also a steel “skirt” that extends horizontally to control the shape and direction of the splines. The fiberglass splines formed the guidework (Figure 9). Fiberglass was preferred over other materials because of its uniform elastic behaviour. If the curve of the vault is flat then simply fixing the extremities of the splines is sufficient to describe the curve. If the curve is taller, then extra control points are needed. The curves extracted from the vault are close to a catenary and required 4 points to accurately describe the shape. The design of the formwork fed back into the design of the vault i.e. the shape of the structure was adjusted so that the curves extracted from the digital model could be described by the fiberglass rods. In comparison, the drone port from the Venice Biennale project used a scaffolding to have many more control points but at the same time be more free on the shape of the vault.

For the “*Volta Porosa*” 6 splines were used and placed diagonally making a diamond grid. During the progress of the construction the splines were adjusted to describe the unbuilt portions. However this adapting feature of the guidework was not a success and it was sometimes difficult to see the correct location of bricks. Nevertheless the guidework was stiff enough to support the AAC tiles during the construction making the 10 seconds time for holding in place the tile for adhesion not required. The splines helped also keeping the area under the vault clear of any supports, thus making the work easier when need of manoeuvre or when the mason wanted to lay bricks from above or below. Finally even if splines were used to reduce the formwork required this project still uses a stiffening steel arch and horizontal steel supports. A full bending-active grid shell could be investigated.

Finally concerning guidework, Augmented Reality (AR) and Mixed-Reality (MR) are becoming possible options to be used as virtual guides, making the guidework fully dematerialized (Jahn et al. 2019). However, using these virtual guides would for now only be possible for projects with sufficient technological knowhow and means.

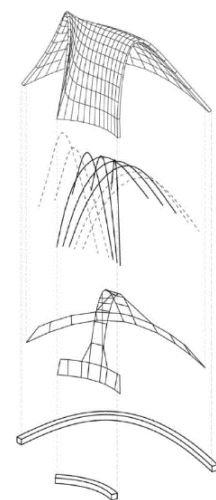


Figure 9 : *La Volta Porosa*, Cambridge MIT, 2016<sup>4</sup>

<sup>4</sup> <https://jdovaults.com/La-Volta-Porosa>

## 2.2.2 Bending active formwork

For free-form tile vaulting a formwork is usually used. Early solutions were investigated in part 2.1.3. In this part bending-active structures that can bear load are explored.

The University of Manitoba and the Vrije Universiteit Brussels (VUB) work on using a bending-active gridshell as a formwork. The principle stress lines (PSL) of a vault are used to determine the topological pattern of the gridshell elements. As a proof of concept the project “Ice bloom” was built. It is a shell made from ice constructed with a formwork that is a bending active gridshell designed with the PSL (Coar et al. 2017) (Figure 10).

To improve the bearing capacity of the bending-active formwork tensioning cables can be used. It also allows to manipulate the shape. Firstly, post tensioned bending active frames have been tested with significant improvement of the bearing capacity for point load and distributed load (Coar et al. 2018). Secondly, the same principle is to be applied to a bending active vault gridshell with post tensioning cables. The numerical model was made and further experiments will be performed on a physical one. However cable reinforced elastic gridshell have not been used yet for free-form tile vaulting but seem to be a promising solution to be investigated.



Figure 10 : Ice Bloom 2017<sup>5</sup>

In 2019 a 3D print lightweight and stable formwork was investigated for unreinforced shell structures with traditional masonry and concrete (Yuan et Block 2019). The formwork was printed flat then bended. This introduction of curvature through bending was utilised to enhance its structural stability (Yuan et Block 2019). It led to a second workshop for constructing the “red pavilion brick shell” (WANG et al., s. d.). The final shell geometry was found using both TNA with RhinoVault and Particle-Spring (PS) method with Kangaroo2 plugin for Grasshopper. The formwork was 3D printed after which a layer of polyurethane was cast on it for the insulation. Still the printed formwork was placed on a temporary steel frame support. This project shows mainly the possibilities of additive manufacturing to make the construction process more efficient, reducing human labour and wastes.

---

<sup>5</sup> <http://lancelotcoar.com/icebloom>

## 3 Research objectives

### 3.1 Problem statement and research goals

As we have seen, to build a traditional tile vault no formwork is required except for the supporting arches. Nevertheless a guidework is needed. For more complex forms, like free-form vaults, the challenge is to describe accurately enough the desired shell shape with a relatively dense guidework in order to guide the mason. Also, for these more complex forms, the falsework usually becomes costly and generates waste. Bending active gridshells seem to be a promising solution for the falsework as they are constructed from initially linear elements that are bended in place. The challenge is then to get the final equilibrium shape to correspond to the compression shell, and to have a dense enough description of the shape for the mason. **Therefore the main goal of this research is to investigate the use of bending-active elements as guidework for tile-vaults.**

### 3.2 Research questions

The main research questions are: How to approximate a compression only shape with a bending active gridshell ? And, how to design a low-cost and reusable bending active gridshell to serve as a guidework ?

Secondary research questions are: how precisely does this guidework needs to describe the final shape, i.e. how dense the grid shell needs to be ? And, can this bending-active guide work be generated in an automatic way for new tile vaults or does every vault shape need a special study for its guide work ?

### 3.3 Research methodology

The research core is the design of a low-complexity, low-cost and kit-of-part guidework. It will be done through the design of a prototype gridshell to serve as falsework for a compression only shell : here a half scale of the “drone port”.

After having initially learned about how to form-find a compression only shell with TNA and the particle spring method, we will consider the compression shape as a given for our work. From there we will first define a general algorithm for the definition of the target falsework, i.e. the gridshell we would want to ideally achieve without considering the bending active behaviour.

Then we will investigate on the computational strategies that enables to model the bending active behaviour of the elements of the gridshell. The obtained deviation, from the target falsework, will be used as a feedback to adapt the initial gridshell. We will test the complete workflow of the computational design of the bending active falsework firstly for a simple compression shell and secondly for the drone port shell which is more complex and presents synclastic and anticlastic areas.

In parallel, investigation will also be made on the materials used for the falsework regarding cost and availability. We will also interview an experienced mason to know more about the problematics of the construction of tile vaults.

Finally, the materials will be ordered and the prototype falsework will be built. Feedback on construction issues, and on the final accuracy of the falsework to describe the shell shape, will be regarded.

## 4 Choice of the target falsework

### 4.1 General scheme of the algorithm

To help us design a correct falsework for the construction of a tile vault we wrote an algorithm with Grasshopper for Rhino. An overview scheme of it is shown in Figure 11.

First, we need to have a 3D model of the shell. Because the tile vault is a compression only structure, we need to form-find its geometry to have static equilibrium. For form-finding, we have used two numerical methods : TNA with RhinoVault, and Particle Spring method with Kangaroo2<sup>6</sup>.

Remark :

- The research part of this thesis work focuses on the falsework, i.e. the bending active gridshell. However to design the falsework we also obviously need the geometry of the tile vault. Thus we investigated on how to form-find compression only structures also, and we describe that state-of-the-art in Annex : 0. We strongly invite to read Annex 0 if you are not familiar with the form-finding for compression only structures. From this point we will take the shell geometry as a given.

Secondly, from that shell model, we define a target falsework. The target falsework approximates exactly the shape of the compression shell, and it is the gridshell we want to achieve with bended elements. Here we define the number of rods, their position, and where they are connected (nodes). But the physical behaviour of the rods is not yet simulated. We just have geometrical curves on the surface or mesh of the shell.

Thirdly, we model the physical behaviour of the rods and we evaluate the deviation of the gridshell from the target grid. We also include the displacement in case the falsework needs to sustain temporarily construction loads. (For example, depending on the geometry of the tile vault, we might need to start by building arches which need to be supported during their construction). We also do a structural analysis of the grid to evaluate if the internal stresses are admissible by the material. In chapter 5 we will explain numerical possibilities for how to model the bending active behaviour of the gridshell.

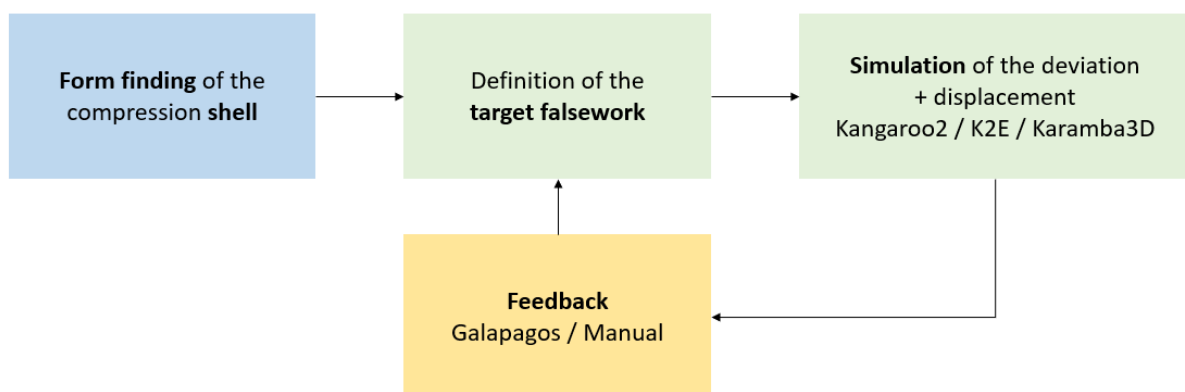


Figure 11 : scheme of the algorithm

---

<sup>6</sup> Kangaroo2 is a plug-in for Grasshopper itself a plug-in for Rhino.

Finally we do a feedback loop from the simulation results to the choice of the target guidework. This is done by adapting the position of the rods, their density and diameter, but also by adding stiffening cables or extra anchors. In chapter 6 we show a case of performing this feedback loop with Galapagos<sup>7</sup>, however we mostly do it in a manual way in this work.

## 4.2 Curves on a surface

To define the target falsework we need to choose which type of curve to draw on the surface of the shell.

Figure 12 show images from the PhD thesis of Eike Schling (Schling 2018) that illustrates the different choices for possible curves that simplify construction of a double curved structure. For a given point of a curve on a surface we can draw the Darboux frame that is composed of the normal vector  $n$ , the tangent vector  $t$ , and their cross product the vector  $u$ . The rotation around  $n$  gives the geodesic curvature  $k_g$ , around  $t$  gives the geodesic torsion  $\tau_g$ , and around  $u$  the normal curvature  $k_n$ .

If two of these curvatures are set to zero then the achievable shapes are a plane ( $k_n=\tau_g=0$ ), a double ruled surface ( $k_n=k_g=0$ ), or a sphere ( $\tau_g=k_g=0$ ) as shown in Figure 12. These are not suitable solutions for our falsework because it restricts too much the freedom of shapes.

If only the geodesic torsion is set to zero ( $\tau_g=0$ ), then we obtain principal curvature curves. They have the property of being tangent to the principal curvature directions for any point of the surface, thus making the nodes orthogonal (the principal curvature directions are always perpendicular (Schling 2018)). This simplifies fabrication. The principal curvature curves can be built from planar strips but that still present a curvature in plan, i.e. they are not straight slats when unrolled. We first thought of constructing the falsework from linear slats and not rods, thus this would have been a problem if going with principal curvature curves. The strong axis of the strips can be oriented perpendicular to the surface which is good for load bearing. Finally these curves tend to present some high curvature portions which is strongly limiting the maximum diameter cross section admissible for rods and thus limiting its bending stiffness.

If only the normal curvature is set to zero ( $k_n=0$ ) then we obtain asymptotic curves. They can be built from flat and linear slats that would bend around the  $n$ -axis (and no bending around the  $u$ -axis because  $k_n=0$ ), which simplifies construction. Also, the strong axis of the slat is then oriented perpendicularly to the surface and thus enables good structural performances<sup>8</sup>. However the achievable forms are limited to anticlastic surfaces (i.e. surfaces with negative gaussian curvature), which is usually not the case for compression only structure.

If only the geodesic curvature is set to zero ( $k_g=0$ ) then we obtain geodesic curves. As for asymptotic curves, they can be built from straight slats, enabling for simple fabrication. Geodesics are bend around the  $u$ -axis, and so if slats are used then they sustain load with their

---

<sup>7</sup> Galapagos is an evolutionary solver for optimisations in Grasshopper.

<sup>8</sup> Eike Schling uses these advantages for the fabrication of the “asymptotic gridshell” pavilion. Also, its surface is a subcategory of anticlastic surfaces : a minimal surface (negative gaussian curvature and mean curvature of zero), which adds the benefit of making orthogonal node, which simplifies further the fabrication.



weak axis which is structurally non-optimal. There is a compromise here between having a thick enough slat for structural performances, but thin enough to bend into the desired geodesic curve. Luckily for us, this is not a big problem because we are focusing on tile vaults which mainly need a guidework, and so the gridshell does need to sustain high loads. Finally, the geodesic lines have to property to follow the shortest path between two points on a surface.

Remark : when rods are used (instead of slats) these considerations may actually become less relevant. Nevertheless we chose to keep working with geodesic lines because it gives us more freedom in the choice of the element (slats or rods) and also because it is not a bad choice.

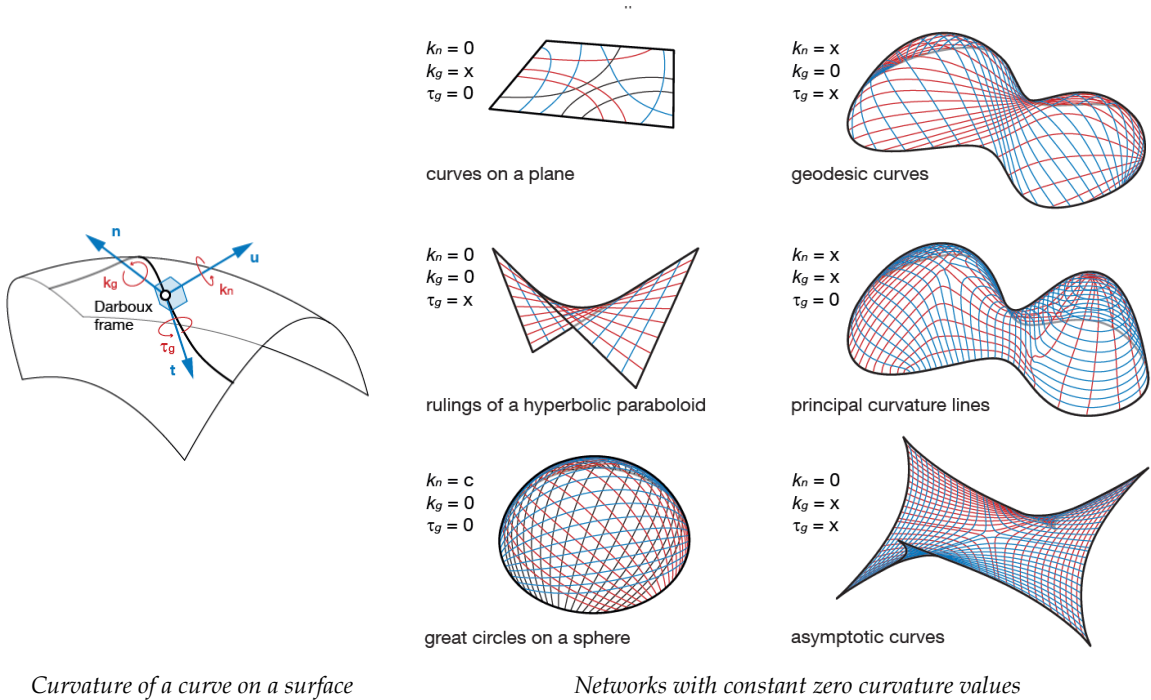


Figure 12 : Curves on a surface<sup>9</sup>

### 4.3 Finding geodesic curves on a surface or a mesh

To draw a geodesic curve on a surface there are two strategies : you can define a start and end point, or you can define a point on the surface and a direction. This makes that it can be challenging to find a satisfying density of rods. The anticlastic regions will tend to bring closer geodesic curves and the synclastic tend to seclude them.

Grasshopper gives the component “geodesic”, for which you need define the end points of the geodesic curve and a surface. It only works for surfaces. However, the form finding of the compression shell with RhinoVault outputs a mesh. Thus you can either transform the mesh into a surface (which is not always trivial), or you can use a strategy to draw geodesic curves directly on a mesh.

To draw a geodesic curve on a mesh we use the property of the geodesic curve of being the shortest path between two points on a given surface (approximated by a mesh). Figure 14 shows the grasshopper code to draw geodesic curves on a mesh, and Figure 13 shows an illustrative example. First two points are defined and a straight line is drawn between the two.

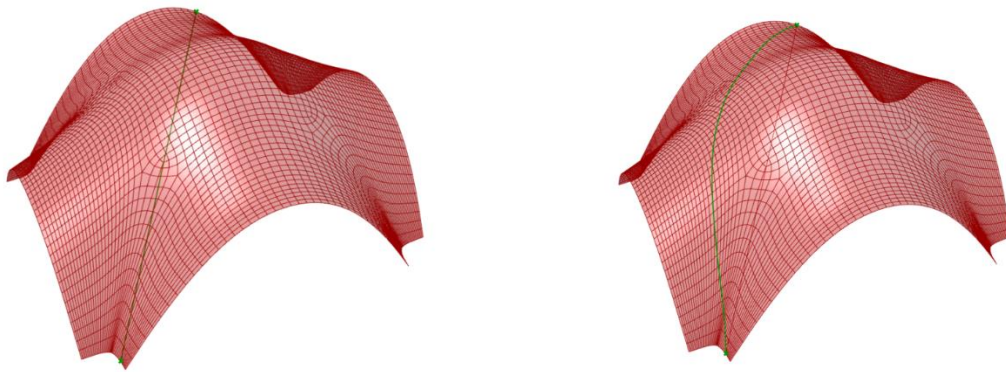
---

<sup>9</sup> All images of Figure 12 from (Schling 2018)



Then this line is divided into a polyline (here 50 segments). The segments are given the target goal of zero length. This will make kangaroo minimise the path length between the two points that are anchored. Then we use the component “OnMesh” that attracts the vertices of the polyline to the mesh if the “strength” variable is set sufficiently high (compared to the zero-length strength variable).

We note that the smoothness of the mesh impacts the results. Also if we want to define a geodesic that passes through the summit of this shell, the geodesic may slip on the side of the summit because of the roughness of the mesh. In that case it may be needed to help the geodesic by setting an additional anchor point in the middle for example.



(Green) Start from straight line (the line is here under the shell)  
 (Red) Mesh of a compression shell

(Green) Geodesic curve  
 (Red) Mesh of a compression shell

Figure 13 : Finding a geodesic curve on a mesh

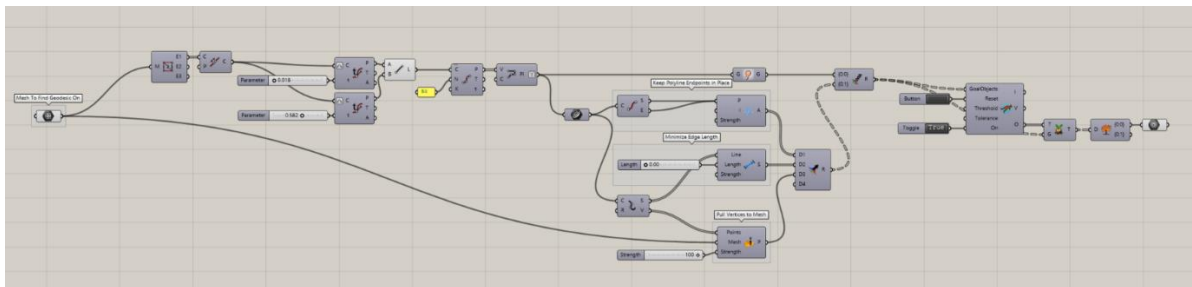


Figure 14 : Grasshopper code with Kangaroo2 to find a geodesic curve on a mesh

## 5 Investigation on computational strategies for modelling a bending active gridshell

“Bending-active structures are structural systems that include curved beam or shell elements which base their geometry on the elastic deformation from an initially straight or planar configuration.”(Lienhard 2014).

### 5.1 Bending active theory

Like for compression only structures, the shape of a bended active element cannot arbitrarily be drawn by hand but has to be form-found from its mechanical behaviour. However unlike compression only structures, the shape of bending active structures do not only depend on geometrical consideration for obtaining a static equilibrium, but also depends on the material properties of the bended elements. This relation between the mechanical behaviour and the form is described by theastica curve that is the equilibrium final curve that minimises the potential bending energy under constraints. For the equations giving the analytical description of bending active structures we invite reading chapter B of the PhD thesis of Julian Leinhard (Lienhard 2014).

In this thesis the form-finding of the bended shape is performed by numerical simulations that will be explained further. However we will still need to check if the radius of curvature at each point of an element is larger than a minimum radius, in order that the local stress in the element does not exceed its design strength, for it not to yield or break.

From the Bernoulli-Euler theory we have for a beam the equation :

$$\varepsilon = \frac{\Delta dx}{dx} = \frac{y}{R}$$

Where

- $\varepsilon$  is the strain,
- $dx$  the initial length of the element,
- $\Delta dx$  the variation of the length of the element,
- $y = t/2$  is the perpendicular distance to the neutral axis,
- and  $R$  is the radius of curvature ( $r$  in Figure 15).

Figure 15 show the geometrical relation in a deflected beam for the parameters above.

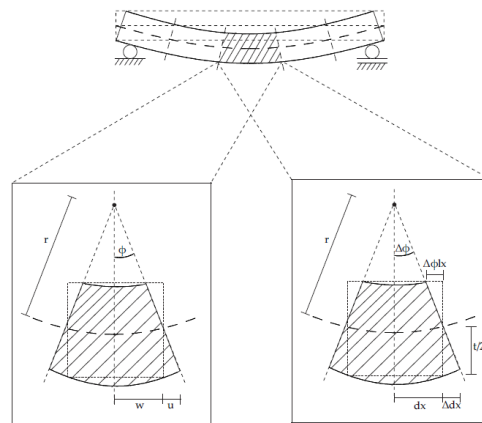


Figure 15 : geometric relation in a deflected beam (image from (Lienhard 2014))

Then, combined with Hooks law we obtain :

$$\sigma = E \cdot \varepsilon = \frac{E \cdot y}{R} = \frac{E \cdot t}{2 \cdot R}$$

Where :

- E is the Young's modulus
- t the thickness of the element

Thus the minimum radius of curvature ( $R_{min}$ ) is given by :

$$R_{min} = \frac{E \cdot t}{2 \cdot \sigma_{Rd}}$$

Where :  $\sigma_{Rd}$  is the permissible stress.

## 5.2 Numerical modelling of the rods

### 5.2.1 Rod modelling with Kangaroo2

To find the equilibrium shape of a bending active element we use Kangaroo2 which is a optimisation solver that tries to minimise the energy of the system. In Figure 16 we show the grasshopper code and in Figure 17 the results of the simulation of a bending rod with kangaroo2. First a line of 3m is defined, then it is divided in 10 segments. The "Rod" component enables to model the axial stiffness ( $E \cdot A / L$ ) of each element and the bending stiffness ( $E \cdot I$ ) between the elements. For the axial stiffness the lengths is not the total length but the length of each small segment. The bending stiffness is modelled by the resistance to variation of the angles between the segments, and the segments stay straight and do not bend themselves. Thus it is important that the lengths of the segments are equal (it is the case here) in order to model properly the bending stiffness of the overall rod. Finally an "angle factor" has to be defined, by default set to 1 i.e. the target angle is the initial angle. In this case the initial rod is straight then the right end point is move by 1m to the left which makes the rod bend. We note that it is needed to add a small initial upward force to make the rod bend because in the simulation there is no buckling, then once the rod is bended this lateral force is set to 0 again but the rods stay in its elastica shape.

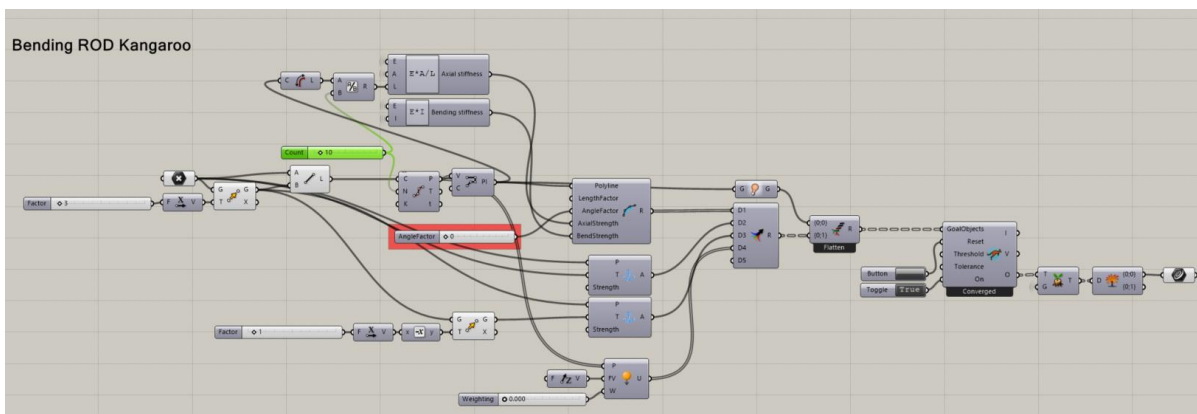


Figure 16 : grasshopper code of the simulation of a bending rod with kangaroo2

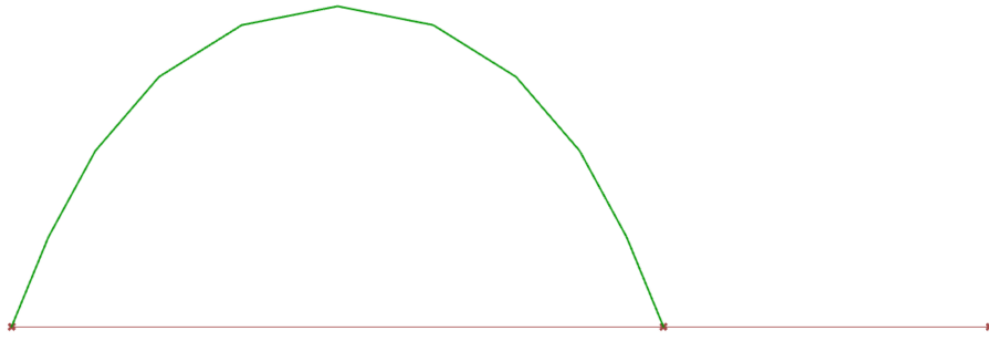


Figure 17 : (Green) Simulation of a bending rod with kangaroo 2, (red) initial state : flat rod

In Figure 17, a 3m steel S235 rod of 2mm diameter and circular cross section is used.

To avoid using this “initial lateral force” another practice is to model prebending with kangaroo2. This is done by setting the “angle factor” to 0 in case the rod would initially be straight. We will mostly use this second modelling strategy in the following of the thesis. Figure 18 shows the grasshopper code of the simulation of the prebending of the rod with kangaroo2. We note that there are no more “initial force” and that the anchor definition is simpler, there is no initial displacement i.e. the target anchors are the initial points. Figure 19 show the results of the simulation of the prebended rod. The initial form (in red) is an arc of radius 1m and the green curve shows the deviation to the equilibrium curve. As previously a rod made of 3m steel S235 and 2mm diameter and circular cross section is used

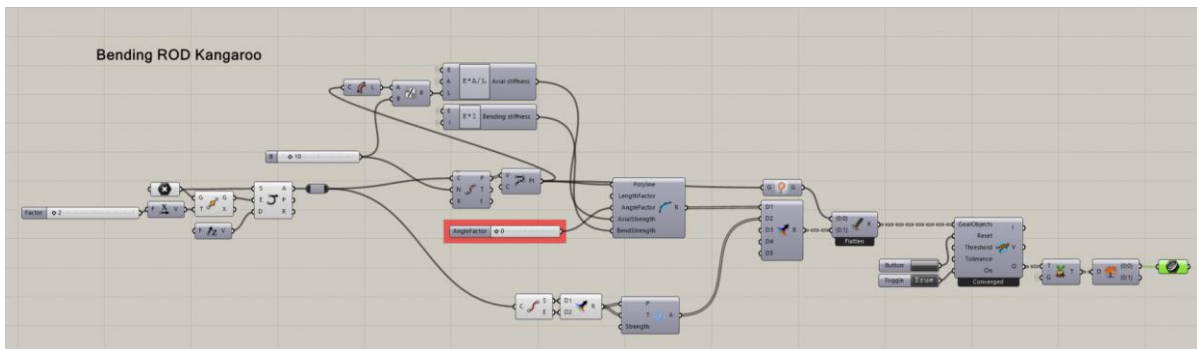


Figure 18 : Grasshopper code for a prebended rod

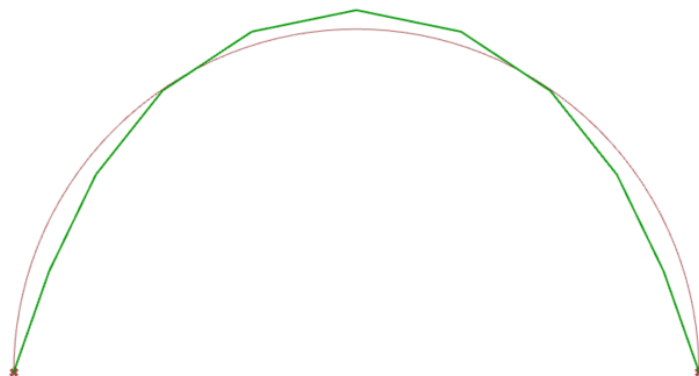


Figure 19 : (Green) Simulation of the deviation of a prebended rod, (Red) initial state

## 5.2.2 Comparison with a catenary shape

A challenge of this work is to approximate in 3D a compression only shape with a bending active grid. Here, we first look at the approximation of a 2D catenary curve with a 2D bending active curve. Figure 20 shows the deviation of a bended curve from a catenary curve for the following ratios  $f/L$  : 0.1, 0.2, 0.3, 0.5, 0.7, 0.9 where  $f$  is the rise and  $L$  is the span. The rods are also made of steel S235 of 2mm diameter and with a circular cross section.

We observe that the elastica curve approximates well the catenary curve for the ratios  $f/L$  lower or equal to 0.3. For ratios above 0.3 we observe an increasing deviation. This deviation will increase if we apply a load because the deviation makes that the load will be taken by bending moment which will create a displacement, generating itself an extra bending moment etc. resulting in an exponential increase of the difference between the two curves. The 0.3 limit on the ratio  $f/L$  for the approximation of a catenary curve by the elastica curve is further detailed in (Lienhard 2014). This limit is interesting to keep in mind if we want to build a compression structure from bended element little connected, like we saw for the Volta Porosa (Figure 9).

For our case of building a falsework, this result means that if the ration  $f/L$  become larger than 0.3 then using a series of single rods is not satisfactory. Two solutions are proposed for the following of the work. First stiffening cables can be added to adjust the shape of the rod. Second, the equilibrium shape of the rod can also be adjusted by connecting it to other rods in a 3D grid. This second solution will be used for the falsework of our scaled drone port, further in the thesis, where the boundary arches have a ratio  $f/L$  higher than 0.3.

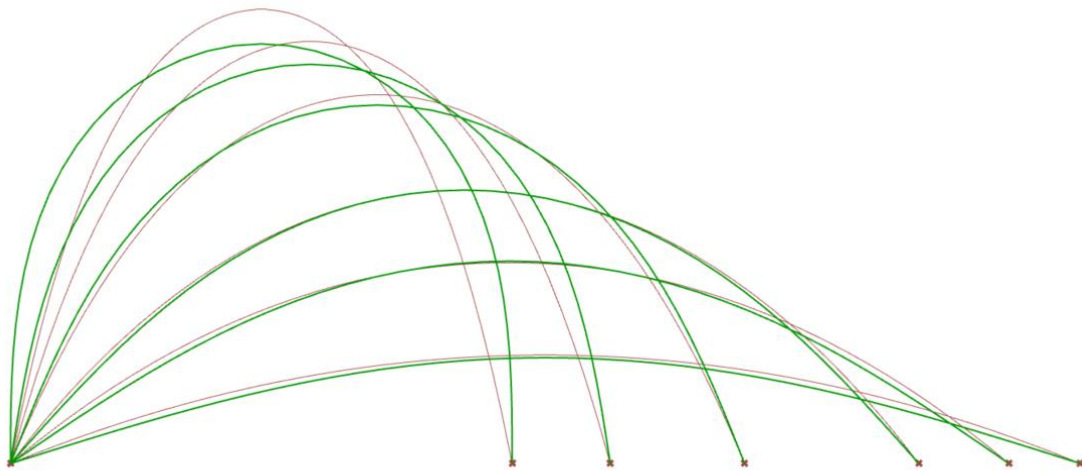


Figure 20 : comparison between catenary curves (red) and bended curves (green), for  $f/L$  ratios from top to bottom of 0.9, 0.7, 0.5, 0.3, 0.2, 0.1 for the catenary curve.

### 5.2.3 Rod modelling with Karamba3D

Modelling the rods with Karamba3D<sup>10</sup> has also been investigated in order to have more possibilities in the structural analysis. Two solvers are used. The dynamic relaxation solver is used when large displacements are expected like when form-finding. The 1st order solver is used when only very small displacements are expected.

We consider a rod of 3m in steel S235 with a circular cross section of 2mm diameter. Three cases are investigated.

The first case is a flat rod that is bended by imposing a displacement of -0.5m with the component “Prescribed displacement” of Karamba. The initial flat rod is a polyline of 30 segments. Here the dynamic relaxation solver is used. To enable the bending a small eccentricity of 5mm is introduced in the middle of the initial rod, which makes it be a nearly flat curve instead of a line. Figure 21 shows the bended rod obtained with Karamba (green) and the previous one with kangaroo2 (red). We see that the results are mingled, showing the methods give the same elastica solution. To calculate the bending moment Karamba “really” bends each segment whereas kangaroo2 “bends” the angles between the segments. To check the bending moment in each segment we calculate the radius of curvature of an interpolation curve of the bended polyline vertices, for each middle point of the segments (see Figure 22). Then from this radius we calculated analytically the bending moment and we observe the results match the bending moment calculated by Karamba.



Figure 21 :Bending rod with karamba (green), and kangaroo2 (red), from a prescribed displacement

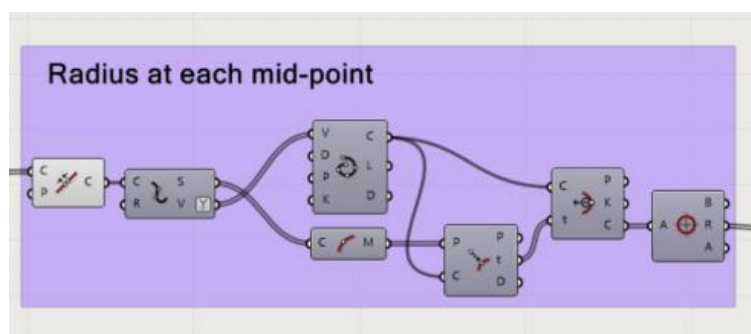


Figure 22 : radius of curvature at the middle points of the segments

In the second case we give to Karamba in input the elastica shape obtained with kangaroo2 and we apply a prebending load to each segment with the component “initial strain”(Figure 23). The initial curvature is calculated from the interpolation curve of the polyline (Figure 23).. The anchors are both pinned. The resulting shape does not change, no

<sup>10</sup> <https://www.karamba3d.com/>



displacement are observed. The bending moment is calculated in Karamba with the 1st order solver and with the dynamic relaxation and both are compared to the analytical calculation, see Figure 24. We observe that in this case the 1st order solver gives results closer to the analytical calculations. We note that the results of the dynamic relaxation can be improved by increasing the “nloadincs” variable of the solver but at a high cost in computational time.

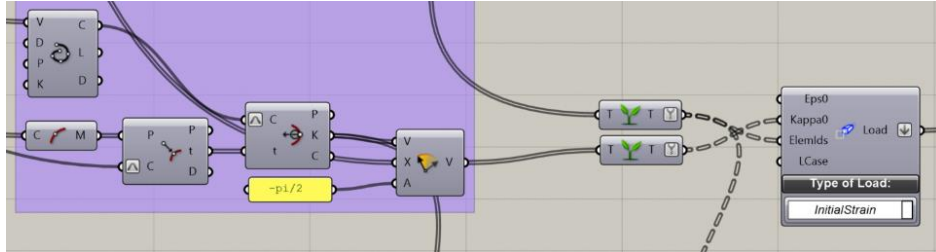


Figure 23 : prebending with Karamba

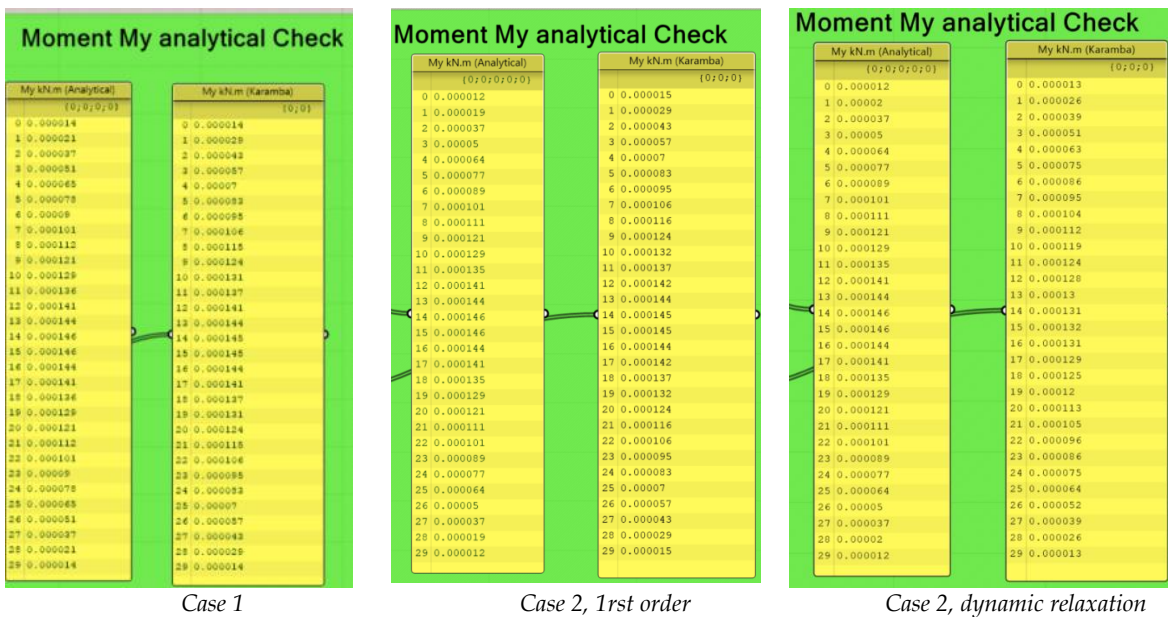


Figure 24 : Bending moment values

The third case is the same as the second case but with the right support being a roller (Figure 25). Thus large displacements are expected. The dynamic relaxation solver gives a correct flat final curve and conserve the total length, whereas the 1st order solver does not give a final flat rod and changes the total rod length, confirming that this solver is not suited for large displacement analysis. In both cases the resulting moments calculated by Karamba are close to 0 which is correct in regard to theory.

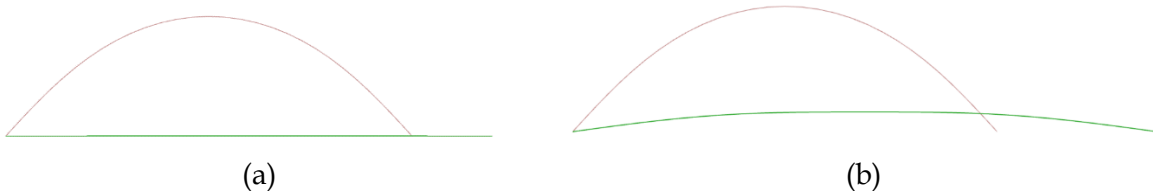


Figure 25 : prebending with Karamba. (red) initial curve. (green) equilibrium curve with roller at right side and the solver : (a) with the dynamic relaxation solver, (b) with the 1st order solver.



## 5.2.4 Rod modelling with K2Engineering

Finally we model the rods with Kangaroo2 Engineering<sup>11</sup> (K2E) which is a plug-in for grasshopper using the Kangaroo2 solver and especially suited for the structural analysis of bending active structures. In our final computation design for the falsework of the scaled drone port we use K2E because it combines the adequacy of Kangaroo2 for form-finding with the possibility to perform structural analysis and define more precisely elements (ex : extra cables).

For this study we use GFRP rods (Glass Fiber Reinforced Polymer) and steel cables. Both cross sections are circular. The material properties and diameter are given in Table 1.

	Rods	Cables
<b>Material</b>	GFRP	SteelS355
<b>Young's modulus : E (MPa)</b>	40000	210000
<b>Yield strength : fy (MPa)</b>	900	355
<b>Density : rho (kg/m3)</b>	2100	7850
<b>Diameter (mm)</b>	10	2

Table 1 : material and geometrical properties

The rod is modelled as a polyline, made of 30 segments here. To model the bending active behaviour of the rods we use the component "rod" from K2E that enables model the stiffness of the angle between each segment of the polyline (Figure 26). The "Rest angle" is set to "0" in order to model the prebending if the initial polyline is not straight. The axial stiffness is modelled by the component "bar" of K2E.

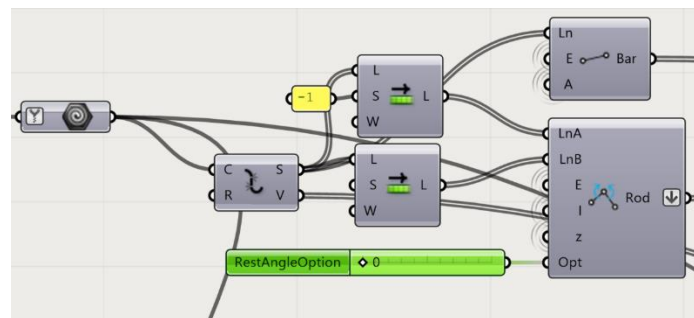


Figure 26 : modelling of the rods with K2Engineering

Figure 27 shows with K2E the deviation of the elastica equilibrium curve from the initial curve which is a semi-circle of 1m radius. The anchors are pinned supports. The perpendicular lines are proportional in length to the bending moment. The colour of the rod tends toward red when the deviation from the initial curve is maximum.

First we check that the bending moment calculated by K2E is coherent with the analytical calculation of the bending moment (Figure 28), and they are nearly equal. Contrary to Karamba, the bending moment is calculated at each angle, between the segments and not at the middle of each segment, thus the analytical calculation is done by calculating the radius of curvature at all the vertices of the interpolation curve of the polyline.

<sup>11</sup> <https://formatengineers.com/research/k2-engineering.html>

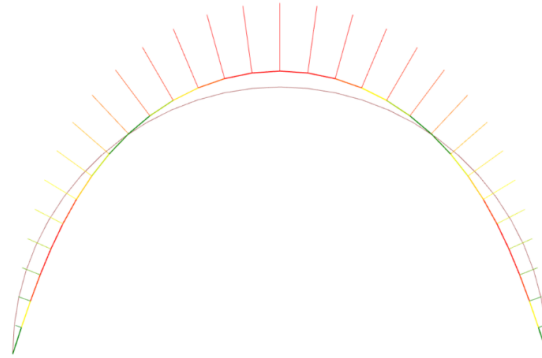


Figure 27 : Prebending with k2Engineering ,max bending moment = 25.5N.m  
(Rods : green to red = 0 to max deviation), (Moment : green to red = 0 to max moment)

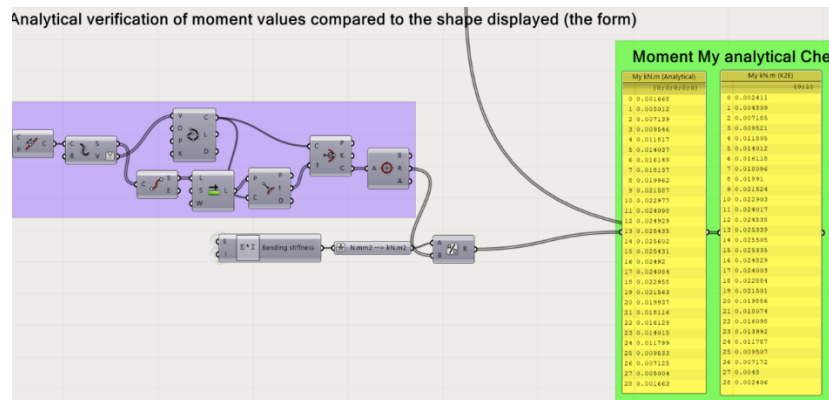


Figure 28 : analytical check of the bending moment calculated by K2E.

Secondly we check that the maximum stress (here 260MPa) is below the yield strength (900MPa). The maximum stress in the rod is calculated from the maximum bending moment, and parameters of Table 1, by using the equations of the bending theory 5.1. It is equivalent to check if the radius of curvature is above the minimum radius.

If we transform the right anchor to a roller then the rod tends to flatten but not entirely. We observe also that there is a remaining bending moment as shown on Figure 29 (a). This problem can be removed by lowering the number of segments, as shown on Figure 29 (b) where the number of segments is lowered from 30 to 10. Thus for each simulation a balance has to be found between the division of the initial polyline (the number of segments) which gives "local precision" and the expected displacement which requires less segments.

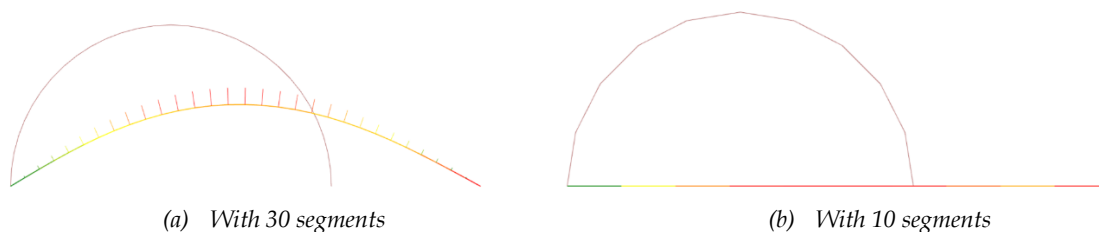


Figure 29 : Prebending. Pined support left and roller right  
(Rods : green to red = 0 to max deviation), (Moment : green to red = 0 to max moment)

Then if we add a cable between the two supports we retrieve previous results and with a force in the cable of 24N which generates a stress of 7.7MPa in the cable of 2mm diameter which is below the yield stress of steel. Results are shown in Figure 30.

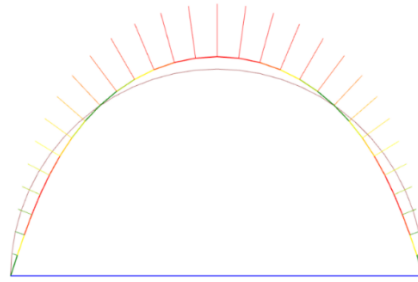


Figure 30 : prebending with. Pinned support left, an roller support right + cable, force in cable = 24N  
 (Rods : green to red = 0 to max deviation), (Moment : green to red = 0 to max moment),  
 (cable, blue = tension, green = neutral)

Finally we add loads by putting 20N on each node. Figure 31, shows that the rod presents very large deformations. To prevent failure we can use stiffening cables. Figure 32 shows two example where we add such cables. We observe that the combination of the displacement with the deviation stays small : 42mm in case (a) and 13mm in case (b). This shows that the addition of cables is an effective way to make the rod able to sustain load. This can be an interesting strategy for stiffening the boundary cables of our falsework that will need to behave as a formwork for the erection of the first arches of the shell, before the rest of the shell is built by cantilevering from those first arches. An in depth study about post-tensioned bending active frames can be found in (Coar et al. 2018). Figure 32 also shows that the deviation is small making the addition of cables a suitable strategy for describing curves different from the elastica curve with bended rods (for example narrow catenary curves). We note that the bending moment obtained is uniform in Figure 32 (b), which present low deviation and displacement and thus the rod describes the initial semi-circle, which has a constant curvature, leading to a constant bending moment. Finally we observe on Figure (b) that some cables carry no load (the green ones), showing that this cables configuration can be optimized.

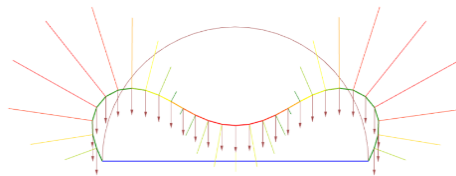
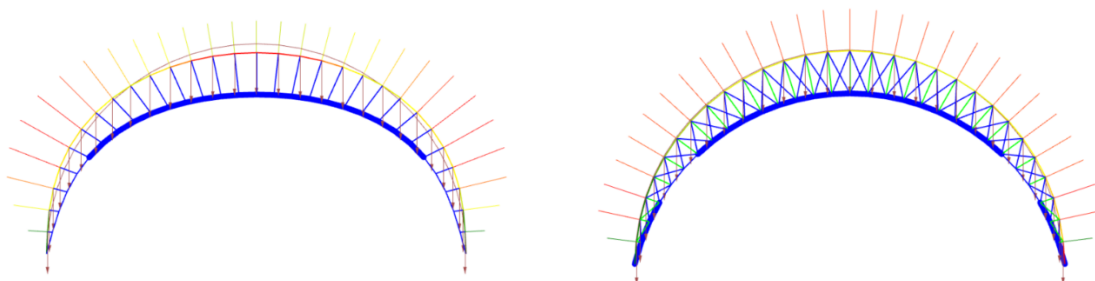


Figure 31 :External load : 20N/node, prebending with. Pinned support left, an roller support right + cable  
 colour legend : idem Figure 30



(a) Straight cables

Max stress in rod = 275 Mpa  
 Max displacement = 42mm  
 Max force in cable = 603N

(b) Addition of cross cables

Max stress in rod = 210 Mpa  
 Max displacement = 13mm (but 3.6mm Zaxis)  
 Max force in cable = 764N

Figure 32 : rod with stiffening cable (colour legend : idem Figure 30)

### 5.3 Modelling of a 3D bending active gridshell

This part shows computational strategies that we investigated to model a bending active gridshell. Here we consider the input to be the geodesic lines of the target falsework. First we want to model the deviation of the falsework when the curves of this target falsework are transformed into bending active elements. Second we want to evaluate the internal stresses and to model the displacement of the falsework if some parts of it need to sustain loads.

#### 5.3.1 Modelling the deviation of the gridshell with Kangaroo2

This part of the program takes as an input the target falsework. Figure 33 shows arbitrary geodesic lines drawn on a compression only shell calculated with RhinoVault2. We will come back on the choice of the best guidework for this shell later (that is not the one of this example).

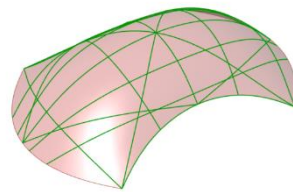


Figure 33 : geodesic lines on a compression only surface

We chose to design the guidework with 4 direction layers for the rods. Figure 34 shows these direction layers names u, v, w, x. The layers u and v are the 2 main directions and then the other layers are diagonals that prevent deformations of the guidework by giving geometrical stiffness.

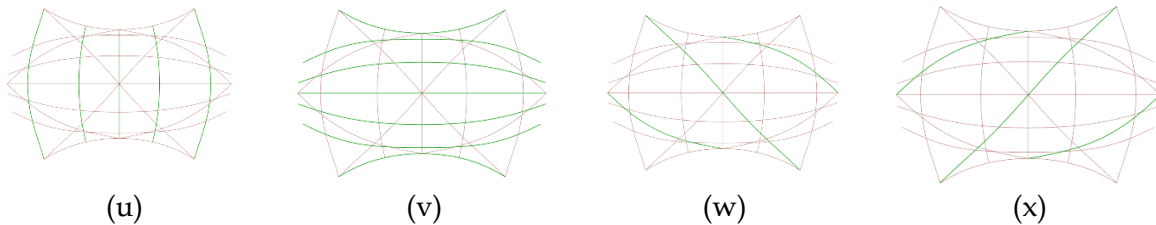


Figure 34 : direction layers of the rods

Then we find the intersection points between the curves (Figure 35). This will enable to define the nodes. As we saw previously the geodesic lines can be drawn on a surface or a mesh. On this second case the curves do not necessarily intersect because the curves are not really projected on each face of the mesh but approximate the mesh. Thus the intersection are found with a tolerance on a small distance between two curves. The end points are also added for each curve in case they do not correspond to intersection nodes in order to include the supports.

#### Remark :

- We note that another possibility to model the nodes, if the points of the two rods are not exactly the same, is to use the component "coincident" of Kangaroo2. However by having directly the nodes be defined in both rods by the same point enables not to use that component and gain some computational time.

Then the curves are rebuilt from these nodes in order to be sure both curves have in common a same point for each of their intersection nodes (Figure 35).

However if we use these rebuilt polylines as inputs for the rods in Kangaroo then we encounter two problems. First, if the number of intersections is low or if even no intersections, then the resolution of the polyline can be insufficient to approximate the target geodesics curves. Secondly the disposition of the nodes on the polylines can be non-uniform which leads to a bad modelling of the bending stiffness. This is because the bending stiffness is modelled by the strength of the angles, between to segments of the polylines, to go towards a target angle (by default their initial angle, but can be set to 0 to introduce prebending i.e. the target angle will be a straight rod).

In order to solve these two problems additional points are added to create the polyline. This is shown on Figure 36. A “number of point factor” is defined, here 10. Each segment of the polyline is divided in a number of intermediate points depending on its length and on the previous factor. This enables to reduce the difference in distances between points in order to model more properly the bending behaviour. Then these points are projected on the geodesic curve to gain resolution. Finally a new polyline is created from these new points.

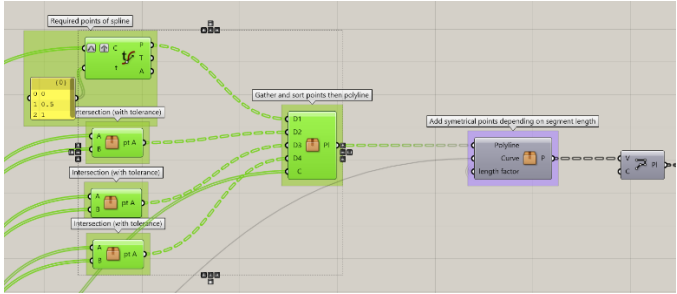
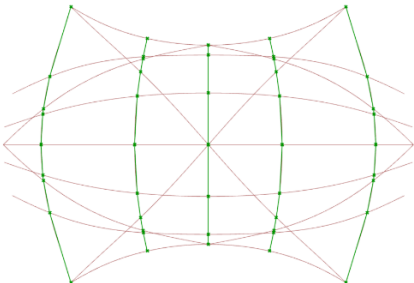


Figure 35 : finding the intersection nodes with tolerance and rebuilding the curves (example with direction layer u)

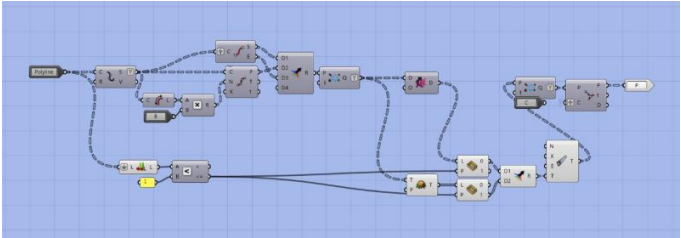
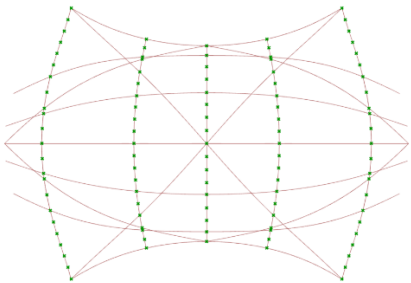


Figure 36 : adding points to create the polyline rods in order to increase the resolution and to model properly the bending stiffness of the rod (example with direction layer u)

These geodesics then serve as inputs for the “rod” component of kangaroo and the angle factor is set to introduce prebending by informing kangaroo2 that the rest angle is so that the rod is straight (see, part 5.2).

Remark :

- A strategy that we first used but that revealed being less efficient than the one above is to first model the rods vertically, then to define on these rods the nodes and the intermediate additional points similarly as above, and finally to bend the rods in place by giving the target points for the end point anchors and using the “coincident” component for the nodes. An example with another shell is show in Figure 37. Firstly, that modelling strategy takes a lot more computational time. Secondly, it is source of imprecisions because the rods are here imposed a large deviation from their vertical position to the bended position, but the final measured deviation that interests us is

the one from the target guidework, whereas in the strategy above the curves are directly transformed into bended rods and thus the deviation calculated by kangaroo is less prone to errors.

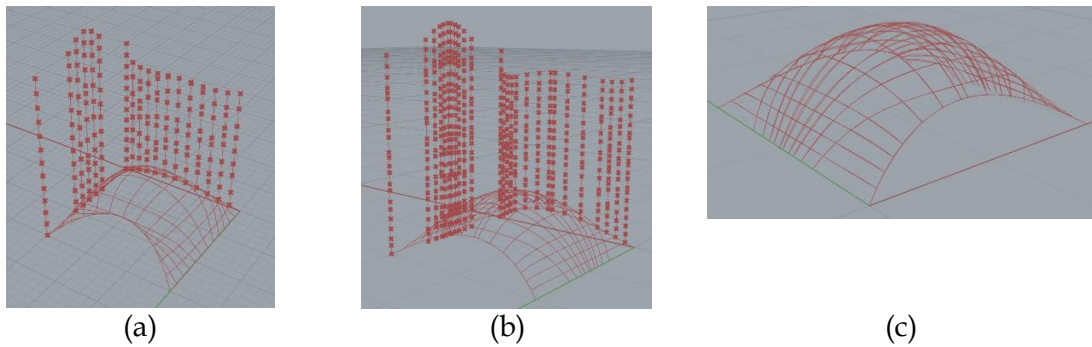


Figure 37 : alternative strategy to model the gridshell (that we don't recommend).  
 (a) Vertical rods with the position of the nodes, and target guidework, (b) additional intermediate points for modelling the bending behaviour, and target guidework, (c) bended rods and target guidework

### 5.3.2 Modelling the gridshell with Karamba3D

Modelling the gridshell with Karamba enables to perform a structural analysis of the gridshell. However in the rest of the thesis we have used for this Kangaroo2 Engineering because it is more suited for the study of bending active structures. For a deep comparison of Kangaroo2, Karamba and Kangaroo2Engineering we refer to the work of Cecilie Brandt-Olsen (Cecilie 2016). Nevertheless we chose to briefly present some particularities of the modelling of bending active gridshells with Karamba3D as it is commonly used for structural analysis and was our main tool in the first period of our research.

The input are the polylines rods approximating the geodesic curves described in 5.3.1. We first thought of using slats instead of rods. Thus their orientation is important and the local coordinates of the segments are reoriented by aligning their z-local-axis to “their” curvature vector obtained from the interpolation curve of the polyline vertices. From the value of the curvature we also assign a prebending to the elements by using the component “load>initial strain”. (Figure 38).

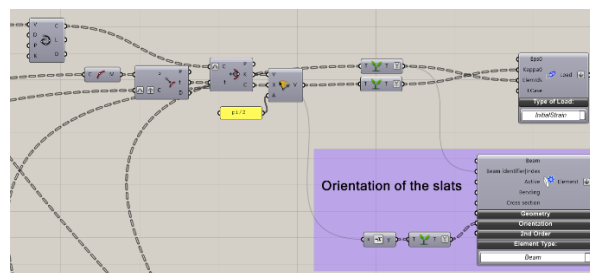


Figure 38 : reorientation of the slats and prebending.

We want the slats to be continuous and nodes to be modelled like scissors. For that the classic way to define nodes in Karamba (“beam-joints”) is not satisfactory because it would create either non-continuous slats (hinged at each node), or a complete rigid gridshell with stiff nodes preventing the scissor behaviour (which would be a too much optimistic hypothesis). The solution is to model the nodes as zero-length springs (Figure 39). This implies that each node is represented by two different points belonging respectively to the two slats but that have the same coordinates, i.e. the two points are the same point spatially but they have two different names and are rigidly attached to two different slats.



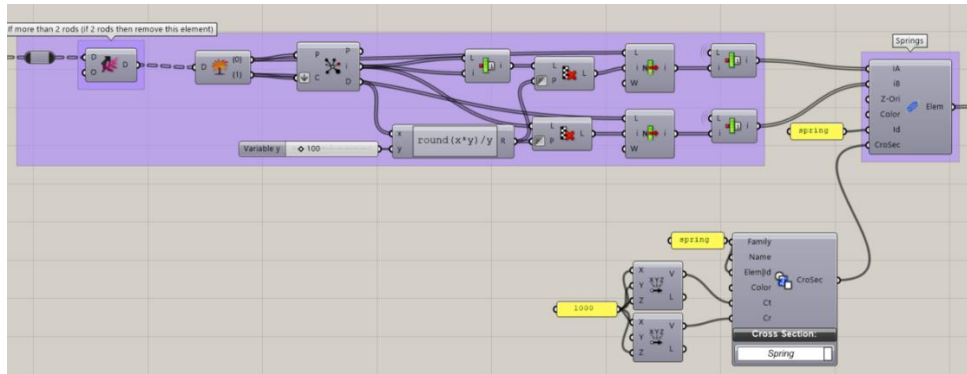


Figure 39 : nodes modelled as zero-length springs

In Karamba the slats are made of segments named “beams”. These beams are not created in Karamba by the classic way (“line to beam”) but by using the component “index to beam”. This enables to create beams from points that have different names but with the same coordinates, which enables to create rigid slats of a continuity of beams but independent from other slats (Figure 40). Finally, we can chose to stiffen some slats by adding a second slat and connecting the two by shear blocs which locks the deformation du to prebending and also creates a double slat structural element with a higher moment of inertia to make to falsework able to sustain higher external loads. An example of a gridshell made with karamba with some elements that are made of two layer slats is show in Figure 41.

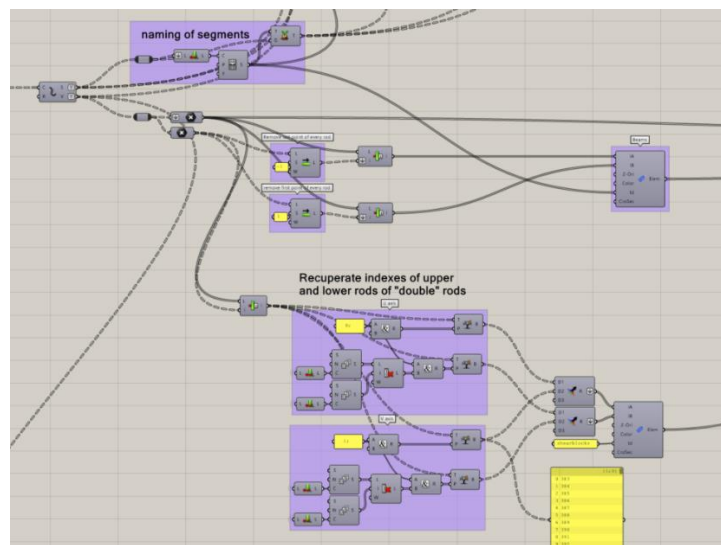


Figure 40 : “index to beam” to model slats as rigid group of beams, and independent from other slats. Also shows how to create the second layer of stiffening slats.

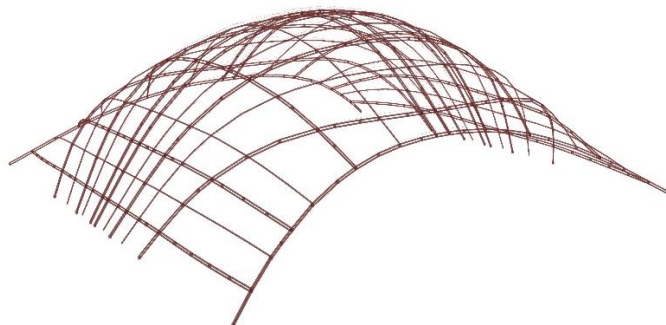


Figure 41 : Gridshell modelled with Karamba and with some elements that are made of 2 layers of slats connected by shear blocks.

### 5.3.3 Modelling a bending active gridshell with Kangaroo2 Engineering

Kangaroo2Engineering is a well suited tool to model bending active gridshells (Cecilie 2016). Figure 42 shows a general overview of the grasshopper code to model with K2E the falsework used for the scaled drone port (chapter 7). First a set of geodesic lines are found on the mesh of the compression only shell. Here there is a manual feedback to adjust the choice of the geodesic lines from the results of the deviations and displacements calculated by K2E. Then the target falsework is transformed into the polylines representing the rods by identifying the intersection nodes and adding in between additional points to increase the accuracy of the approximation of the geodesic curves by polylines, but also to have a constant lengths of the segments in order to model properly the bending behaviour of the rods, the same way we did it with kangaroo2 previously (see part 5.3.1).

Then all the goals necessary for Kangaroo2 are defined with components from K2E. The rods are modelled like we did in 2D for a single rod (see part 5.2.3). We note here the easiness of defining the prebending, by simply setting the angle factor to 0, compared to Karamba where we had to approximate the curvature of each segment and set it as an initial strain load.

K2E offers components to define materials, cross sections, and cables (only takes tension). Self-weight is applied thanks to the component "BarLength" which calculated the lengths of a bar coming at each node. Then we use the "Zombie" solver of Kangaroo2 which does the calculation in one step and shows only the final equilibrium state and skips the dynamic display of the classic Kangaroo2 solver. We adjust the equilibrium threshold to 10e-20 to increase the precision of the equilibrium form-found.

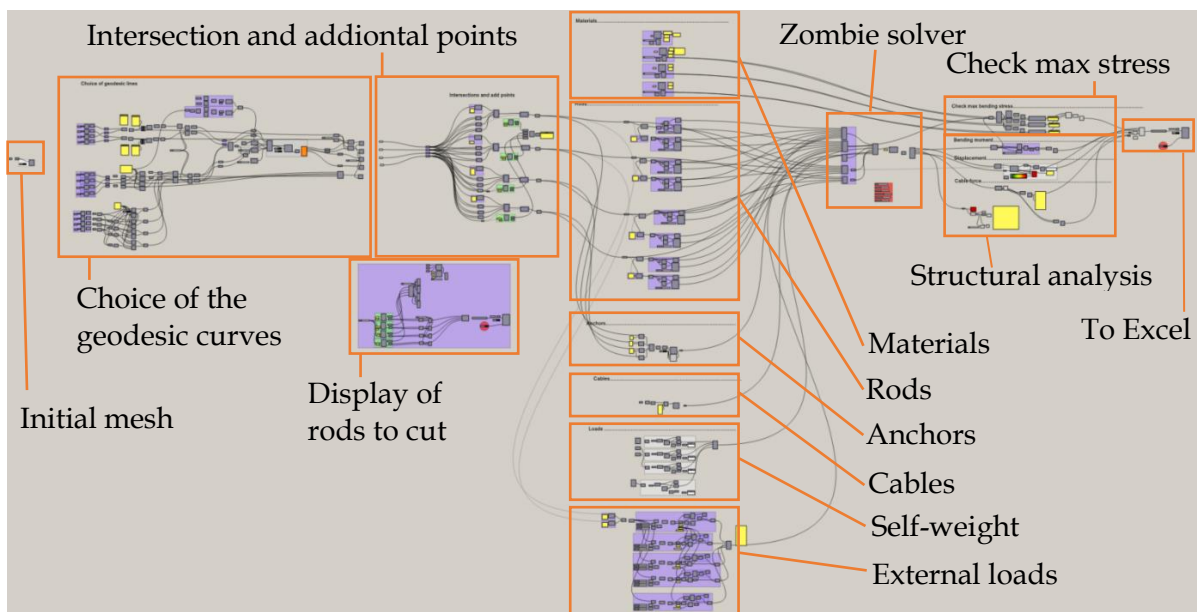


Figure 42 : general overview of the grasshopper code for the modelling with K2Engineering of the falsework for the scaled drone port

## 6 Computational design of a bending active falsework based on geodesic curves for a simple compression only shell

Now that we know how to model a bending active gridshell we will try to use it to create a falsework that approximates a simple compression only shell.

### 6.1 The compression shell

To investigate the complete workflow from a compression shell to its bending active falsework, we chose a simple shell in order to not overlap the main issues with extra specific constraints. The shape of the shell is found with RhinoVault2 (RV2) by the Thrust Network Analysis (TNA) method (Figure 43). Then the resulting shape is passed to Grasshopper and transformed into one single mesh by the component “join meshes and weld” of the plug-in Weaverbird<sup>12</sup>.

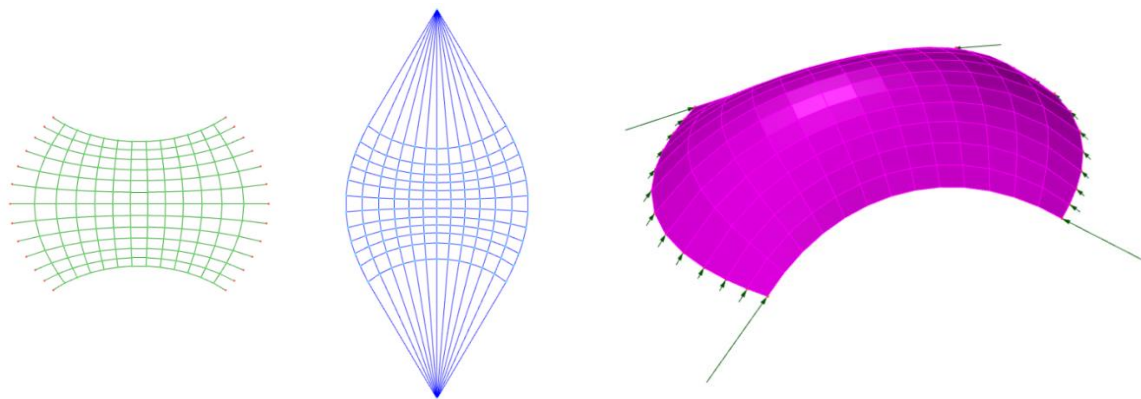


Figure 43 : Left : Form diagram (green), force diagram (blue), right : RV2 shell

The shell dimensions are 3m length, 2m wide and 0.7m height (Figure 44). The shell model here has no thickness. For designing the guidework the thickness is only important to evaluate the admissible displacement of the bending-active grid so that the resulting compression shell has its thrust lying within the thickness of the masonry. Here we expect the shell to be made of several layers of tiles. The first layer of tiles would have a thickness around 15mm and the final shell thickness is expected to be between 60mm and 120 mm. The boundaries of the shell on the ground are curved to avoid creating a hinged line support that would be a bad design because resulting in bending moment in the shell against horizontal loads.

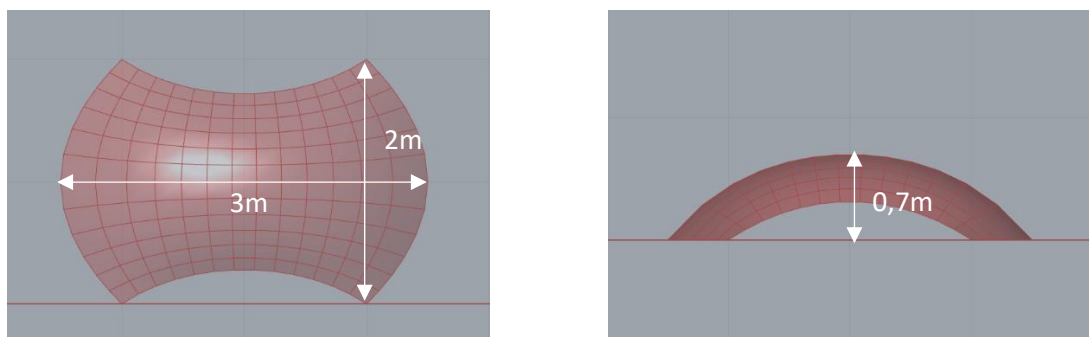


Figure 44 : Dimensions of the shell

<sup>12</sup> <http://www.giuliopiacentino.com/weaverbird/>

## 6.2 Choice of the target guidework

### 6.2.1 Mesh to surface to finding geodesic lines

The geodesic curves are found thanks to the component “geodesics” of Grasshopper. This component needs a surface as a input. Thus the RV2 mesh needs to be transformed into a surface. This is done by using the component “SrfGrid” which requires in input the vertices of the initial mesh to be sorted. To sort correctly these vertices they are projected on a reference surface and sorted according to their (u,v) local coordinate (Figure 45). Note that the vertices could not be directly sorted by their (x,y,z) coordinates because of the curved edges, that make for example some points of the second column have a smaller x coordinate than vertices of the first column.

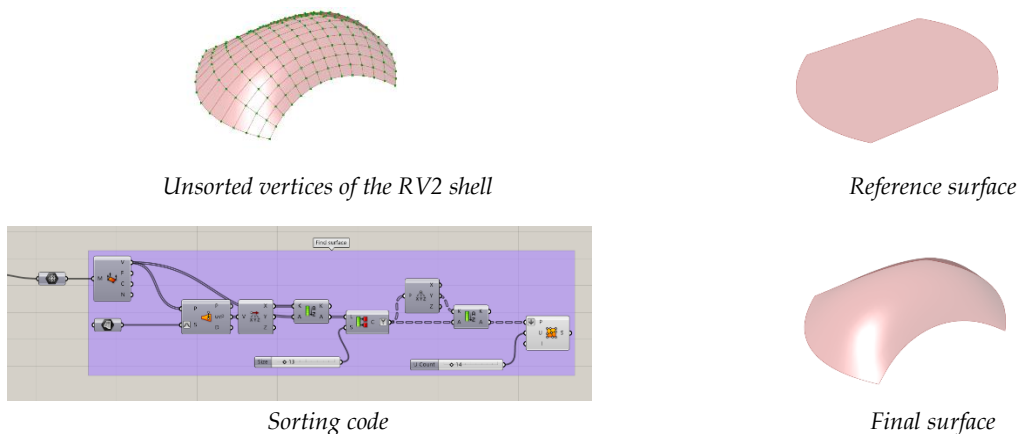


Figure 45 : mesh to surface

### 6.2.2 Optimized guidework with Galapagos

If the bending active behaviour of the guidework is modelled with the “ZombieSolver”<sup>13</sup> of kangaroo2, then it is possible to run a optimisation algorithm with “Galapagos”<sup>14</sup> which is an evolutionary solver for Grasshopper. The kangaroo solver needs to be the Zombie solver that does the calculation in one loop and outputs directly the final result by keeping its intermediate iterations results internal. The general algorithm is shown below on Figure 46. The Galapagos component creates a feedback loop in grasshopper. Here the optimisation algorithm tries to minimize the deviation of the rods of the guidework when modelling it with kangaroo2.

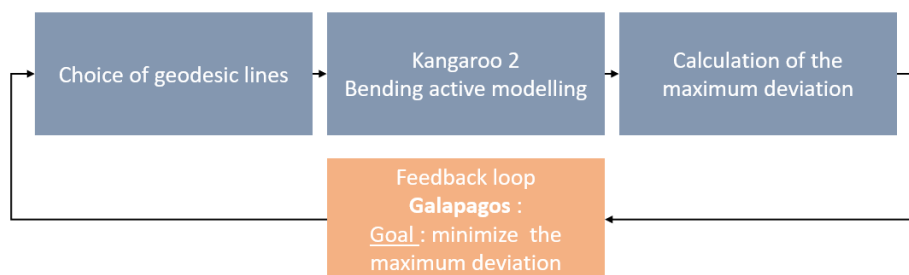


Figure 46 : Optimisation algorithm

<sup>13</sup> <https://grasshopperdocs.com/components/kangaroo2/zombieSolver.html>

<sup>14</sup> <https://grasshopperdocs.com/addons/galapagos.html>

Many variables could be used for the optimization, like the rods number, position (density and distribution), orientation (layers : perpendicular, diagonal,...) and diameter. We chose here to limit the variables to 5 in order to keep the optimization time reasonable. For the two main layers, u and v, bridging opposite boundaries, Galapagos can vary the number of rods between 3 to 10 (min 3 because we impose to have at least the 2 boundary rods and the middle rod for these 2 layers). Galapagos can also vary, for these two layers, the distribution of the rods by dividing the distance between rods by a step that varies linearly. The distribution is impose to be symmetrical compared to the middle rod. The final variable for Galapagos to play with, is the number of diagonal rods that can vary between 2 and 10. This acts identically on the two diagonal layers because we chose to have a symmetry, and the distribution is chosen linear. We have in the direction layers a minimum number of rods (3 and 2) because no rods would lead to an optimal goal of no deviation but is obviously also no guidework.

Figure 47 shows the guidework resulting from the optimization. However this results is not really satisfactory because the density of the rods seems to high on top to lay bricks easily for the mason, and to low on the side to guide properly. Actually the algorithm “dodges” the difficult part of the guidework.

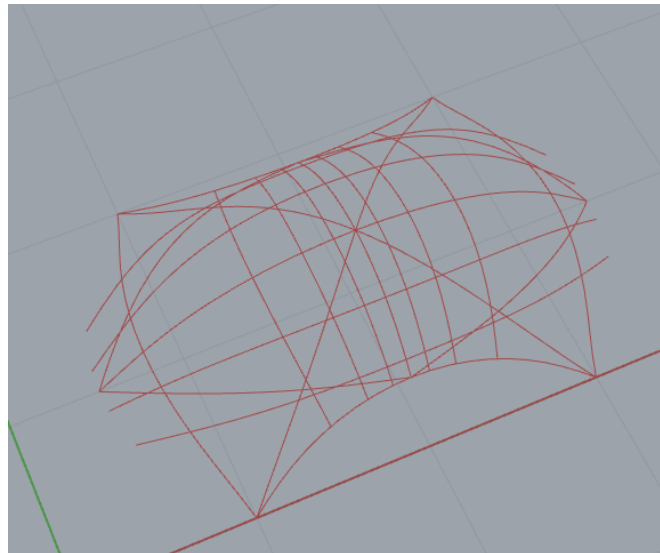


Figure 47 : Optimized guidework with Galapagos

### 6.2.3 Manual choice of the guidework

We chose then to perform the feedback loop in a manual way, i.e. we adjust the values of the entry variables manually to have a satisfactory guidework. The criteria we use are:

- The deviation of the rods. (The deviation is calculated as the distance between the initial vertices of the polylines modelling the rods before and after the kangaroo2 solver).
- Having only 2 rods crossing in each node to simplify construction.
- A “gut feeling” of a density of rods that is not too high to let the mason work, but also sufficiently high to describe accurately enough the compression shell. This depends on the experience of the mason and the complexity of the shell.

The final falsework is show in Figure 48.



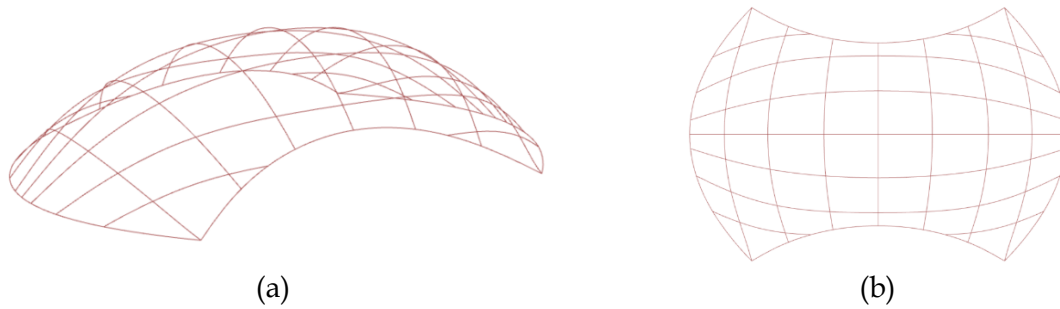


Figure 48 : Manual choice of the target guidework, (a) 3D view, (b) top view

### 6.3 Material choice and modelling of the rods

The rods are in Glass fiber reinforced polymer (GFRP) of 10mm diameter. That value is chosen from manual feedback of the simulation results. Cables will be added further to minimize deviations and displacements. Steel cables of 2mm diameter are chosen, their diameter is less important than for the rods because for the rods it impacts their bending stiffness, whereas for the steel we simply need to sustain the load with little elongation. The values of the material properties where given in Table 1 (page 19).

The rods are grouped as shown in Figure 49. We do the distinction between these direction of rods so that rods in one of these layers do not intersect each other, and then we can find the intersection with other “layers” of rods. Here the rods w and x intersect the ones in u and v. We could have put w and x together, but these diagonals layers can intersect each other in some case (ex : Figure 47) and thus for the more general case we keep them separated.

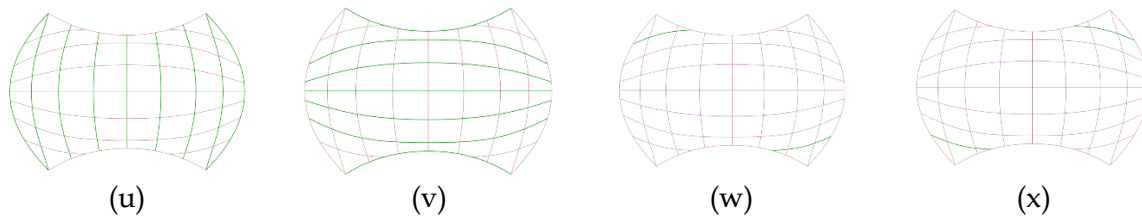


Figure 49 : naming of the direction layers of the rods

For modelling the bending behaviour of rods, the geodesic curves have been approximated by polylines as explained in section 5.3.1. The general steps are summarized in Figure 50. First the nodes are identified then additional points are added in between to refine the approximation of the target guidework curve, and to have a constant distance between two points to model properly the bending stiffness of the rods.

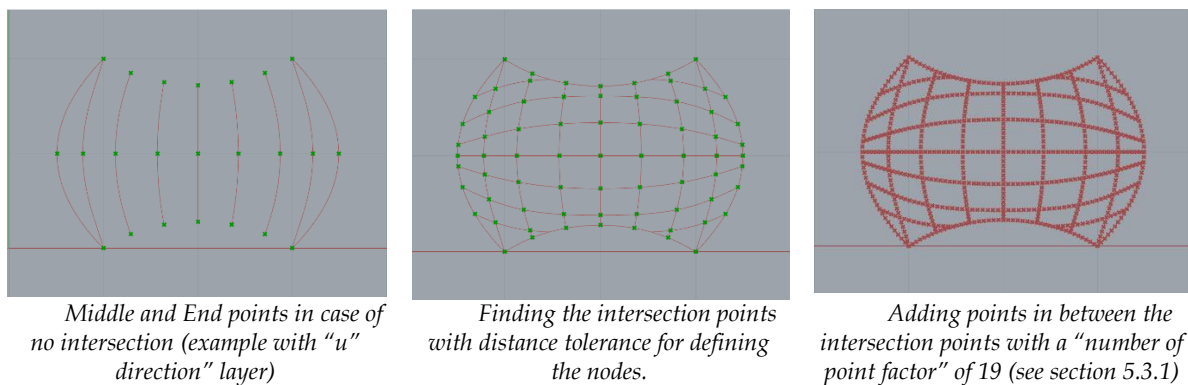


Figure 50 : Modelling of the rods

### 6.4 Analysis of the structural behaviour of the guidework and adjustments to reduce deviation

First the boundaries of the guidework are laid on the ground and bended with cables (Figure 51). This boundary will serve as a attaching curve for the other rods. We observe that the deviation is very low. This is by “chance” that the bottom boundary line of the compression shell is close to the elastica shape and is specific to this simple shell. So here a unique cable is sufficient, otherwise more cables can be used to approximate the curve with a rod like in Figure 32). Thus when designing directly the boundaries of the compression shell it is interesting to do it in order that they fit the elastica curve (nearly like here), if this falsework strategy is used.

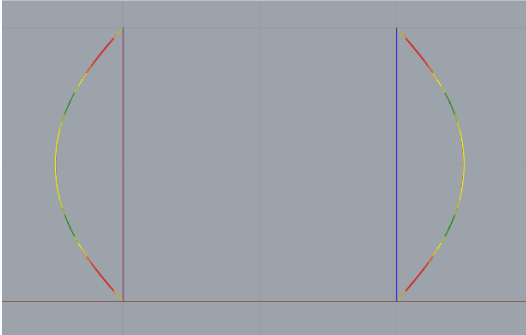


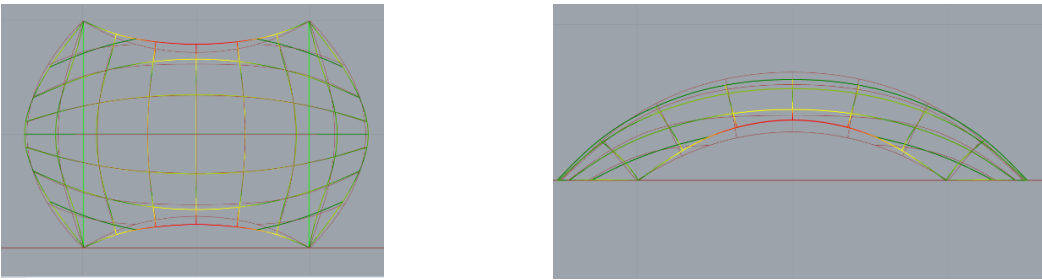
Figure 51 : Construction of the bottom boundaries

Colour legend : (Rods : green to red = 0 to max deviation), (cable, blue = tension, green = neutral)

Max stress in rods	200 MPa
Max stress in cables	12.55 MPa
Max deviation	5.6 mm

Table 2 : Numerical values of Figure 51

Then the other rods are added and Figure 52 shows the obtained deviation. We observe that the deviation is the largest at the middle of the standing boundary rods (the top and bottom boundary rods in the top view of Figure 52). This is because the rods of the u layer are pushing out these boundary rods. We note that the 2 bottom cables are no more necessary once the gridshell is built in this state of the gridshell. Here and for further simulation we just indicate the maximum stress in the rod and cables as a check for being under the design permissible stress (the yield stress).



Top view

Side view

Figure 52 : Guidework deviation, with the 2 additional boundary cables

Colour legend : (Rods : green to red = 0 to max deviation), (cable, blue = tension, green = neutral)

Max stress in rods	358 MPa
Max stress in cables	0 MPa
Max deviation	105 mm
Max vertical deviation (z-axis)	76.5 mm

Table 3 : Numerical values of Figure 52

In order to reduce the deviation observed in Figure 52 we add a cable joining the middle of the standing boundary rods, as shown in the perspective view of Figure 53. We observe that it reduces greatly the maximum deviation down to 31.7mm. However we can see in Figure 53 in the top and side views that these boundary rods still present a deviation around the location of  $\frac{1}{4}$  and  $\frac{3}{4}$  of the rod.

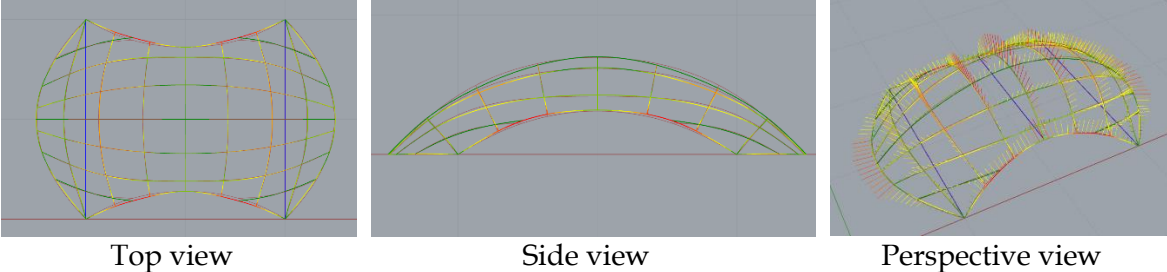


**Figure 53 : Guidework deviation, with 3 additional cables**  
 Colour legend : (Rods : green to red = 0 to max deviation), (cable, blue = tension, green = neutral)  
 (Bending moment : green to red = 0 to max bending moment)

Max stress in rods	254	MPa
Max stress in cables	94	MPa
Max deviation	31.7	mm
Max vertical deviation (z-axis)	22.2	mm

Table 4 : Numerical values of Figure 53

To improve more the accuracy of the guidework and reduce the deviation 2 additional cables are added around  $\frac{1}{4}$  and  $\frac{3}{4}$  of the boundary rods as shown in the perspective view of Figure 54. This enable to reduce further the deviation down to 13.3mm maximum. We also note that the 2 cables of the bottom boundary rods are no more useful (no force), however we let them there because they were necessary to construct the first two boundaries on the floor.

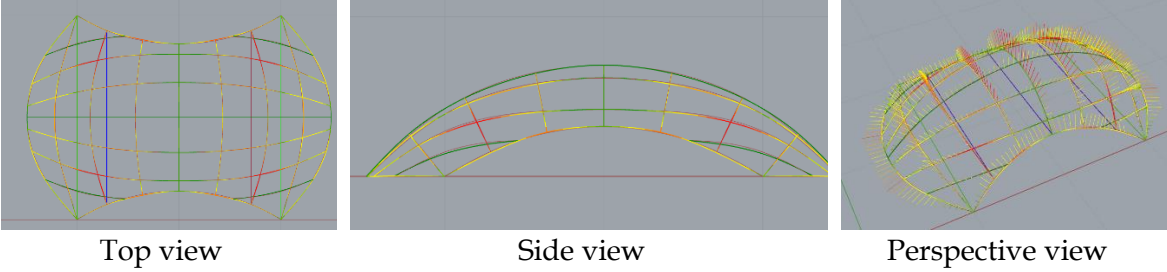
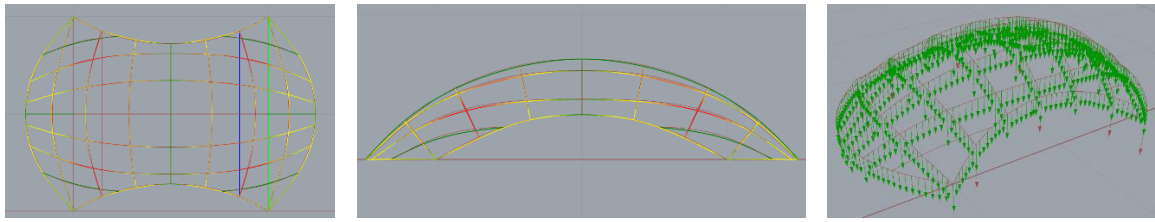


**Figure 54 : Guidework deviation, with 5 additional cables**  
 Colour legend : idem Figure 53

Max stress in rods	260	MPa
Max stress in cables	68	MPa
Max deviation	13.3	mm
Max vertical deviation (z-axis)	12.4	mm

Table 5 : Numerical values of Figure 54

We then add the self-weight of the rods and cables with the components “BarSelfweight” of K2E that requires the material density, the cross section area and the lengths of the bars coming in each vertices of the polylines (including nodes) that is done with the component “BarLenght” of K2E. We observe by comparing the results of Table 6 with Table 5 that the extra displacement generated by the self-weight is of  $15-13.3 = 1.7\text{mm}$  is added to the deviation. As we could imagine the bending property of the rod is more impact full here.



Top view

Side view

Self-weight load

Figure 55 : Guidework deviation and displacement, with 5 additional cables and self-weight load  
 Colour legend : (Rods : green to red = 0 to max deviation), (cable, blue = tension, green = neutral)

Max stress in rods	260	MPa
Max stress in cables	68	MPa
Max deviation and displacement	15	mm
Max vertical deviation and displacement (z-axis)	14.3	mm

Table 6 : Numerical values of Figure 55

From the results of Table 6 we observe that the maximum deviation plus displacement is 15mm which is an acceptable precision for building the shell, because the resulting thrust network would still be kept within the thickness of the masonry shell, that is usually around 10 cm<sup>15</sup>. We also note that 5 extra cables are needed here in order to attain this precision, otherwise the gridshell alone would display 105mm displacement that are not acceptable.

We can conclude at this stage, building a guidework, by combining bended rods with “adjusting cables” is a suitable solution for this simple shell. It is also an encouraging result to use this guidework strategy as a low tech solution for even more complex guideworks.

## 6.5 “Formwork behaviour” of the guidework for constructing the first arch

In order to construct the tile vault, we actually need to construct a first arches from which the other tiles will cantilever. The choice of the arches depend on the shell. Here We chose to construct a first central arch that goes from the middle of the boundary rod on the floor to the one of the other side. Then the arch will be built from constructing progressively the base legs up to the top, and both balancing each other thanks to the central arch.

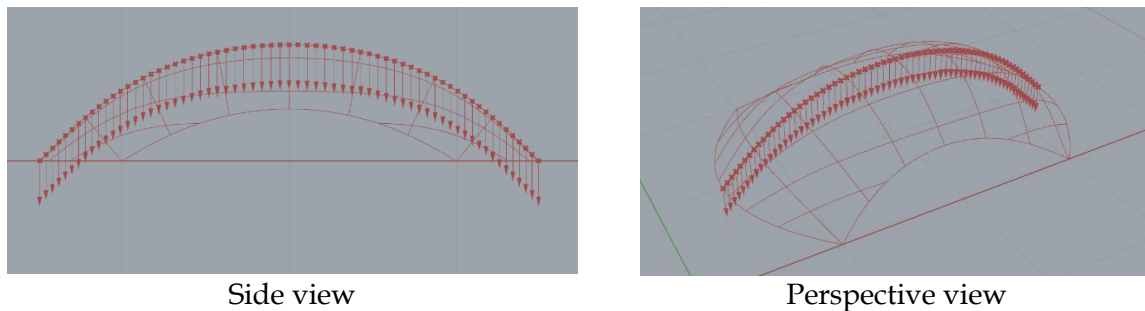
One tile is 280\*140\*15mm and weights 1kg. That makes 1kg/280mm is the tiles are led on their short side. It gives us a load of 37.7N/m. With a safety factor of 2 we obtain 71N/m and can round the load to 0.1 kN/m for extra safety.

The brick load applied on each segment is divided in two and distributed between the two end points of that segment. So each vertices of the polyline has two loads : one from the right segment and one from the left segment, except the extremities of the polyline that have only a half segment load (but it doesn’t matter because these two points are actually the anchors on the ground).

The load is applied at each node vertically as show in Figure 56. This is not representative of reality where actually the bricks below take a part of the load, but our simplification is conservative (more load is applied on the vertices than is reality) so it is not a problem for the moment. We say “for the moment” because we will see further that if we want to pre-

<sup>15</sup> For example the Brick-topia project has a first layer of 15mm tiles, then a second layer of 40mm hollow bricks and a third layer of 43mm solid brick, plus mortar between each layer (López López, Domènech Rodríguez, et Fernández 2014).

compensate the displacement of the rods under loads by playing on the value of the deviation, then we will need to be more precise on the load definition (see next chapter).

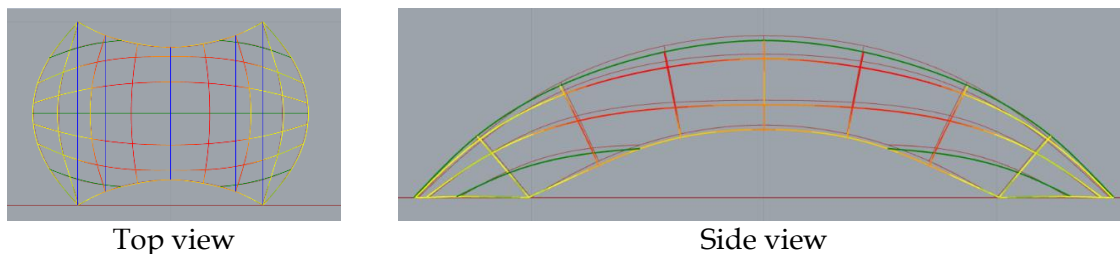


Side view

Perspective view

Figure 56 : brick load on the falsework for the construction of the first arch

Figure 57 shows the displacement plus deviation results. We observe that the maximum deviation is 27.22 mm, which is an acceptable value. Thus it means that this guidework can also serve as a formwork for the erection of the first arch. No extra formwork is needed.



Top view

Side view

Figure 57 : Falsework deviation and displacement, with 5 additional cables and self-weight load and 0.1kN/m brick load applied like in Figure 56.

Colour legend : (Rods : green to red = 0 to max deviation), (cable, blue = tension, green = neutral)

Max stress in rods	258	MPa
Max stress in cables	74	MPa
Max deviation and displacement	27.22	mm
Max vertical deviation and displacement (z-axis)	27.21	mm

Table 7 : Numerical values of Figure 57

However, we try to reduce that increase in displacement by adding another cable stiffening the central rod, on which the brick load is applied, by joining its end points. Figure 58 shows that this extra cable enables to reduce the displacement to 15.75 mm which is fine.



Top view

Side view

Figure 58 : Falsework deviation and displacement, with 6 additional cables and self-weight load and 0.1kN/m brick load applied like in Figure 56.

Colour legend : (Rods : green to red = 0 to max deviation), (cable, blue = tension, green = neutral)

Max stress in rods	258	MPa
Max stress in cables	71.8	MPa
Max deviation and displacement	15.75	mm
Max vertical deviation and displacement (z-axis)	14.76	mm

Table 8 : Numerical values of Figure 58



To analyse the hole construction of the arch we apply a progressive loading on the falsework, beginning from the extremities of the central rod up to the top, in a symmetrical way. Figure 59 shows the step by step loading, for the load cases of 0%, 25%, 50%, 75%, and 100% of the rod. It is not the value of the load that changes but the portion of the rod on which the load is applied that increases. The numerical results are shown in Table 9. It is interesting to observe that the extra stiffening cable of the central rod reduces the deviation (14.29mm down from 15mm in Table 6) in case there is no brick load (0% load case) i.e. the gridshell is “just” a guidework. It is also interesting to note that adding brick load up to 75% of to the rod actually creates a displacement that goes against the deviation, and reducing the total movement of the nodes. Thus the falsework actually approximates more accurately the compression shell during the construction of the arch than when used solely as a guidework. However, when the brick load reaches the top the falsework (load case 100%) it tends to push the side of the central rod “out”, (in the intermediate load cases, the brick load pushes the side of the central rod “In”) and creates the opposite effect, that is why then we see that the displacement adds to the deviation up to 15.75mm. Nevertheless, the load case 100% is not really significant because at that moment the arch is built and thus stands by itself, and we retrieve the load case 0%, and the falsework from that moment is only used as a guidework for the rest of the construction of the tile vault.

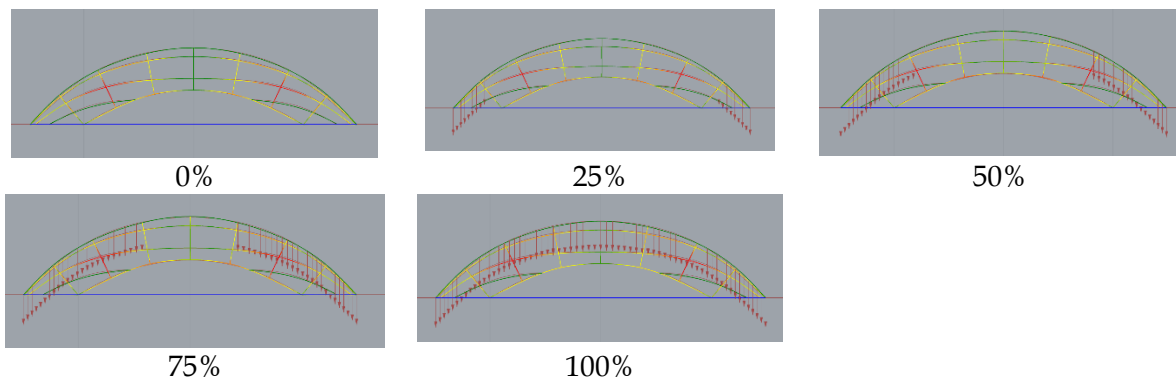


Figure 59 : step by step load increment

Colour legend : (Rods : green to red = 0 to max deviation), (cable, blue = tension, green = neutral)

Load case	Max stress cable (MPa)	Max stress Rod (MPa)	Max displacement plus deviation (mm)	Max Z-axis displacement plus deviation (mm)
0%	66.87	260.21	14.29	13.36
25%	66.12	260.95	13.61	12.71
50%	64.2	264.32	13.07	12.29
75%	64.24	270.32	14.01	13.22
100%	71.86	258.09	15.75	14.76

Table 9 : Step by step load increment

From the results shown in this chapter we can concluded that this bending active gridshells adjusted and strained by extra cables is stiff enough to carry the load of the bricks during the erection of the first arch without showing significant deformation (it is even more precise during the construction), and is also accurate enough to serve as a guidework for this simple compression shell.

## 7 Computational design of a falsework for a more complex shape : the drone port

In this chapter we will investigate the use of a bending active gridshells as a low tech solution for the falsework of a more complex compression only structure: the drone port.

### 7.1 The drone port shell : using new technological advancements at the service of the poorest

The drone-port is a real built project for the architectural Venice Biennale in 2016, introduced in the state of the art (Figure 8). The project aims to contribute to open remote regions in Africa and help transport medical and emergency supplies by drone. It is a compression only shell built from a first layer of tiles and two layers of DuraBrics (stabilized compressed earth bricks developed by LafargeHolcim). The advantage of these bricks is that the main material (earth) is available and affordable worldwide, and thus the vault can then be built everywhere in the world with local labour and with a low carbon footprint. Because the bricks are weak in bending it is important that the shell has a compression only shape. This was achieved by the BRG by form-finding the shape of the shell using TNA with RhinoVault.

For the construction they say “We are trying to develop a kit of parts which is as lightweight as possible and which capitalize on local resources” (« A’A » 2016). That is also what we are trying to contribute to with this master thesis work. The idea is that the complexity of the shape is embedded in the falsework such as unskilled labours could construct the shell. In our case we want that the shell form is the equilibrium state of the bending active gridshell so that the falsework finds itself the correct shape.

The same goal for the falsework and the fact the shell is constructed with the tile-vaulting Catalan technique makes this drone port a very relevant case study for our work. Figure 60 shows the drone port under construction for the 15<sup>th</sup> architecture Biennale in Venice. We see that the guidework is held by a dense scaffold that also serves for the masons to stand on during construction. We also see that the construction of the vault starts by erecting the four boundary arches which need a temporary formwork.



Figure 60 : Construction of the drone port in Venice, 2016<sup>16</sup>

---

<sup>16</sup> Image from : (« A’A » 2016)

Philippe Block kindly shared with us the 3D Rhino model of the drone port (Figure 61). The shell occupies an area of 10m\*8m and is 5.5m high. We observe that it presents synclastic and anticlastic double curvatures making it a more complex shell than the one of chapter 6.

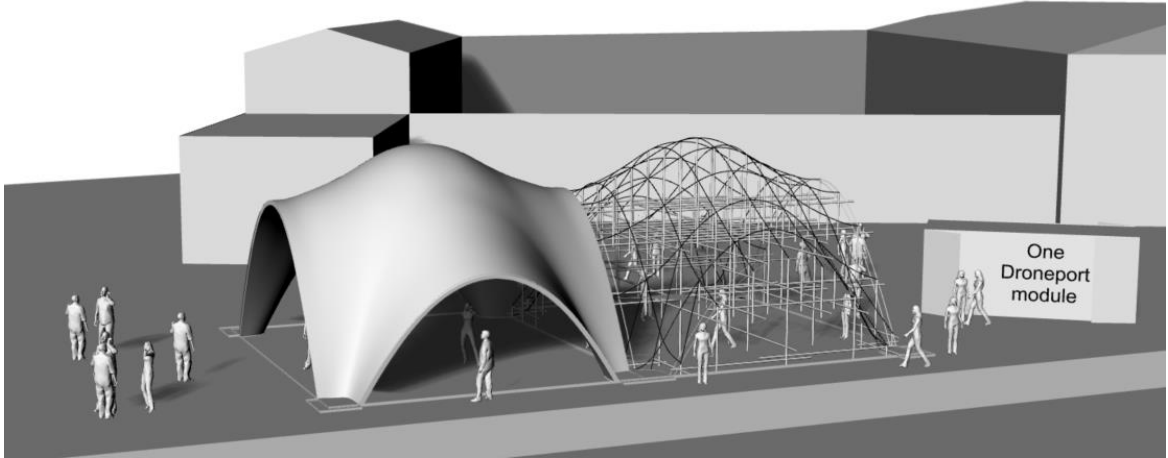


Figure 61 : Rhino model of the drone port shell and of its falsework (given by Philippe Block)

### 7.2 Choice of the target falsework

We have the project to build a physical model of the falsework. We chose to focus on a smaller version at a scale of 50%. This is more manageable for a first experiment, but still stays at an architectural scale. Figure 62 shows a top view and elevation of the target guidework and dimensions. Figure 63 shows a perspective render of the target falsework.

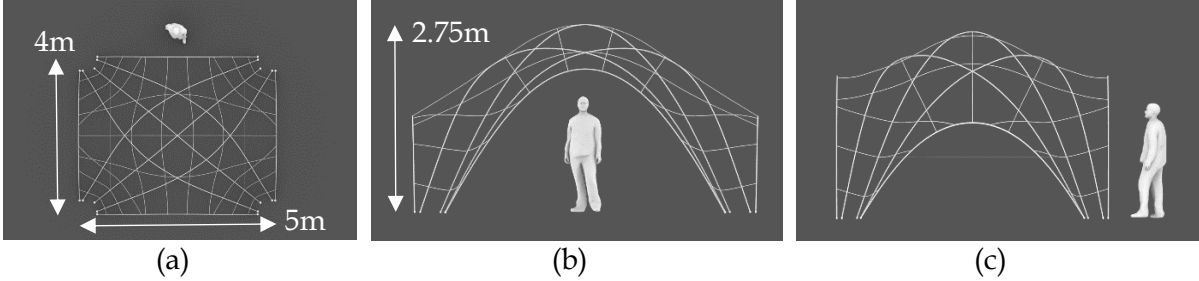


Figure 62 : target false work (a) top view, (b) front elevation, (c) side elevation

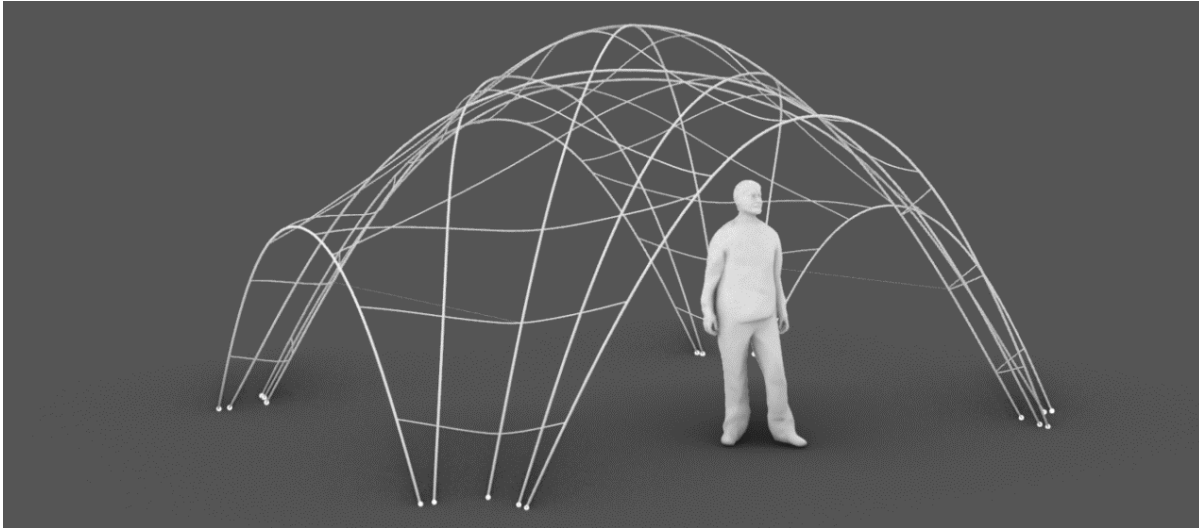


Figure 63 : perspective render of the target scaled 50% falsework

To find a suitable guidework we perform a manual feedback by adjusting the rods position, number and diameter. This feedback considers the deviation from the bending behaviour of the rods but also the displacement when working under brick load for the erection of the boundary arches. From this feedback, two different diameters are used for the rods.

We begin with a primary layer of rods of 15mm diameter : four rods make the four boundary arches, and 6 rods describe the diagonal (green rods in Figure 64). These rods carry the load of the falsework, and their end points are anchored by hinged connections to the ground (red points in Figure 64). The 15mm diameter is also chosen so that the boundary rods can sustain, with little displacement, the load of the bricks during the construction of the boundary arches, from which the rest of the shell is then build by making the tiles cantilever.

The secondary layer is made of rods of 8mm diameter. They enable to adjust the shape of the principal layer rods in order that the equilibrium shape of the gridshell describes the compression target shape. They are also chosen, like for the previous simple shell (section 6.2.3), with a “gut feeling” of the density of the rods, high enough to have an accurate description of the compression shell by the guidework, but also low enough to have sufficient space between the rods for the mason to be able to lay bricks easily from beneath. This depends on the experience of the mason and the change in curvature.

We also chose to have maximum 3 rods crossing in a same node to avoid complex nodes and stay accurate in the description of the shell. (We will already have 1\*15mm +2\*8mm = 31mm of thickness for the gridshell at the location of the nodes where one rod of 15mm rod and two rods of 8mm cross). Finally 2 adjusting steel cables of 1mm diameter will be used. The summary of the material properties is show in Table 10.

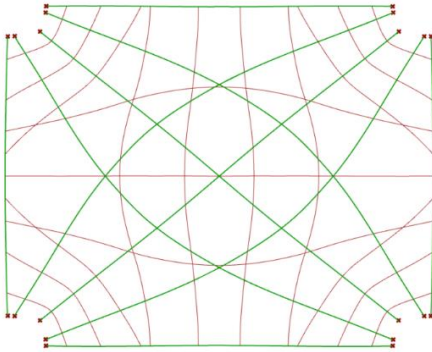


Figure 64 : Rod groups :  
 (green) Primary rods : 15mm diameter rods  
 (red) Secondary rods : 8mm diameter rods  
 (red points) anchors

	<b>Rods</b>	<b>Cables</b>
<b>Material</b>	GFRP	SteelS355
<b>Young’s modulus : E (MPa)</b>	40000	210000
<b>Yield strength : fy (MPa)</b>	900	355
<b>Density : rho (kg/m3)</b>	2100	7850
<b>Diameter (mm)</b>	15 and 8	1

Table 10 : material and geometrical properties

### 7.3 Deviation of the bending active guidework

The modelling to the rods with K2E is done the same way as for the simple shell (see sections 6.3 and 5.3.1). And the general overview of the grasshopper code with K2E for the case of the modelling of the drone-part falsework was presented in section 5.3.3. In all simulations the self-weight of the rods and cables are taken into account like in section 6.4 .

First we look at the deviation of the principal layer rods (the 15mm rods) alone. Figure 65 shows a large displacement of 70.8mm on the two boundary rods of the larger arches. This is due because the equilibrium shape of the bended rod that is the elastica curve does not correspond to the compression arch.

At first sight we could imagine that it is because the ratio  $f/L$  is here of 0.51 and larger than 0.3, and thus the elastica shape can no more approximate well a catenary shape as we saw in section 5.2.2. However it is not that because Figure 66 shows that the boundary arch is not exactly a catenary shape, which is maybe because the TNA in 3D allows for more freedom of shape, or the thickness of the arches is enough for the catenary thrust to be kept in the masonry.

Anyway, we have two options to adjust the shape of the boundary rod to fit the boundary of the shell. We could use “adjusting stiffening cables” like in Figure 32. Or we can adjust the shape by adequately choosing the number, position, and diameter of the rods of the secondary layer. The second option is preferred.

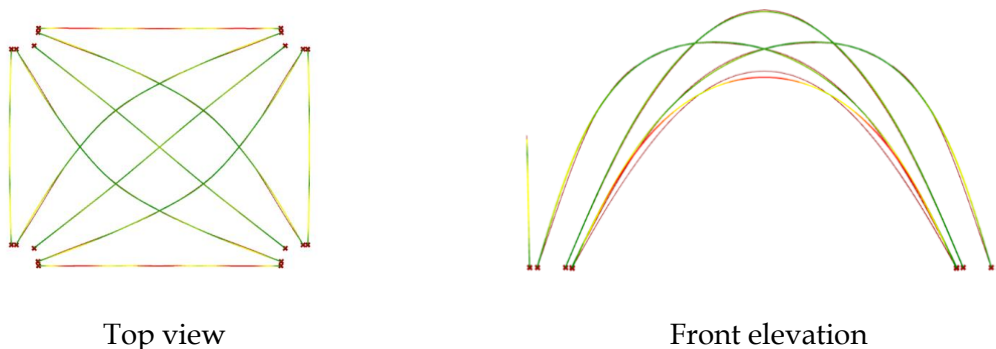


Figure 65 : Deviation of principal rods alone  
colour legend : (rods : green to red = 0 to max deviation)

Maximum deviation	70.8 mm
Maximum Z-axis deviation	-65.5 mm
Max stress rods	233.6 MPa
Max moment in rods	0.1 kN.m

Table 11 : Numerical results of Figure 65

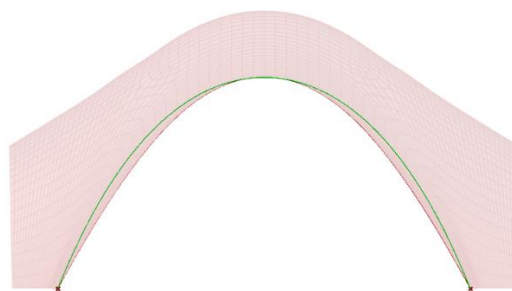
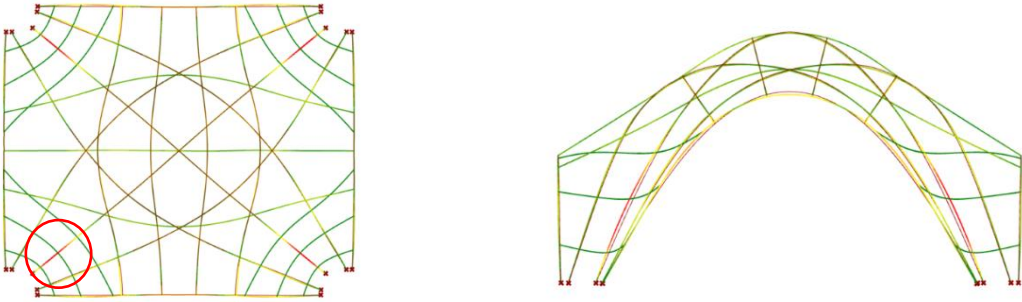


Figure 66 : (green) Catenary curve, (red) Compression shell



Thus, the secondary layer of rods is chosen from a manual feedback loop. The more influential rods of the secondary layer, on the shape of the boundary rods of the primary layer, are the 4 groups of 3 rods in the legs of the gridshell. These rods tend to narrow the boundary arches by “pushing in” the sides of the boundary rods. They also “push out” the diagonal rods. This can be observed on Figure 67 : the boundary rods now correctly approximate the target boundaries, however the legs of the gridshell present a deviation of 51.8 mm (red circle in Figure 67) because of the bending stiffness of the added rods of the secondary layer that want to be straight.



Top view

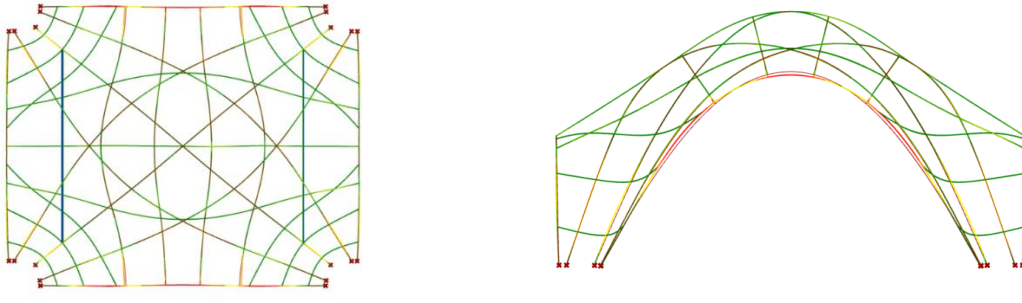
Front elevation

Figure 67 : Deviation of the gridshell (without extra cables)  
 colour legend : (rods : green to red = 0 to max deviation)

Maximum deviation	51.8 mm
Maximum Z-axis deviation	-31.6 mm
Max stress rods	366.4 MPa
Max moment in rods	0.1 kN.m

Table 12 : Numerical results of Figure 67

To prevent the deviation in the legs, two cables are added. Figure 68 shows that it works, and no significant deviation is observed in the legs. The remaining deviation of 36.4 mm is located on the boundary rods. It is an acceptable deviation compared to the thickness of the shell.



Top view

Front elevation

Figure 68 : Deviation of the gridshell with 2 extra cables  
 colour legend : (rods : green to red = 0 to max deviation) (cables : bleu = tension, green = neutral)

Maximum deviation	36.4 mm
Maximum Z-axis deviation	-36.1 mm
Max stress rods	395.4 MPa
Max moment in rods	0.1 kN.m
Max stress in cables	156 MPa
Max force in cables	0.1 kN

Table 13 : Numerical results of Figure 98

## 7.4 Modelling of the brick load

The construction of the compression shell starts by building the boundary arches. During their erection, these arches need to be temporary supported. Once they are finished they can stand by their own if their thrust line, which is a catenary (in case identical tiles are used), is kept within the thickness of the tiles. Otherwise, either some bending moments will appear and the tiles and mortar will need to take some tension, or the formwork needs to stay and we continue to build the rest of the shell until the 3D thrust can be taken by what is constructed of the shell. For us it is not a problem because the formwork is also the guidework and so will stay in place until the end of the construction.

First we could model the brick load as a constant linear load applied vertically. A tile of 280\*140\*15mm weights 1kg. If the tiles are laid on their long side then it leads to a linear load of 71N/m. This would lead at the load case of Figure 69.

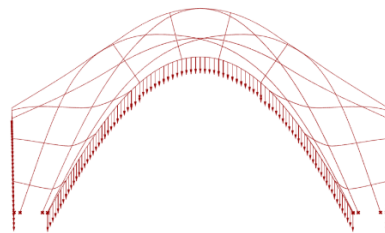


Figure 69 : Load of the bricks without considering that a part of the load is taken by the arch in construction

However, as shown on Figure 70, a part of the load of the brick is taken by the bricks below. We chose to take it into account and to use a “safety factor” of 1 in order that we do not overestimate the displacement due to the brick load. It is important so that when we do the feedback loop to choose the position, number and diameter of the rods, we do not overcompensate the displacement by an opposite “pre-deviation”. Thus when doing the choice of the geodesic lines for the guidework and running the simulation we try to estimate the real load. Then in a second time, we will apply a safety factor of 3 on the falsework to check if the displacement stays correct in that case also.

So, because the arch in construction takes part of the load, the applied brick load to the boundary rod is actually perpendicular to the rod and has a lower value. To recalculate the value of the load we chose to divide half of a boundary arch in 4 load cases shown in Figure 71. The inclination angles of the segments enables to calculate the projection load  $F_n$  from  $F$ ,

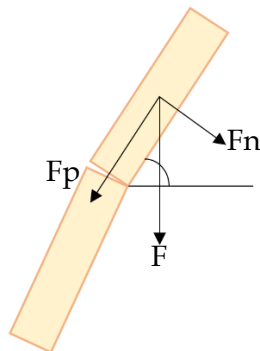


Figure 70 : repartition of the load of the brick  
 $F$  : load of the brick  
 $F_p$  : load on the brick below  
 $F_n$  : load on the gridshell

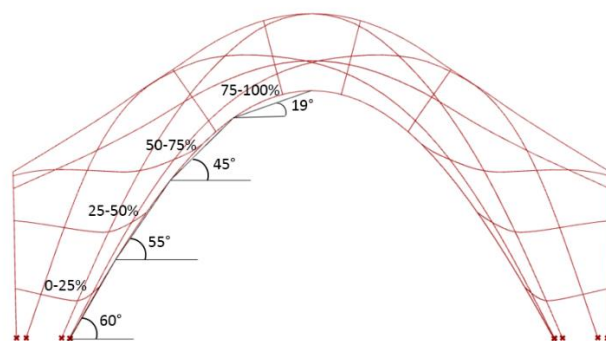


Figure 71 : Approximation of half the boundary arch in 4 segments to define 4 load cases “ $F_n$ ” from 4 inclination angles of the segments.

that is applied on the gridshell. Then the load are applied incrementally, and symmetrically on each side of the rod, by adding each time a load case.

The load case 100% that considers the 4 load segments is shown in Figure 72. We observe that the loads are well oriented perpendicularly to the boundary rod and that the magnitude of the vector increases in 4 steps. The small “gaps” observed in the loading are actually the superposition of 2 adjacent half load, because the corresponding segment of the polyline, at the border of the load cases zones, has a load distributed between these two. Finally we can observe a small variation in the magnitude of the vectors for a same load case zone. This is due to the segments of the polyline being not exactly equal in length (but the impact on the results it is negligible). A summary of the values of the brick loads applied is give in Table 14.

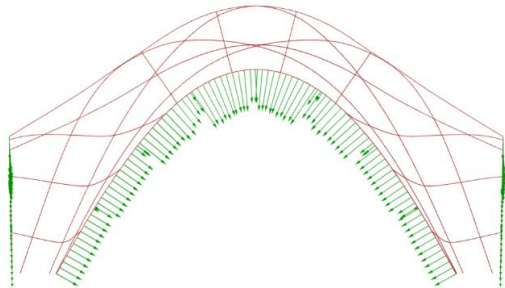


Figure 72 : Final modelling of the brick load on the falsework

Portion of the half boundary rod	Inclination angle (°)	Brick load on falsework (N/m), safety factor of 1	Brick load on falsework (N/m), safety factor of 3
0-25%	60	35.5	106.5
25-50%	55	40.7	122.1
50-75%	45	50.2	150.6
75-100%	19	67.1	201.3

Table 14 : A summary of the values of the brick loads

### 7.5 Displacement of the falsework under brick load

The figures of Table 15 show the displacement and deviation obtained when adding incrementally the load cases. This models the behaviour of the falsework when constructing the boundary arches. The numerical results are given in Table 16 and Table 17, and the maximum moment in rods and the maximum forces in cables are respectively of an order of 0.1kN.m and 0.1kN. The maximum stress in rods and cables is below the yield strength.

We observe in the first load cases that the displacement tends to reduce the deviation, making the overall falsework more accurate. This is because the portion of the arc under construction pushes the sides of the rod towards the inside. This is why it is interesting to design the falsework so that its initial deviation is opposite to the displacement, which is the case here. However, when the load is applied on the upper part of the boundary rod, we observe a re-increase of the total displacement plus deviation because that load tends to push outside the its sides which adds a displacement in the same direction as the deviation.

Finally, we observe that, in the case of no safety factor (sf = 1), the final loaded falsework describes even more accurately the target shape. In the case of a safety factor of 3, the final maximum displacement plus deviation is of 53.4mm which is also acceptable.

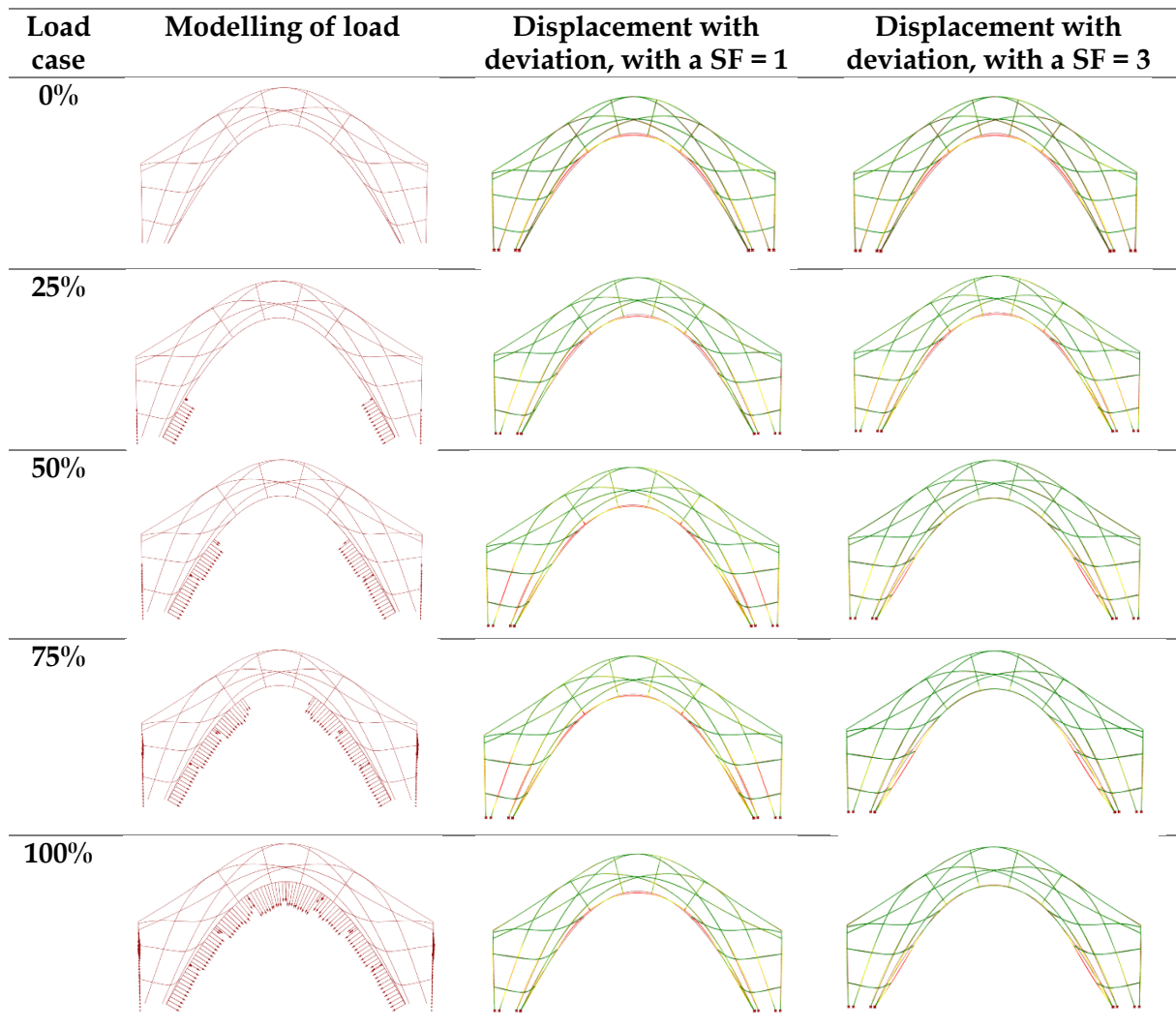


Table 15 : Displacement plus deviation during the construction of the boundary arches

Load case (SF=1)	Max displacement plus deviation (mm)	Max Z-axis displacement plus deviation (mm)	Max stress rods (MPa)	Max stress Cables (MPa)
0%	36.4	-36.1	395.4	156
25%	34.2	-34	392.5	157.3
50%	27.7	-27.6	387.7	160.4
75%	23.5	-22.3	387.1	163.2
100%	29.7	-29.6	390.4	160.7

Table 16 : Displacement and stress values for a step by step brick loading, Safety factor = 1

Load case (SF=3)	Max displacement plus deviation (mm)	Max Z-axis displacement plus deviation (mm)	Max stress rods (MPa)	Max stress Cables (MPa)
0%	36.4	-36.1	395.4	156
25%	30	-29.8	386.7	159.7
50%	50.9	-25.5	369	168.5
75%	69.4	-35.3	363.5	176.4
100%	53.4	-27	373.7	172.8

Table 17 : Displacement and stress values for a step by step brick loading, Safety factor = 3

## 8 Construction of a physical model of the falsework for the scaled drone port

From previous chapter, the numerical simulations show that the designed bending active gridshell succeeds to describe accurately enough the target shell to serve as a guidework but also to sustain the brick load during the erection of the boundary arches.

In this chapter we investigate how we can build in reality this falsework in a low tech way.

### 8.1 Interview of a master mason : Carlos Martin

On Monday 8 February (2021) we had the chance to meet in videocall with Carlos Martin who is an experienced mason. He has in particular participated to build the drone-port of the Venice Biennale. Some of the insights of the discussions are summarised here.

First, some parts of the vault need a temporary support that can bear some load. For example for the construction of the drone-port four supporting arches were used to build the boundary arches with the tile. The rest of the structures only required a guidework made of a grid of quads of 1x1m<sup>2</sup>.

The density of the guidework can be a tricky part because it depends on the experience of the mason. High experienced mason working on a simple barrel vault or dome may not even need any guidework and a low density one for more complex shapes, whereas low experienced masons will need a dense one. However the guidework needs to be not too dense in order not to annoy the mason when lying the tiles when he works from a scaffold under the structure.

According to Carlos Martin his biggest challenge when construction tile-vaults is getting the good materials i.e. having adapted tiles and a gypsum mortar that hardens not too fast nor too slow. Also the bounding direction of the tile layers is very important. A common mistake is that joints overlap between the different layers of tiles which can cause weak points. Thus a good practice tip is to start constructing the second layer in a perpendicular direction of the first one and to cut the first tiles at one third in order that a joint of one layer will always be next to a tile of another layer. For example he confessed the initial tiling of the drone-port wasn't correct and he had to change it.

Carlos Martin also explained that when constructing a tile-vault, he would operate in a symmetrical way from each support. Finally, Carlos Martin pointed the importance of building first good foundations that can also take the horizontal component of the thrust generated by the vault.



Figure 73 : Carlos Martin working on the Droneport, (« A'A » 2016)



## 8.2 Rods

We contacted the company VINK<sup>17</sup> to order the rods. The material properties of the GFRP rods of VINK are given in Table 18. We can compare those values to the one we used for the simulation, given in Table 10. The flexural modulus we used was 40 GPa, which is sufficiently close the one of VINK which is 41.2 GPa. The density we used for the self-weight was 2100kg/m<sup>3</sup> which is consistent with the value of VINK. Finally, we considered a tensile strength of 900 MPa whereas VINK gives a value of 687.5 MPa, but which is not a problem because the maximum stress in the rods we got from the simulations is 395.4 MPa (Table 16 and Table 17). Thus we are confident that our numerical simulations are still valid to model correctly the structural behaviour of VINK's rods.

Property (coupon values)	ASTM Test	Units	Test Results
<b>Mechanical</b>			
Tensile Strength (LW)	D638	MPa	687.5
Tensile Modulus (LW)	D638	GPa	41.2
Compressive Strength (LW)	D695	MPa	412.5
Flexural Strength (LW)	D790	MPa	687.5
Flexural Modulus (LW)	D790	GPa	41.2
Notched Izod Impact (LW)	D256	J/m	2,135
<b>Physical</b>			
Barcol Hardness	D2583		50
Water Absorption	D570	% Max	0.25
Density	D792	Mg/m <sup>3</sup>	2.01-2.10
Coefficient of Thermal Expansion (LW)	D696	10 <sup>-6</sup> K <sup>-1</sup>	5.5

Table 18 : material properties of the GFRP rods of VINK

The maximum rod length they could have for us was 6m. The length of the rods of the falsework of chapter 7 are given in Table 19. We see that some of the rods are too long : the 6 diagonal rods of the principal layer (15 mm diameter rods) and the 2 boundary rods of the larger side. However we observe that these later ones are only 4 cm too long (604cm rods). Thus we chose to reduce slightly the scale of the falsework, from 49.45%<sup>18</sup> in chapter 7 to 49.10% for the physical model, in order to limit the size of the boundary rods to 6m, to be able to have them in one piece. The length changes are summarized in Table 19.

**Remark** : The behaviour of a compression only structures is based on its geometry for static equilibrium. Material properties are not taken into account in the TNA of RhinoVault for example. Thus we can here (and we could in chapter 7) reduce the scale of the drone-port shell without expecting structural problems. However for the bending active gridshell this is not true because its form depends on the material properties and cross sections of the rods. Thus the previous numerical results are in theory not scalable (the equilibrium shape is governed by non-linear equation)<sup>19</sup>. Nevertheless we do a very minor change in the scale (-0.35%) and thus we still have confidence that the falsework form will accurately describe the compression shape with admissible deviation.

<sup>17</sup> <https://www.vink.be/>

<sup>18</sup> A scale of 49.45% was done to have rods of 8m length maximum, but actually only 6m max length were in stock when we wanted to order.

<sup>19</sup> For more information about scalability we invite to read Annexe : 10.2.

	In the simulations of chapter 7			For the physical model		
	Rods (cm)	number	diameter (mm)	Rods (cm)	number	diameter (mm)
<b>Diagonal layers</b>	241	4	8	239	4	8
	165	4	8	164	4	8
	104	4	8	103	4	8
	800	4	15	794	4	15
	798	2	15	792	2	15
<b>V direction layer</b>	604	2	15	600	2	15
	559	2	8	555	2	8
	573	1	8	569	1	8
<b>U direction layer</b>	447	2	15	444	2	15
	420	4	8	417	4	8

Table 19 : Rod length used in chapter 7, and rod lengths used for the physical model, in red the rods that are too long to be in one piece

Figure 74 shows for the physical model the length and diameter of each rod. We also note that the new dimension of the gridshell are : 4.97m x 3.93m, and 2.70m height. Figure 75 shows a photo of all rods used for the construction.

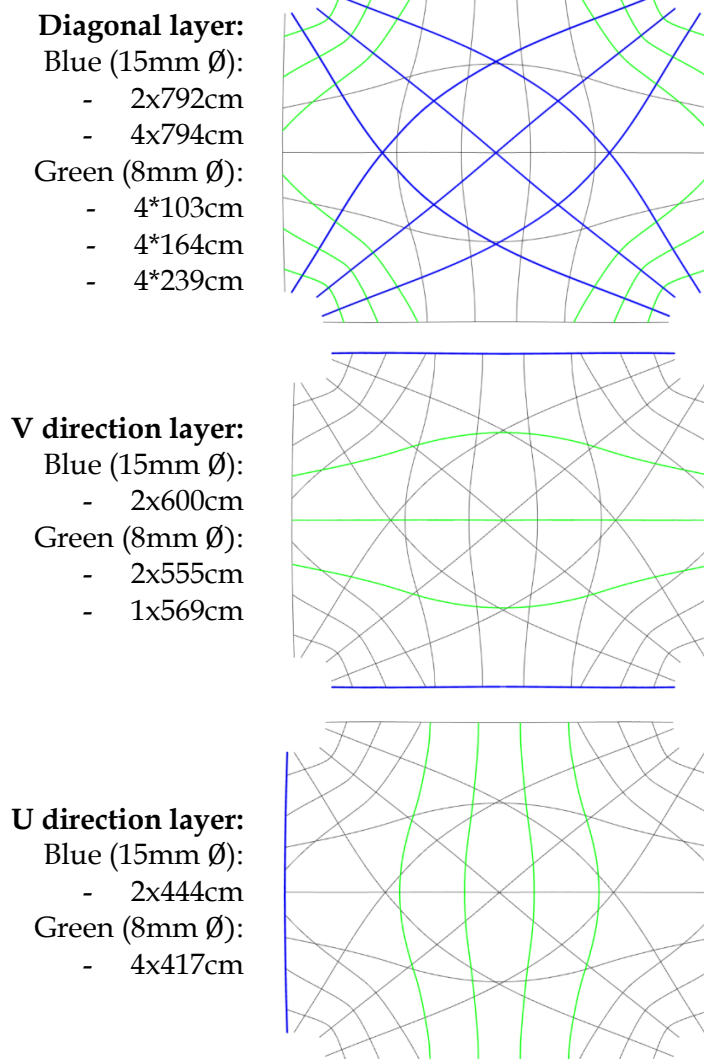


Figure 74 : Physical model rods lengths and diameter



Figure 75 : All rods used for the construction

The rods exceeding 6m length need to be constructed from 2 smaller rods. This concerns the six diagonal rods in blue of Figure 74. The two central ones are constructed each from two rods of 396cm and the four other one each from two rods of 397cm. The two rods are attached together with a steel tube. Figure 76 shows a schematic section of the connection. The rods are inserted in the tube, then two M4 bolts enable to fix each rod in the tube. Figure 77 shows photos of the realized connection.

Having this connection is important because it enables to create larger gridshells without being limited by the length of the available rods. For example it would be necessary for nearly all the rods if we would want to construct a falsework of the full scale drone port shell.

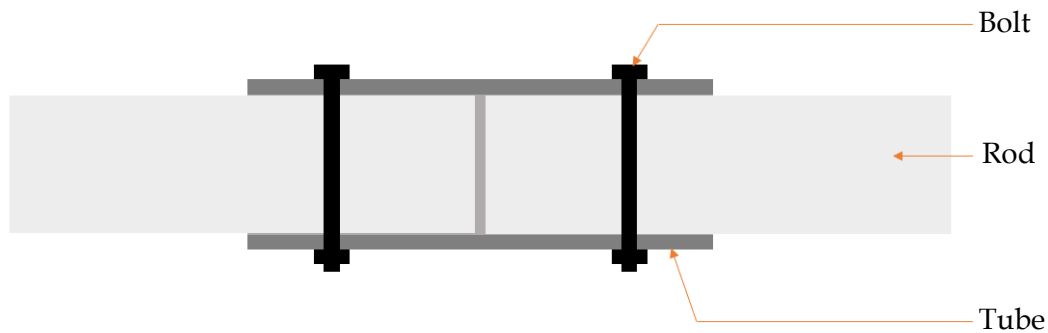


Figure 76 : schematic section of the construction of the longer rods with a connecting tube

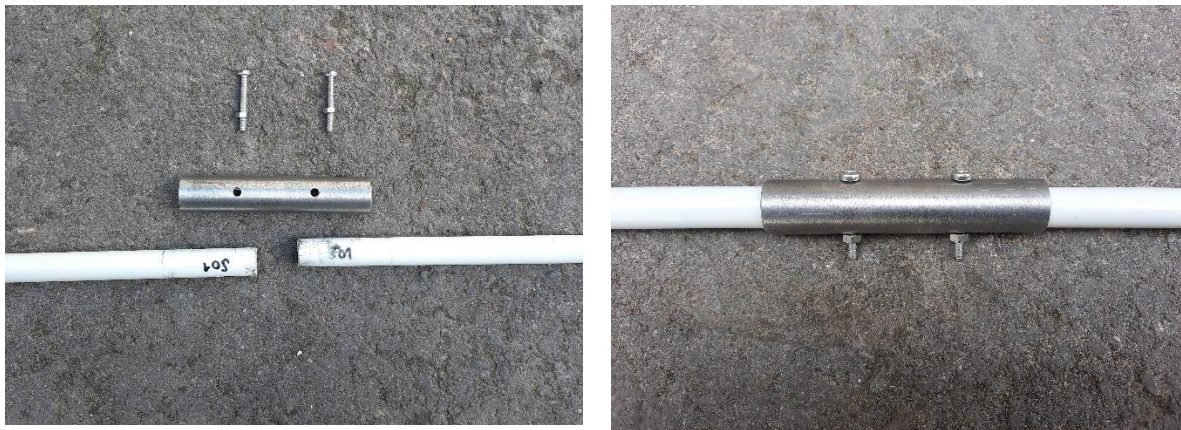


Figure 77 : photos of the tube connection for the fabrication of the longer rods

### 8.3 Investigation about nodes

The position of the nodes for each rod is indicated precisely in Annex 11.

Here we investigate how to connect the rods together with a low-tech and low cost solution. First there are the classic plastic connectors (Figure 78). The orthogonal connector would not be suitable for use and we would need to use the variable angle one. However it is not very low tech and it takes a lot of space.

Second there is the steel ring possibility (Figure 79). It is low price and can be used when three layers cross as shown on the assembly node example from Figure 79. This solution also suits well larger project and is used for example in the “cathédrale-éphémère”<sup>20</sup> project.

Third, a low tech possibility is to use plastic from bottles and rubber from old bike air chambers. The plastic has the advantage to shrink when heated and the rubber prevents sliding. Julien Toussaint shows that by following traditional lacing techniques with plastic and using rubber to increase the grip, he manages to obtain a perpendicular assembly 13 times more resistant to slipping than an assembly by sisal cord (Toussaint, s. d.). The solution is low tech, cheap and easy to perform, however because we need to dismantle the falsework we prefer to search for a reversible connection.

We initially chose to use the idea of the rubber to prevent sliding, and we chose to connect the rods with two reusable tie-wraps. It is low tech and cheap. It is also an easy and rapid method, that is reversible for dismantling. Finally, the total node is also thin, which is important so that we do not add inaccuracies in the guidework. Figure 81 shows a drawing of the node connection.



Foot connector

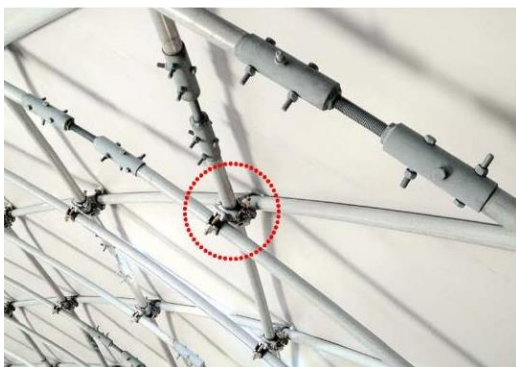


Orthogonal connector



Variable angle connector

Figure 78 : Plastic connectors<sup>21</sup>



Assembly node<sup>22</sup>



Steel ring<sup>23</sup>

Figure 79 : connector with steel ring

<sup>20</sup> “Cathédrale-éphémère”, Créteil 2013, Laboratoire Navier, architect : Tom Gray, engineer : TESS

<sup>21</sup> <https://www.carbonetube.net/produit.php?cat=RACCP>

<sup>22</sup> <https://www.tess.fr/projet/cathedrale-ephemere#>

<sup>23</sup> <https://gigatek.be/fr/obo-betterman-collier-d-ecartement-pour-cables-et-tubes--obo1360205>



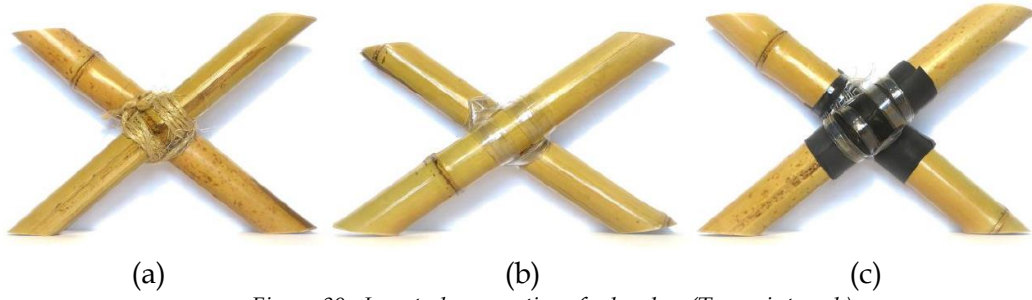


Figure 80 : Low-tech connections for bamboo (Toussaint, s. d.)  
 (a) Node with rope, (b) node with plastic from bottle, (c) node with plastic from bottle and rubber from old air chamber

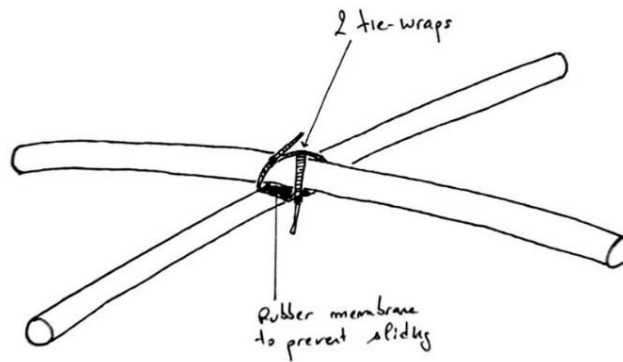


Figure 81 : Chosen connection solution with reusable tie-wraps and rubber membrane.

For the physical model, instead of using rubber, we used non-slip adhesive tape, that is easy to install on the rods and cheap. The grains makes it very resistant to slip. Also classic tie-wraps have been used. Figure 82 shows images of the nodes realized.



Figure 82 : Photo of the nodes realized, (a) Crossing node, (b) Boundary node



The rods of 8mm diameter were cut 1cm longer at each side to prevent them slipping off. However this was not sufficient for some of the boundary nodes. To solve the problem we added a bolt at the end that acts as an anchor with the tie-wraps and prevents the node to slip. This is illustrated on Figure 83.

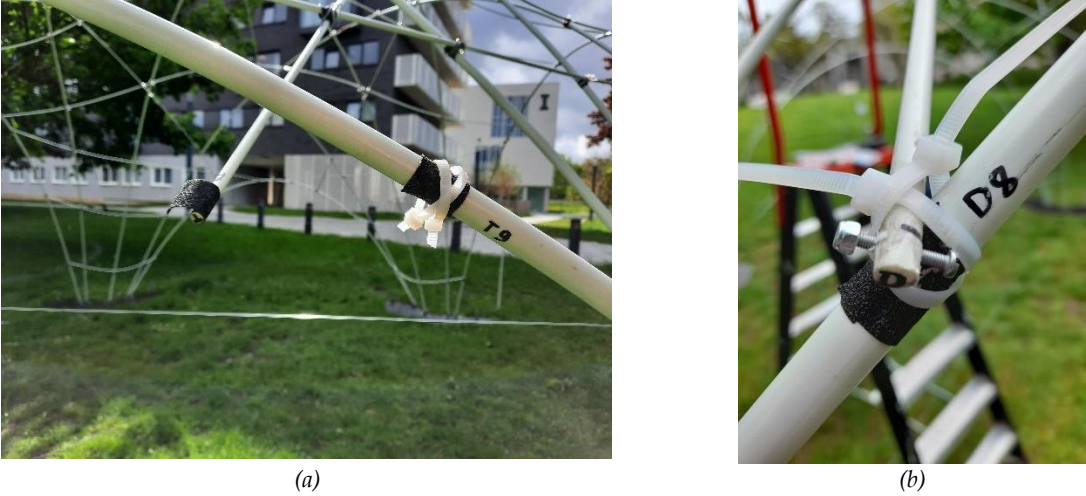
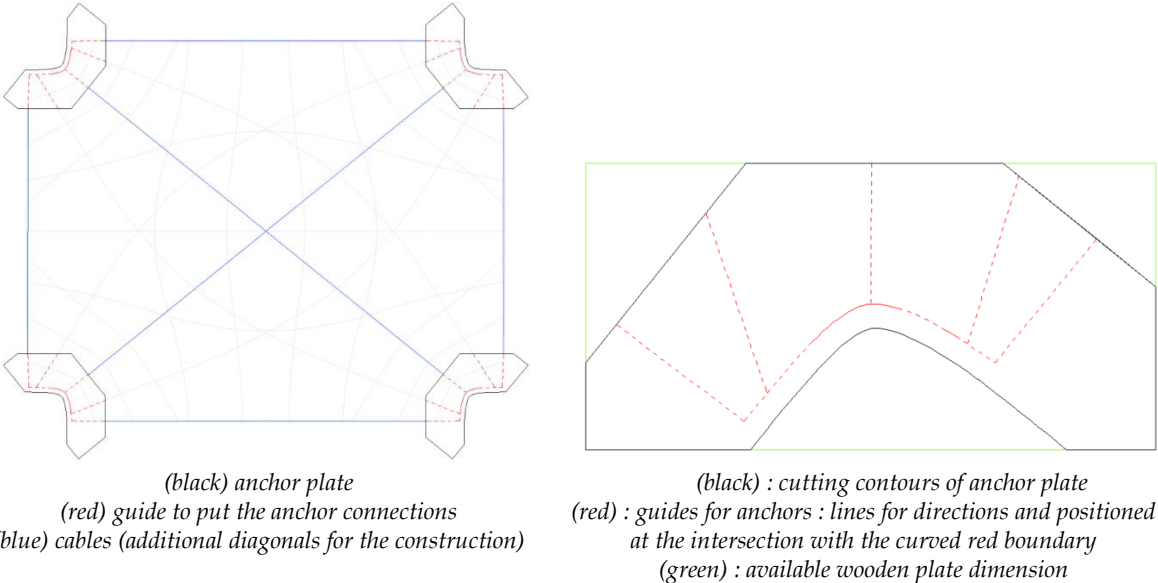


Figure 83 : (a) Slipping of the boundary nodes, (b) Addition of a bolt to act as an anchor

### 8.4 Anchors

The 15mm rods are fixed to wooden plates. These anchoring plates are cut from available planks of 62.5 cm x 125 cm as shown in green on Figure 84. Guiding lines are drawn (in red) to help positioning the rod anchors. The exterior boundary of these plate follow the curve of the legs of the shell. This is because the bricks would need to be placed on a foundation on the ground and not on the plate. The interior boundaries of these plates are perpendicular to the cables. The cables (blue) serve to take the horizontal thrust of the resulting force in the plates. The two diagonal cables have been added to take the horizontal thrust during the construction phase, because we plan to start putting in place the diagonal rods first. These diagonal rods are placed first in order that the structure can stand by itself during the construction.



(black) anchor plate  
 (red) guide to put the anchor connections  
 (blue) cables (additional diagonals for the construction)

(black) : cutting contours of anchor plate  
 (red) : guides for anchors : lines for directions and positioned at the intersection with the curved red boundary  
 (green) : available wooden plate dimension

Figure 84 : design of anchor plates

The reaction forces in the plates are given in Figure 85. Available cables of 2mm diameters have been used, which have enough strength, and negligible strain for the resulting horizontal component (over dimensioned).

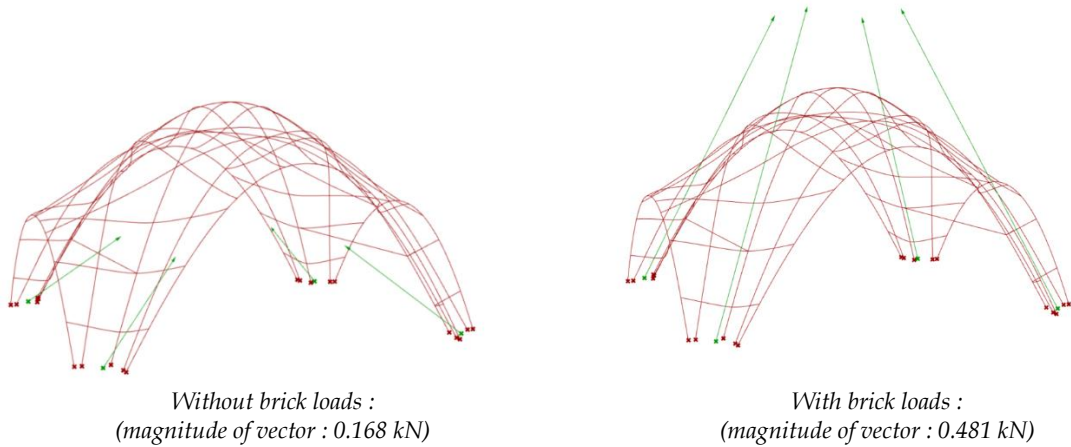


Figure 85 : Reaction forces in the anchoring plates

Actually, to prevent the gridshell to be moved under wind or by people, we chose to fix the base plates to the ground with available big “tent-pegs” at the laboratory. This makes the cables in reality not needed to take the horizontal forces, because the anchors are strong enough. However the hole for the anchors is large and the cables enable to be more precise. Also, the cables still make the process of positioning correctly the plates at the start a lot easier (Figure 86).

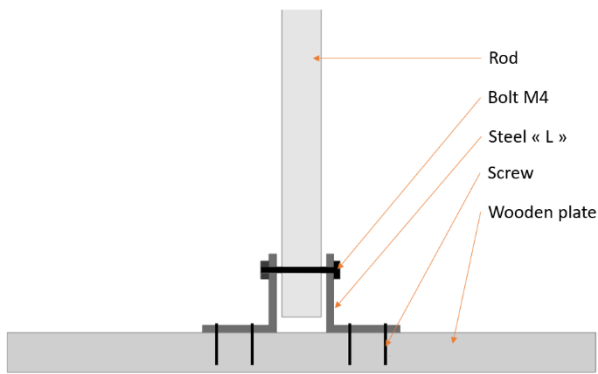


Figure 86 : Positioning then anchoring of the plates

The rods are attached to the wooden plates by hinge connections each made of two steel angles in “L” shape screwed to the plate, and a bolt passing through the rod (Figure 87). Because we create a hole of 4mm in the rod to pass the bolt we check that the rod at that location is still resistant enough. Thus we loaded the bolt passing through the rod incrementally up to 47 kg (0,47kN), which is the maximum load we could put with our loading system, as shown in Figure 88. The rod did not break for perpendicular nor parallel loading to its fibers. This compared to the maximum load of 0,12kN expected on a rod anchor enables us to conclude that this anchoring system is strong enough for our application.

The final entire anchoring system is show in Figure 89.





(a)



(b)

Figure 87 : Rod anchors, (a) Schematic section, (b) Photo



(a)



(b)

Figure 88 : testing of the resistance of the rod at its anchoring location

(a) loading perpendicular to fibers (0,47 kN)

(b) loading parallel to fibers (0,47 kN)



Figure 89 : Final anchoring of the gridshell

## 8.5 Construction steps of the gridshell

To construct the gridshell started by the positioning of the base plates as discussed above. Then the rods are placed starting by the diagonal rods of 15mm diameter. The images of Figure 91 show the different steps of the placing of the rods. These steps are ordered such as the structure can stand by itself during the construction.

First the two middle diagonal rods are anchored and attached together. Then the diagonal layer of the rod placed below is completed. After this the other layer of diagonal rods is placed above and attached. This enables that the rods of a same direction are in a same layer for the crossing, and avoiding “weaving” between rods.

Secondly the four rods of 8mm diameter of the U direction layer (going from the front to the back of the gridshell) are fixed above the diagonal layer. Then the two boundary rods of the V layer are anchored, i.e. the boundaries of the larger opening (front and back). These boundaries are attached to the extremities of the rods of the U direction layer so they can stand by themselves. Then the same process is done for the 8mm rods of the V layer that are placed above the gridshell, and the side boundaries (of the U layer) are anchors and attached the the V layer rods.

Finally, the diagonal rods of 8mm diameter of the legs are attached to give the curvature of these legs. The stiffening cables, here 1mm diameter steel wire, are also attached to help creating the legs curvature.

Figure 90 shows a photo of the gridshell, and Figure 92 front, side, and top views.



Figure 90 : Photo of the gridshell





(a)



(b)



(c)



(d)



(e)



(f)

*Figure 91 : Construction steps of the gridshell*

- (a) First two diagonal rods so that the structure stands by itself during construction*
- (b) Completion of the first layer of diagonal rods attached from below the other diagonal*
- (c) Completion of the second layer of diagonal rods attached above the other diagonal layer*
- (d) Placing the 8mm diameter rods of the U layer above the diagonal rods, then attaching the boundary rods of the V layer.*
- (e) Addition of the stiffening cables*
- (f) Finished gridshell and construction team (from left to right : Maryllis, Léopold, Arnaud, Aurélie)*

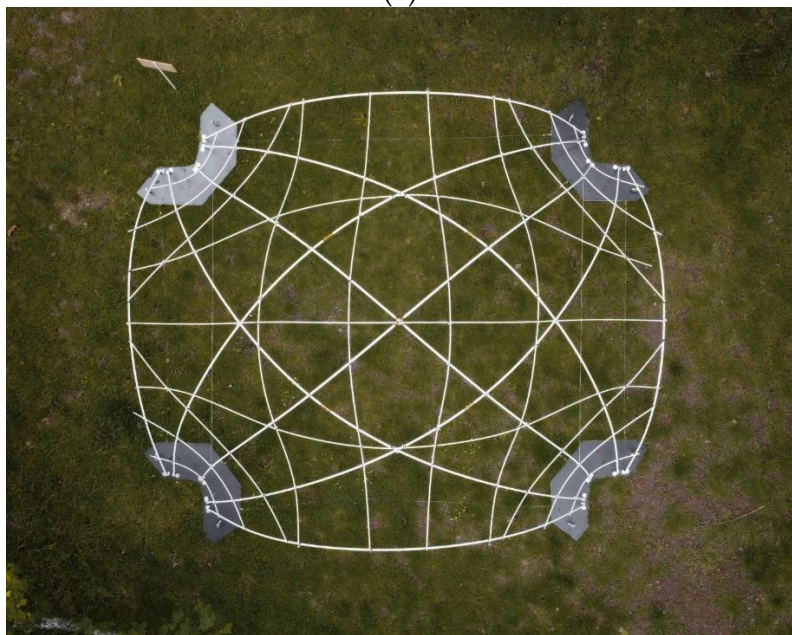




(a)



(b)



(c)

Figure 92 : Views of the gridshell (a) front, (b) side, (c) top.

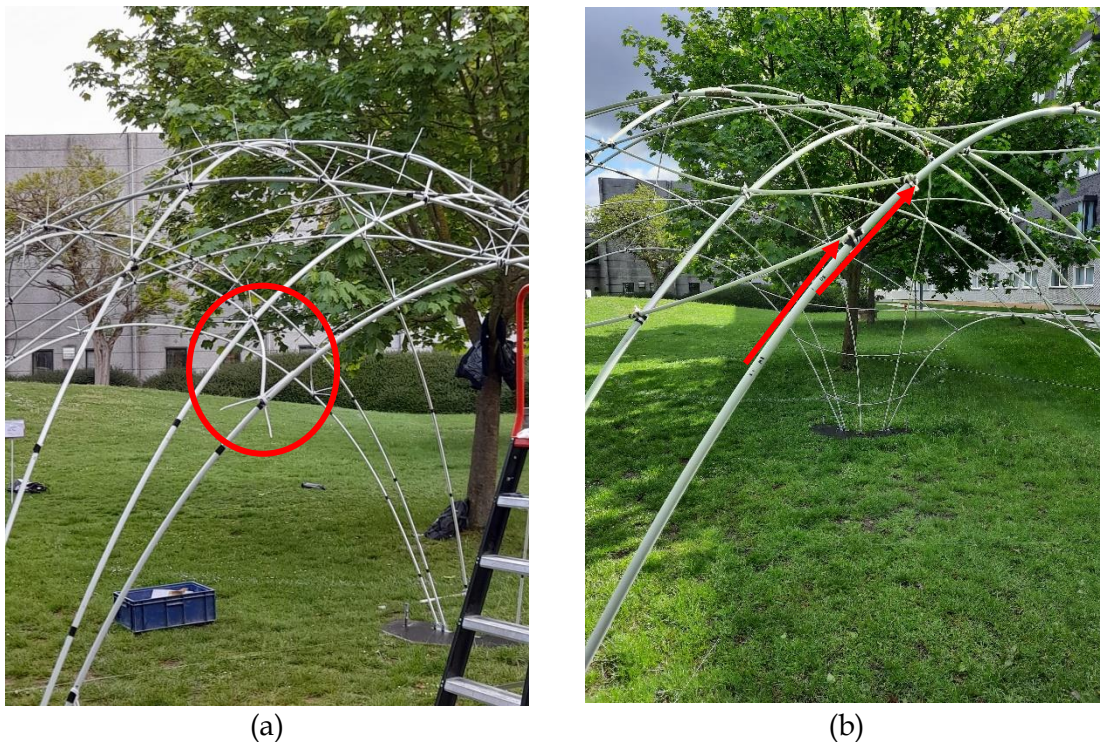


## 8.6 Construction issues, and feedback

We noted two construction issues during the building of this gridshell.

First, the 8mm diameter rods of the legs exceed over the boundary rods. This is because the legs are not as curved as in the theoretical model, thus making the secondary rods of the legs less bended, and so they exceed a little bit.

Secondly, we noted an inaccuracy in the node position indicated on the four boundary rods. On Figure 93 (a) we saw that the rod of the 8mm rod was too much bended compared to what was expected from the numerical model. This also made the rod pull hard on the node which was the source of the problem of the slipping of the boundary nodes stated in Figure 83. To solve during the construction, we chose to change the node position of the boundary rods to what felt right by looking at the numerical model pictures. The solution took onsite is shown on Figure 93 (b). Of course this solution is not precise and generated inaccuracies from the numerical model, but to make it work it was better than going for the seemingly wrong nodal position indicated on the boundary rods. Then we investigate on the reason of this error.



(a)

(b)

Figure 93 : Error in the node position of the boundary rods

(a) We see that the 8mm rod is too much bended compared to the numerical model

(b) Solution decide onsite to relocate the node position of the boundary rods.

The indication of the nodes on the boundary rods were correct to what was planned from Annex 11 Figure 117, thus the error does not come from a bad measurement during execution.

The thickness of the rods make them actually not be in the same “surface” as in the numerical model, but it would only create a small imprecision, and not the observed error.

The cause of the error on the node position indicated on the boundary rods, is in the grasshopper code, when passing from the numerical gridshell to the flat rods. The numerical calculations and results of the previous chapters are correct. The problem is when passing from the calculated gridshell, to its decomposition in straight rods.

To draw the straight rods, we draw lines of the same length of the bended rods, so the rods total lengths are correct. Only the node position needs to be changed.

The guilty component is the “Evaluate Curve”, that takes as input the a curve and a parameter “t” to evaluate the curve. The parameter “t” is from the local coordinate system of the curve but does not actually vary proportionally to the length of the curve ! Arturo Tedeschi write in Algorithm Aided Design : “It’s important to point out that t doesn’t measure distances. We can imagine t as the time a “particle” takes to go from t=0 to the instant position P(t). This time is affected by the position of control-points and, in particular, the motion of the particle slows down when it passes through a concentration of control points. For this reason t=0,5 is not the parameter that specifies the curve’s mid-point” (Tedeschi 2014).

Thus we changed this component by the combination of the components “length parameter” and “evaluate length”. The first one enables to have the length position of the node on the bended rod, and the second one to position de node on the equivalent straight rod depending on this length. The change in the grasshopper code is shown in Figure 94.

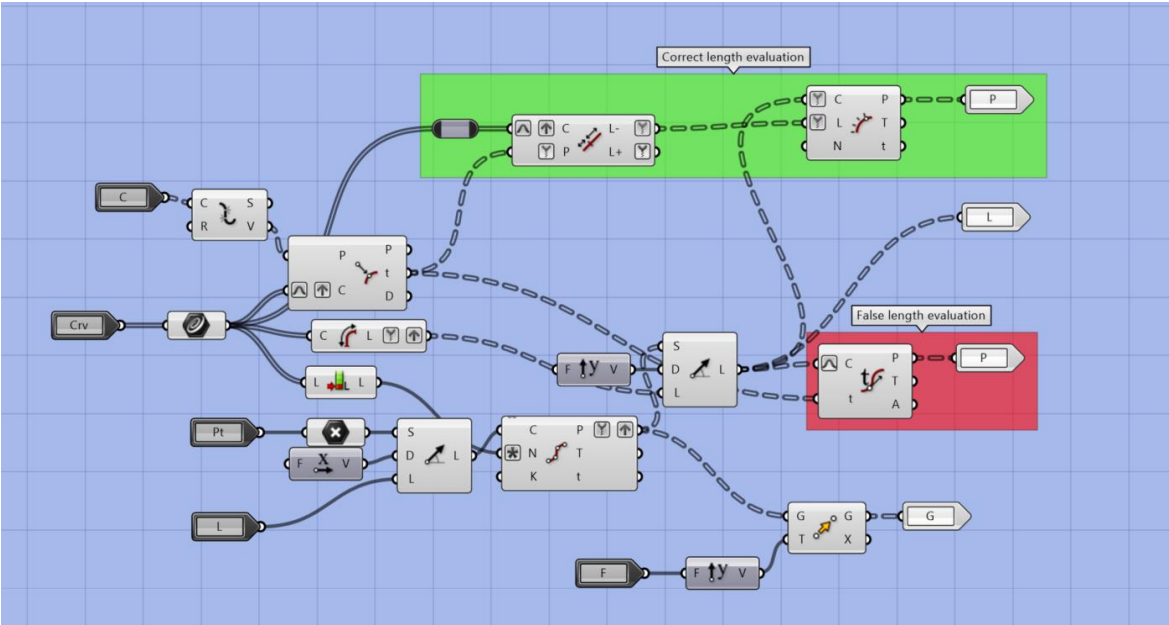


Figure 94 : Node position on the straight rods (red) with “Evaluate Curve”, which is a wrong way to proceed (green) with “length parameter” and “evaluate length”, which is the correct way to position the nodes

Figure 95 shows the difference in the resulting node position with the two methods. We observe that the results from the two methods are nearly identical (green and red nodes superimposed) except for four rods : the two of 600 cm, and the two of 444 cm length, which are the four boundary rods. For these boundary rods we see that the green and red nodes have significant differences which is why we observe this same error in the physical model.

Thus if we want to use the gridshell as a falsework for building a half-scale of the drone port in the future, we will need to dismantle the gridshell then indicate the new correct nodes positions before re-assembling it. The new corrected nodes positions are summarized in Figure 118 of Annex 11.

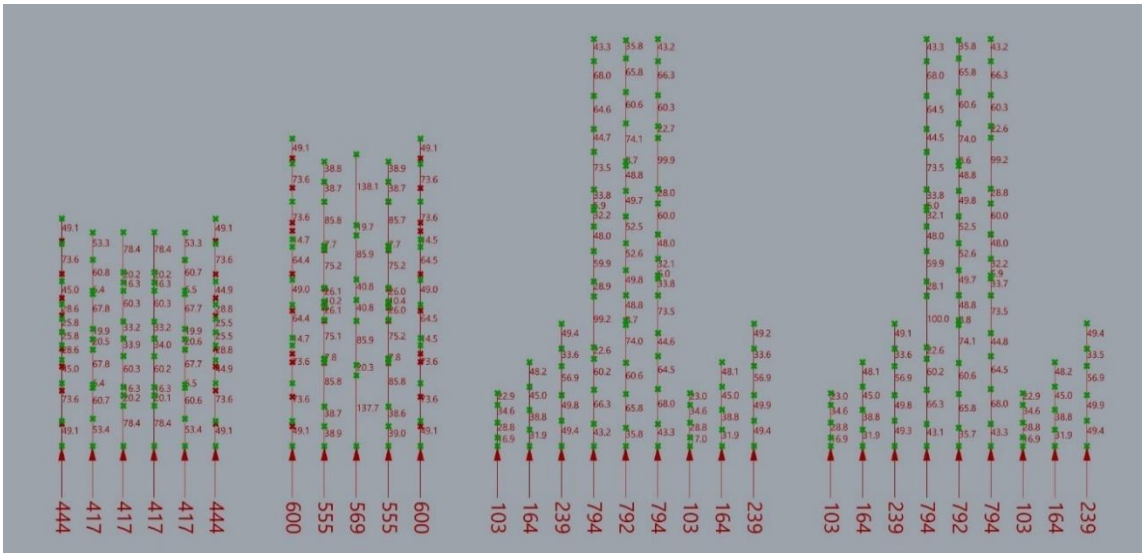


Figure 95 : Node positioning on the rods (cm)  
 (red points) Wrong way with "Evaluate curve" component  
 (green points) Correct way with "length parameter" and "evaluate length"

Finally, in Figure 96 we try to compare the obtained real gridshell to the numerical model. As a disclaimer we mention that the positioning of the camera over the gridshell is approximative which may already add some differences from the Rhino view. Nevertheless we see that the overall result is satisfying. We note that the onsite estimation of the nodes positions on the boundaries are generally quite good. Also we see that the anchors are well positioned. The main observed difference from the numerical gridshell seems to be the rods in the legs due to the difference in curvature.

From this gridshell construction we can conclude that the overall system is satisfactory and seems to approximate quite well the target shape. A deeper comparison could be made in the future with more precise measurement tools. Trying to build a real tile-vault with this gridshell (after the correction mentioned above) as a falsework could be done for pushing further this study. We also learned, from the feedback on issues on the construction, about good practice with Grasshopper, which enabled us to identify and solve the boundary node position problem, but which is also a precious insight for further designs with that software. Finally we conclude that the solutions proposed for the nodes, the anchors and the connections of rods to create a longer ones, are all three successful.

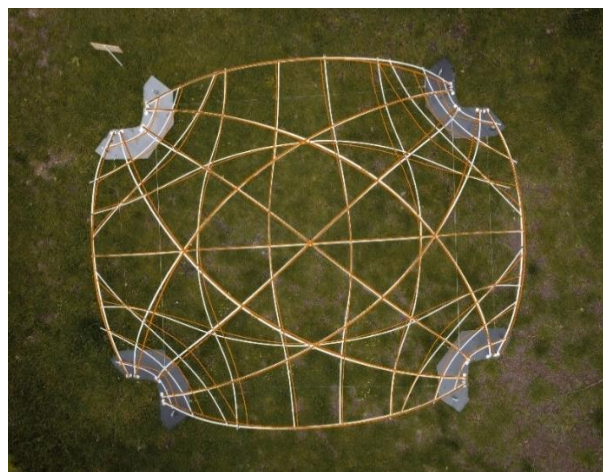


Figure 96 : Comparison between the constructed gridshell (white) and the theoretical model (orange)



## 9 Conclusion

After having carried out a state of the art on the construction of tile vaults, we chose to investigate the use of a bending-active gridshell to serve as the falsework. Its advantage of being constructed from straight elements would enable to reduce the extra cost and waste generated from the fabrication of the falsework and thus making free-form tile vault construction more sustainable.

We started by investigating on the numerical modelling of bending active gridshells, and we chose to go with Kangaroo2 Engineering for the form-finding and structural analysis. More generally the computational approach to design enables to have an integrated design considering geometry, structure, and fabrication. Goals about form can be associated with goals about material and structure. Achim Menges states, “the material through his properties becomes an active generator of design, not a passive receptor of a pre-designed form” (Achim Menges 2014).

We tested our computational design algorithm on a simple shell. The falsework is based on geodesic lines. We saw that using only bending active elements with a gridshell density acceptable for the mason is sometimes not sufficient to approximate accurately the target compression shell, and that extra stiffening cables can be used as an easy and low tech solution to adjust the gridshell shape.

Then we looked at a more complex tile vault shape : the drone port, for which we would also build a half scale prototype model of our designed falsework as a proof of concept. The modelling of the construction incremental loading was important to adjust the rods position and diameter to take into account the expected displacement. The challenge of the falsework lies in minimizing deviation from the target compression only shell to achieve the desired shape, while keeping the rod density in a acceptable range for the mason i.e. dense enough to be accurate for lying bricks in the correct location but not too dense to hinder him in his work. Two stiffening cables have also been used.

To investigate further our concept we built a prototype model of the falsework at half scale of the drone port. The purpose is to design a low-complexity, low-cost and kit-of-part system. Simple and cheap solutions for nodes and anchors have been developed. Connections pieces have been designed and fabricated that enable to connect smaller rods together to achieve longer bending-active elements. Finally the gridshell has been constructed, the overall structure seems to approximate correctly the target shell shape, and the detail designed are successfully working. We note that the curvature of the legs would need to be slightly improved. We also gained knowledge on good practice for using Grasshopper, from a feedback on bad node positioning on the boundary rods.

Finally, among the perspectives of this work we add the following elements: to build real tile vault using this falsework to validate its usability (after the small node adjustment described in chapter 8.6); to investigate other materials for the rods like bamboo or locally available materials in less developed countries; to add a feedback loop in the design that adapts the compression shell shape from the achievable bending-active gridshells.





# **Annex**



## 10 Annex : Form-finding of a compression only shell

First, master builders have built domes and vaults through history with empirical knowledge. Then engineers have tried to describe analytically shells structural behaviour through membrane theory. However, this approach becomes quickly very complex as soon as departure from basic shapes, which has therefore slowed down the use of shells in the past century. Recently, new advances in computation, fabrication and construction has given rise to a revival of shell structures. Some of these computational strategies will be described here.

What is a shell ? “*Shell structures* are a constructed system described by three-dimensional curved surfaces, in which one dimension is significantly smaller compared to the other two. They are form-passive and resist external loads predominantly through membrane stress.” (Adriaenssens et al. 2014). For shells, and especially when using masonry, the membrane stress is a compression only force acting in the plane of the shell surface. *Form-passive* means that the structure does not actively change its shape under varying external loads unlike form-active structures like membranes and cable nets. Nevertheless, shells resist loads through geometry and not accumulation of materials. This is why they are found in nature where material is the scarce resource, which is the reason bones or sea shells try to achieve resistance through shape complexity. That is also why today shells are interesting, in addition to their aesthetical value, when one wants to reduce resource use for economic or environmental reasons.

*Form-finding* means that the final geometry of the shell is the result of a search for a form in which static equilibrium is reached under certain design loads. Here the classic workflow division of an architect that draws a form then gives it to the engineer that makes it structurally viable is no more possible. In shells the shape depends on the flow of forces which is why to design them architects and engineers need to work hand in hand.

### 10.1 Force and form

#### 10.1.1 The hanging chain

The earliest structural form finding of an arch was found by Robert Hook (1635-1703) which he states in this way : “As hangs the flexible line, so but inverted will stand the rigid arch”. (Block, DeJong, et Ochsendorf 2006). He has the intuition that because the hanging chain under self-weight can only take tension force and no bending then the inverted shape, that is an arch, will take only the opposite forces i.e. only compression (Figure 97).

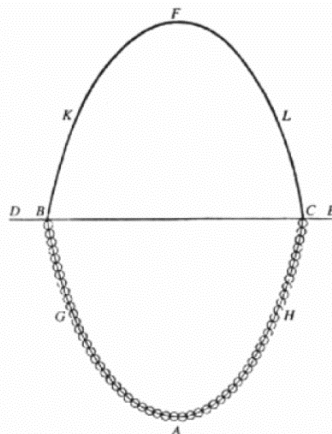


Figure 97 : Hooke's hanging chain, drawing by Poleni (Block, DeJong, et Ochsendorf 2006)

The obtained hanging chain shape, and thus also inverted arch shape is called a catenary and it is the shape that takes the chain under a constant weight per unit length. The equation describing the shape is a cosines hyperbolic equation (Muttoni 2015). However if the weight is uniformly distributed along the horizontal axis then a parabola shape is obtained. Figure 98 shows an example of a roof with a uniform distributed load of the concrete on its length and thus has the shape of a catenary. Figure 99 shows a bridge with a uniformly horizontal distribution of the load thanks to the secondary cables linked to the deck, and thus the obtained shape is a parabola (Muttoni 2015).



Figure 98: Catenary. Dulles airport Virginia<sup>24</sup>.



Figure 99 : Parabola. Golden gate bridge.<sup>25</sup>

### 10.1.2 Graphic statics

Graphic statics is a graphical method to analyse the equilibrium of a structural system. It gives the shape of a hanging cable under a specific load case, by linking geometrical considerations to the equilibrium of internal forces and applied loads. On Figure 100 a force diagram and a form diagram are drawn. The two diagrams are linked and one can be deduced from the other. The force diagram enables to deduce the internal forces and reaction forces. The funicular shape gives the equilibrium shape of the cable or the thrust line in a compression arch. The designer can choose to move the point S closer (respectively further) to the external forces in order to reduce (respectively increase) the internal forces and to elongate (respectively shorten) the funicular polygon. Graphic statics are useful when studying 2D structures with no bending i.e. cables, trusses, compression arches. An example<sup>26</sup> of a work designed by using graphics statics is the vaults of Güell park by Gaudi where the vaults follow the shape of the funicular polygon under self-weight and the pressure of earth.

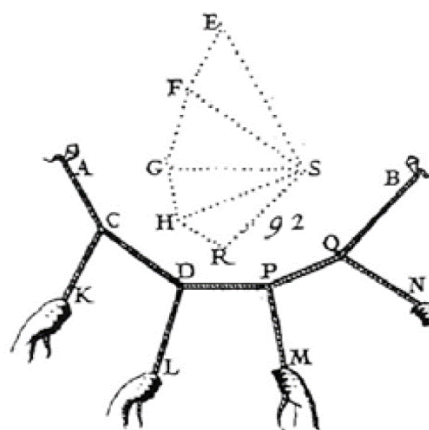


Figure 100 : Graphical analysis of a funicular shape by Varignon, *Nouvelle mécanique ou statique* (1725)

<sup>24</sup> [https://en.wikipedia.org/wiki/Dulles\\_International\\_Airport](https://en.wikipedia.org/wiki/Dulles_International_Airport)

<sup>25</sup> [https://en.wikipedia.org/wiki/Golden\\_Gate\\_Bridge](https://en.wikipedia.org/wiki/Golden_Gate_Bridge)

<sup>26</sup> For further interest about graphic statics one can find many interactive examples on eQUILIBRIUM at : <https://block.arch.ethz.ch/eq/drawing>



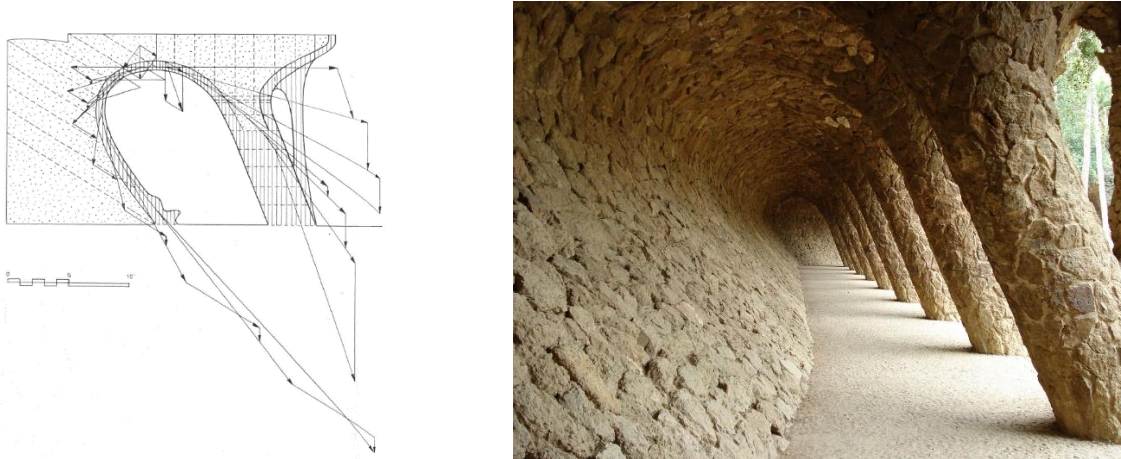


Figure 101 : Vaults of Güell Park, Antoni Gaudi <sup>27</sup>&<sup>28</sup>

### 10.1.3 Fundamentals of structural theory of masonry

Today structural analysis is based on limit states. The main criteria are strength and stability, then secondary limit states can be checked to ensure the structure is serviceable. In historical masonry, stresses are orders of magnitude lower than failure stress and deflection is usually negligible (high stiffness), thus the main structural criteria is stability (Heyman 1997).

To analyse the behaviour of a masonry structure Heyman gives 3 simplifying assumptions: “the masonry has no tensile strength; the stresses are so low that the masonry has effectively an unlimited compressive strength and; sliding failure does not occur.” (Heyman 1997) Therefore to evaluate the equilibrium of a masonry one needs to verify if the thrust line is kept entirely within the thickness of the structure. The thrust line is analogue to the funicular polygon, it represents the path of the resultant of the compressive forces through the masonry structure.

Figure 102 shows an example of a circular arch divided in equivalent sections. An infinite number of thrust line can be drawn in the arch. The ones that give the maximum and minimum internal force and abutment reaction force are drawn on Figure 102.

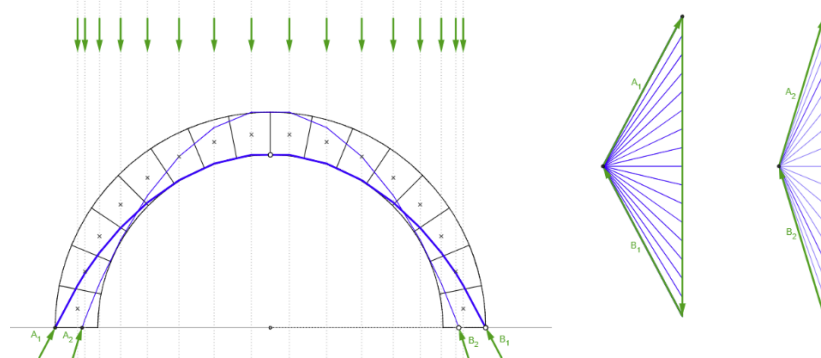


Figure 102 : Minimum (A2-B2) and Maximum(A1-B1) thrust of a semi-circular arch under its own weight. Form diagrams (left) and force diagrams (right).<sup>29</sup>

<sup>27</sup> (Gonçalves 2020)

<sup>28</sup> [https://fr.wikipedia.org/wiki/Parc\\_G%C3%BCell](https://fr.wikipedia.org/wiki/Parc_G%C3%BCell)

<sup>29</sup> <https://block.arch.ethz.ch/eq/drawing/view/16>

Knowing this Poleni proved that the dome of St Peter’s church was safe. He draw a section of the dome that is therefore an arch and divided it into blocks. He used Hook’s hanging chain method but applied loads proportional to the blocks. Finally, he inverted the funicular shape showing the compression thrust line is kept within the masonry (Figure 103).

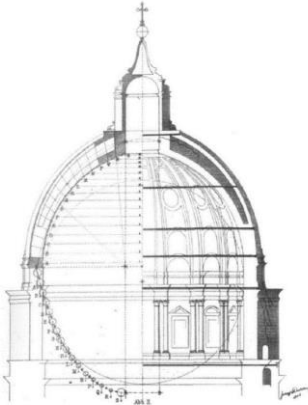


Figure 103: analysis of St Peter’s dome by Poleni

If the thrust line goes outside the thickness of the arch then a bending moment is created and tension appears at the opposite side that leads to a crack. The crack point is considered as a hinge now and the overall structure deforms until at least one line of thrust can be found once again in the structure then it reaches a new equilibrium state. Displacement of abutments (settlement, earthquake...) is a usual cause of the thrust line going out the arch and causing cracks. Figure 104 shows a way the arch may collapse. A points load  $P$  is applied (Figure 104.a). The inverted hanging hook chain with self-weight and the additional load  $P$  is then drawn (Figure 104.b). It’s inversion gives the thrust line (Figure 104.c) and leads to the formation of 4 cracks. At these location hinges are created that leads the arch to become a four bar mechanism leading to collapse (Figure 104.d).

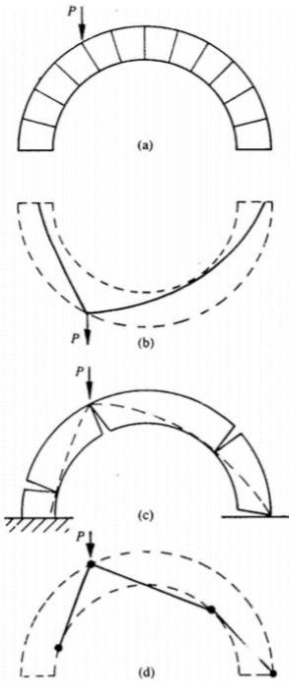


Figure 104 : Collapse of a circular arch under a point load (Heyman 1997)

An example of a design that takes into account a varying point load is the Salginatobel bridge (Figure 105) for which Robert Maillart has designed the thickness of the arch of the bridge so that the resulting thrust line is kept within the structure for every position of a moving point load on the top of the bridge.



Figure 105: Salginatobel bridge, Robert Maillart, 1930<sup>30</sup>

## 10.2 Physical models for form finding

Ancient buildings were based on simple geometries because people believed that efficient structures should be based on simple shapes. The ancestors of modern thin shells were Roman's cylindrical domes and hemispherical vaults. But also these simple shapes are present in more recent structures before the digital age because they are more easily described analytically which was important for engineer hand calculations, but also easier to describe for construction on site. However the pen cannot know physical constraints and engineers have therefore been confronted to the question : "Which three-dimensional forms are most suitable for a shell structure in order that the designer gains sufficient confidence that the structure will work as intended ?" (Adriaenssens et al. 2014).

A first answer is to use physical models for taking into account physical realities to perform form-finding. Hook's hanging chain is an early example in 2D. Before computational methods, form-finding in 3D was first done through the means of physical modelling in the 19th century. Arturo Tedeschi writes: "The conventional drawing was first attacked by a new approach, the form-finding - emerged in architecture in the late 19th century - which aimed to investigate novel and optimized structures found through complex and associative relations between material, shape and structures. Pioneers like Gaudi (1852-1926), Isler (1926-2009), Otto (1925-) and Musmeci (1926-1981) have rejected typology and looked to self-formation processes in nature as a way to organize buildings. Since the form could not descend from proven solutions, the traditional drawing could not be used as a tool to predict design outcomes." (Tedeschi 2014).

Structures can be sorted into two categories : the ones for which their structural behaviour depend on scale and the one that are independent of the scale. The first category of structures need to resist to bending and thus have a structural behaviour that depends on strength, stiffness and may be prone to buckling. Here scaling of the physical model cannot be done because the structure is governed by non-linear equations. This category also regroup structures for which some material properties need to be considered like creep, moisture, temperature.

---

<sup>30</sup> [https://fr.wikipedia.org/wiki/Pont\\_de\\_Salginatobel](https://fr.wikipedia.org/wiki/Pont_de_Salginatobel)

The second category of structures benefit largely from physical model form-finding because the found geometry can be scaled up linearly to predict the full size behaviour. When the structural behaviour is governed by static equilibrium under compression or funicular shapes then the model is independent of scale. Masonry arches, domes, vaults, cable nets etc. are such structures.

For form-finding in 2D the funicular solution gives the equilibrium shape under the external loads. However, when going in 3D, there is no unique funicular solution. Unlike the two-dimensional funicular arch, a shell can carry multiple load cases without bending (Adriaenssens et al. 2014).

Antoni Gaudi (1852-1926), Heinz Isler (1926-2009) and Frei Otto (1925-2015) are well known for their use of physical models in form finding. To model the crypt of Colonia Güell Antoni Gaudi used a hanging models made of strings on which sand bags are attached to model the loads (Figure 106). Instead of using a pen and paper, Gaudi plays with the lengths of the strings and the weights of the bags of the inverted model to the design research of the crypt. This way of designing with forces thanks to the means of a physical models leads to his signature architecture that conveys an organic aesthetic and a rational structure in an integrated way (Figure 107).

Heinz Isler was a shell builder. Like Gaudi he uses hanging models for design research based on Hooks technique. However instead of using hanging strings or chains he makes his models from hanging sheet of cloths. He would soak the fabric in a liquid plaster or resin then hang it and let it dry and harden. Figure 108 shows a physical model of Heinz Isler for the design of the Open air theatre of Grötzingen (Figure 109).

Frei Otto used physical models in the second half of the 20<sup>th</sup> century to find the form of membranes and cable net structure for which analytical calculation were not yet possible. Frei Otto developed technics of model making with soap bubbles which have the characteristic of finding an equilibrium form that is a minimal surface with a constant surface tension. This is well suited for the form-finding of form-active structures like membranes for which self-weight plays a minor role in the structural behaviour. Figure 111 and Figure 110 show respectively a soap bubble model by Frei Otto and the form-active structure roof of the Munich Olympic park.

Today, even with the progresses in 3D computational form-finding, physical models are still relevant (Gonçalves 2020; Gass 2016). First it gives a direct feedback on structural errors that the computer might not give : if it collapse in the model it will likely be the same for the real scale structure. Secondly it give a "hand feeling "feedback on the structural behaviour. It is an interesting way to understand better how the structure works by feeling with the hands the stronger and weaker points (Wanda J. Lewis 2020). Finally physical models are a convincing and pedagogical way to communicate ideas.





Figure 106: Physical hanging model by A. Gaudi<sup>31</sup>

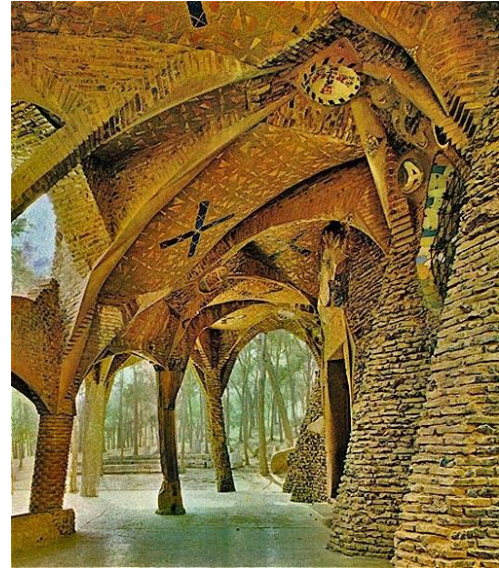


Figure 107: crypt of Colonia Güell, A.Gaudi<sup>32</sup>

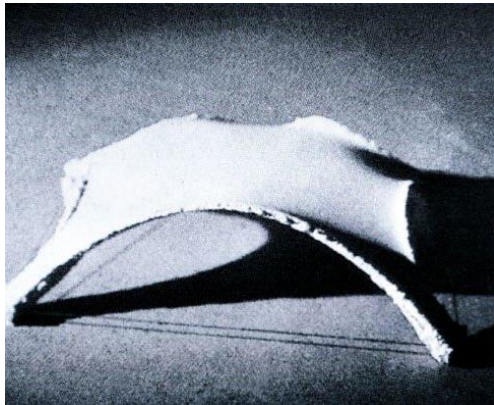


Figure 108: stiffened form-finding model for a compression concrete shell to cover the stands of the open air theatre at Grötzingen, H.Isler (Gass 2016)



Figure 109: Open air theatre at Grötzingen, H.Isler<sup>33</sup>

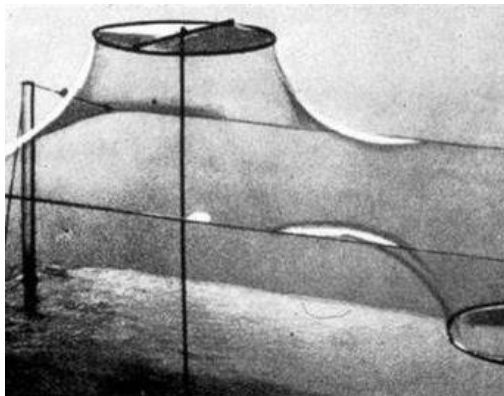


Figure 110 : Soap bubble model, F.Otto<sup>34</sup>



Figure 111 : Roofing of the Munich Olympic park, F.Otto<sup>35</sup>

<sup>31</sup> <https://www.gaudidesigner.com/fr/colonia-guell.html>

<sup>32</sup> Ibid.

<sup>33</sup> [https://fib-ch.epfl.ch/Pubs/2006/9\\_Biography.pdf](https://fib-ch.epfl.ch/Pubs/2006/9_Biography.pdf)

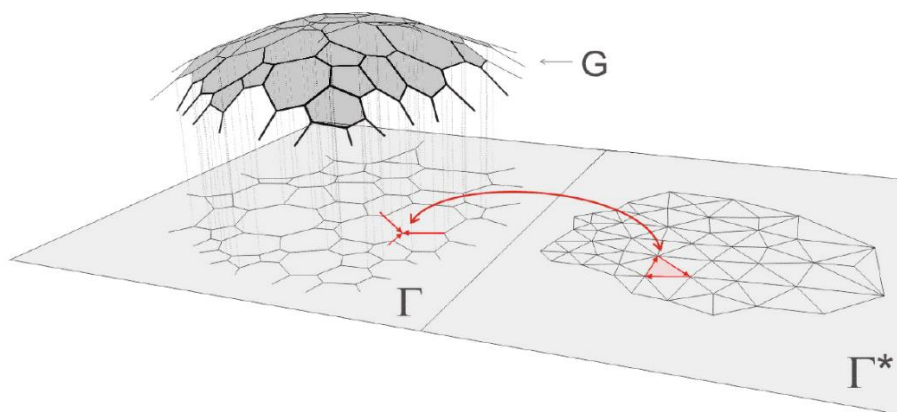
<sup>34</sup> <https://www.archdaily.com/>

<sup>35</sup> Ibid

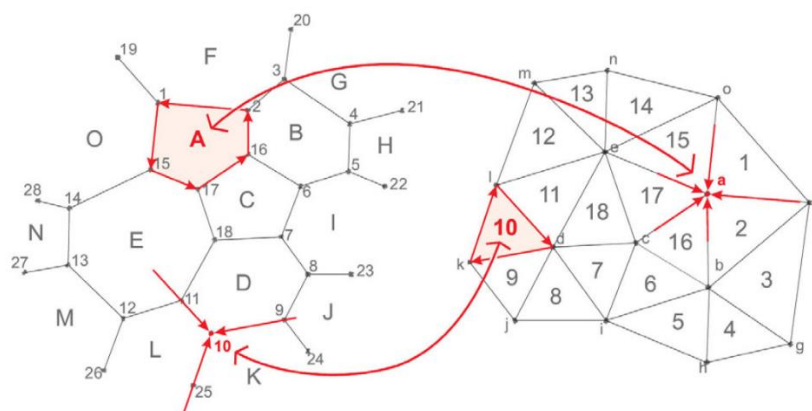
### 10.3 Thrust Network Analysis (TNA)

The thrust network analysis (TNA) is a computational method to form-find the static equilibrium shape of a compressive only funicular shell or unreinforced masonry. It is based on geometrical considerations and does not take into account material characteristics. For two-dimensional problems we saw that graphic statics is a method that enables finding funicular polygon which inverted gives the thrust line. The thrust network is a generalisation of the thrust line for three-dimensional problems. Like the thrust line is the representation of one possible equilibrium state of an arch, the thrust network is one possibility of the static equilibrium of the shell : if at least one thrust network can be found entirely in the masonry then the structure is stable under the loading case. TNA is a method that used techniques from graphic statics to form-find the thrust network. After that buckling, deflection, sliding and other load combinations (asymmetric) still need to be checked (Adriaenssens et al. 2014).

A hypothesis for TNA is that the shell is only under gravity load. This means that only vertical loads are considered in the TNA. This enables to split the form finding in two steps : first the equilibrium of the horizontal component of the forces is found, then vertical loads are added to find the heights of the nodes (BLOCK et Ochsendorf 2007). In TNA two reciprocal diagrams are created : a form diagram which is the horizontal projection of the funicular equilibrium solution, and a force diagram (Figure 112 (a)).



(a)



(b)

Figure 112 : (a) Relationship between the thrust network  $G$ , its planar projection the form diagram  $\Gamma$ , and the reciprocal force diagram  $\Gamma^*$ , and (b) the reciprocal relation between  $\Gamma$  and  $\Gamma^*$  (BLOCK et Ochsendorf 2007)



Figure 112 (b) shows the reciprocal relation between the form and force diagrams. Because of the horizontal projection, these diagrams are planar which enables to use graphic statics to find the equilibrium state. The diagrams are “parallel dual graphs” which means that “branches which come together in a node in one of the diagrams, form a closed space in the other, and vice versa, and corresponding branches in both diagrams are parallel. Structurally this means that the equilibrium of a node in one graph is guaranteed by a closed polygon of force vectors in the other, and vice versa.” (Adriaenssens et al. 2014). If the form diagram has nodes with a valency of three (the one of Figure 112(b)), then the shape of the force diagram is unique (only the scale can still change). However if the valency of the nodes in the form diagram are higher than three then multiple shapes of the force diagram can satisfy a horizontal equilibrium for the same form diagram and lead to different thrust networks.

Then the addition of the vertical loads enables to find the internal forces of the network. Here the scale of the force diagram can be adapted to adjust the “inclination” of the resultant force vectors. This scale factor enable to adjust the height of the thrust network because its lines need to be aligned to the calculated 3d force vectors. Therefore a desired higher structure requires a smaller force diagram and inversely. To control the final funicular shape, the designer can thus play on the horizontal form diagram, the force diagram and the scale factor.

The “Block research group”<sup>36</sup> (BRG) developed a plug-in for Rhino<sup>37</sup>, called RhinoVault, which enables to perform a TNA in the Rhino environment. From an initial pattern it generates a form diagram and a force diagram to perform the horizontal equilibrium. Here the designer can bring change manually on one or both of the diagrams before the equilibrium search, and can also give them a weight to indicate which one RV2 will modify preferably. After the horizontal equilibrium is found, the designer can then define a target height (translated in a scale for the force diagram) and RV2 will calculate the corresponding thrust network.

An example of a project that uses TNA with RhinoVault2 (RV2) is the armadillo vault made by BRG for the Venice Architectural Biennale 2016 (Figure 113).

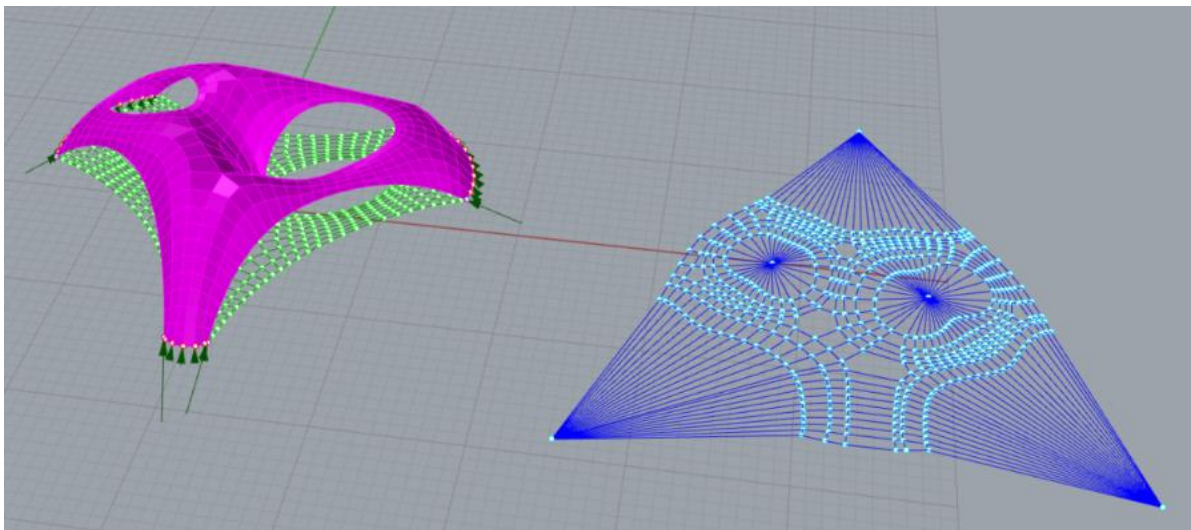


Figure 113 : RhinoVault2 model of the Armadillo Vault

<sup>36</sup> <https://www.block.arch.ethz.ch/brg/>

<sup>37</sup> Rhinoceros 3D : <https://www.rhino3d.com/fr/>

## 10.4 Particle-Spring method

Particle-spring (PS) is another computational form-finding method. It enables to simulate hanging or pretensioned chains and grids, for form-finding respectively shells and membrane structures.

The objective of the particle spring method is to find structures in static equilibrium of a network of particles (the nodes) and springs (the lines). The PS method uses two physical laws: second law of Newton enables to simulate the motion of the nodes, and Hook's law of elasticity is used to calculate the forces in the springs.

The designer starts by defining a mesh, usually a quad mesh. Then he applies anchor conditions to the nodes to define their degree of freedom for each of the three spatial axis. Then each segment is transformed into a spring for which a stiffness and a rest length is defined. After this each node is given a mass and external loads are applied to it. Finally the particle-spring solver calculates iteratively the motion of the nodes and thus the new position of them for an incremental time step of  $\Delta t$ , and depending at each step on the external loads and the internal forces resulting from the elongation or shortening of the springs. (Adriaenssens et al. 2014). To do design research the architect can play with : the boundary conditions, the meshing and its typology, the stiffness of the springs, the masses of the particles and the external loads.

For example, if one takes a flat grid with fixed corners and applies a gravitational loads on the nodes, then the nodes will move downwards which will induce an elongation of the springs that will create in return a counter force because of its stiffness, until the system arrives to a static equilibrium.

Particle-spring analysis can be done with Kangaroo2<sup>38</sup> that is optimisation solver based on the minimisation of the total energy of the system. With kangaroo the springs are modelled with the component "length" which by default wants to keep its initial length with a certain strength (target length = initial length). However one needs to be careful, because the curve obtained is not a catenary shape, as shown in green on Figure 114. If the target length of the spring (its rest length) is set to 0 then we obtain a parabola. To obtain a real catenary with kangaroo you can set a polyline with "infinite" strength (or very high strength springs compared to the loads at nodes), and then move the supporting points closer to each other to make the polyline hang.

This remark also applies in three dimensions as shown on Figure 115. We apply loads in each node of a mesh of 10x10 faces, and the corners are anchored. If the edges are springs with the default "length" settings (i.e. the target lengths of springs are their initial length) then we obtain the green net. If prestress is introduced with a target value of zero for the length the result is the red net. The blue net represents a "real" hanging net, where the edges length remain constant (very high strength springs compared to loads), and the anchors are moved closer to each other. To achieve a geometry with the same height and anchors, this last method

---

<sup>38</sup> Kangaroo2 is a plug-in developed by Daniel Piker for Grasshopper a visual coding language; and Grasshopper, developed by David Rutten, is itself a plug-in for Rhinoceros 3D.  
<https://discourse.mcneel.com/t/how-does-kangaroo-solver-work/92075>

requires to set an initial net larger than for the two other cases (green and red) for which the springs length increases.

Finally, if the mesh is not deformable (like for the quads) then some springs can be in compression, that would mean that the shell presents some areas in tension, and so we do not have a compression only structure anymore. Figure 116, shows an initial triangular mesh on which loads a applied and the edges are defined as springs. The obtained geometry with Kangaroo2 usual "length" component (red), is compared with an inverted hanging net resulting from Kangaroo2Engineering<sup>39</sup> (K2E). In K2E, the springs can be replaced by cables that only sustain tension, which enables to model more properly an inverted hanging net (Figure 116 in blue).

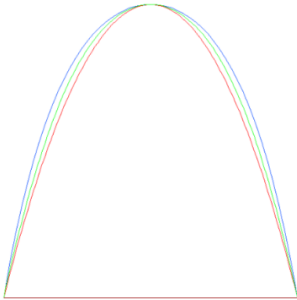


Figure 114 : (blue) catenary shape, (green) Kangaroo2 curve with default "length" component (red) parabola

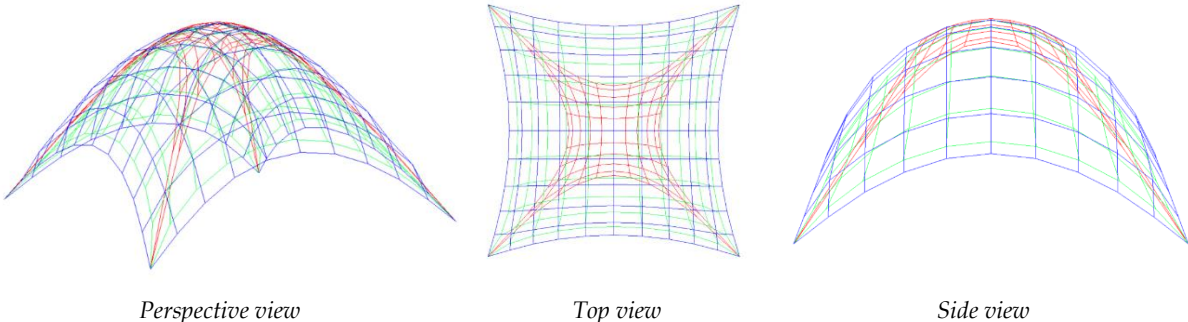


Figure 115 : (blue)"real" hanging net (unchanged spring length)  
 (green) default kangaroo2 hanging net with spring target length as initial length  
 (red) mesh with pre-stress (target edge length = 0), and node loads

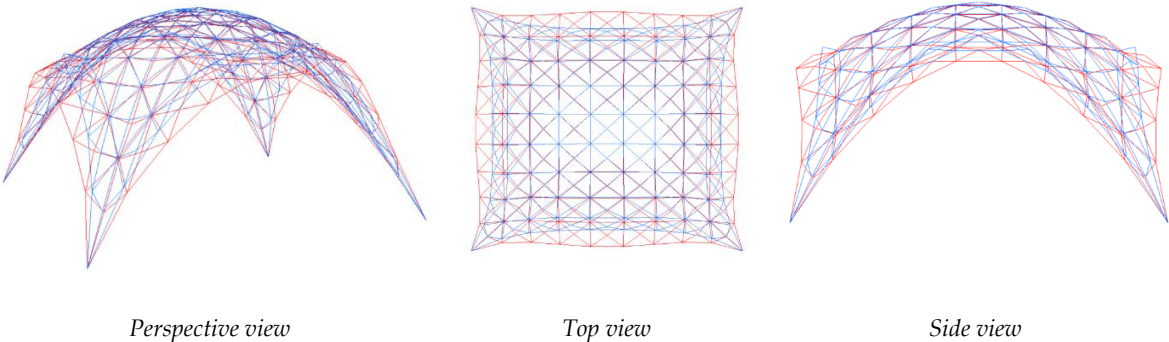


Figure 116: Particle spring method applied on a triangular mesh  
 (red) with kangaroo 2 usual "length" component : some springs are in compression  
 (blue) with k2E : edges are cables i.e. no elements take compression.

<sup>39</sup> <https://formatengineers.com/research/k2-engineering.html>



# 11 Annex : Physical model : rods lengths and node position

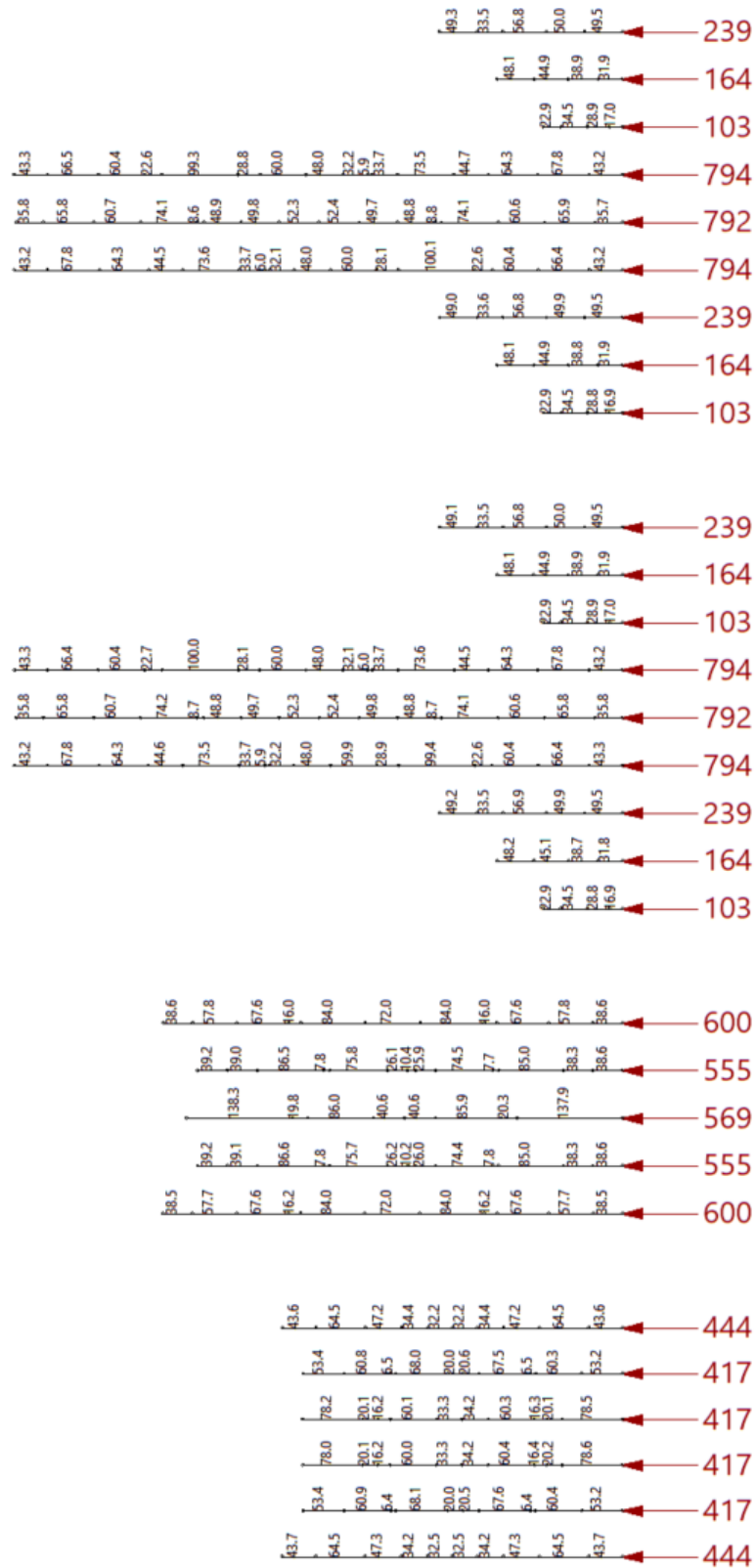


Figure 117 : rods lengths (cm) and distance between nodes (cm) for the physical model (scaled droneport falsework)





## 12 References

- « A'A ». 2016. « The Droneport Project ». 2016, 2016. <https://www.lafargeholcim-foundation.org/media/publications/aa-perspectives-the-droneport-project>.
- Achim Menges. 2014. *Achim Menges: Rethinking Materiality Through Computation in Architecture*. [https://www.youtube.com/watch?v=PbgArau\\_4vI&t=185s](https://www.youtube.com/watch?v=PbgArau_4vI&t=185s).
- Adriaenssens, Sigrid, Philippe Block, Diederik Veenendaal, et Chris Williams. 2014. *Shell structures for architecture: form finding and optimization*. Routledge.
- Block, Philippe, M. K. Bayl-Smith, Tim Schork, James Bellamy, et D. A. Pigram. 2014. « Ribbed tiled vaulting: Innovation through two design-build workshops ». *Fabricate: Negotiating Design and Making*.
- Block, Philippe, Matt DeJong, et John Ochsendorf. 2006. « As hangs the flexible line: Equilibrium of masonry arches ». *Nexus Network Journal* 8 (2): 13-24.
- Block, Philippe, Matthew DeJong, Lara Davis, et John Ochsendorf. 2010. « Tile vaulted systems for low-cost construction in Africa ». *ATDF journal* 7 (1/2): 4-13.
- Block, Philippe, et John Ochsendorf. 2007. « Thrust network analysis: A new methodology for three-dimensional equilibrium ». *Journal of the International Association for Shell and Spatial Structures* 48 (décembre).
- Block, Philippe, Tom Van Mele, Matthias Rippmann, Francesco Ranaudo, Cristian Javier Calvo Barentin, et Noelle Paulson. 2020. « Redefining structural art: strategies, necessities and opportunities ». *The Structural Engineer* 98 (1): 66-72.
- Cecilie, Brandt-Olsen. 2016. « Calibrated modelling of form-active structures ». PhD Thesis, Copenhagen, Denmark: Technical University of Denmark.
- Coar, Lancelot, Young-Jin Cha, Zhiyu Jiang, Jessica Piper, et Lars De Laet. 2018. « The design and testing of post-tensioned bending active spatial assemblies ». *Proceedings of IASS Annual Symposia 2018* (15): 1-8.
- Coar, Lancelot, Michael Cox, Sigrid Adriaenssens, et Lars De Laet. 2017. « The design and construction of fabric formed ice shells with bending active frames utilizing principle stress patterns ». In *Proceedings of IASS Annual Symposia, 2017:1-10*. International Association for Shell and Spatial Structures (IASS).
- Dessi-Olive, Jonathan, Nick Krouwel, Mark West, et John Ochsendorf. 2018. « Tile Vaulting with Lightweight Concrete and Fiberglass Spline Formwork ». In *Proceedings of IASS Annual Symposia, 2018:1-8*. International Association for Shell and Spatial Structures (IASS).
- Gass, Siegfried. 2016. « Physical analog models in architectural design ». *International Journal of Space Structures* 31 (mai). <https://doi.org/10.1177/0266351116642061>.
- Gonçalves, David Afonso. 2020. « Estruturas antifuniculares ». Master Thesis, Universidade de Lisboa, Faculdade de Arquitetura.
- Heyman, Jacques. 1997. *The stone skeleton: structural engineering of masonry architecture*. Cambridge University Press.
- Isler, Heinz. s. d. « Luis Cândia, Pietro Brenni », 9.
- Jahn, Gwyllim, Cameron Newnham, Nick Berg, Melissa Iraheta, et Jackson Wells. 2019. *Holographic Construction*.
- Lienhard, Julian. 2014. « Bending-Active Structures », 116.
- López López, David, et Marta Domènech Rodríguez. 2012. « Tile Vaulting as an alternative ». In *Visions for the future of housing: mega cities: proceedings of the XXXVIII IAHS World Congress*.
- López López, David, Marta Domènech Rodríguez, et Mariana P. Fernández. 2014. « "Brick-topia", the thin-tile vaulted pavilion ». *Case Studies in Structural Engineering* 2: 33-40.
- López López, David, Tom Van Mele, et Philippe Block. 2016. « Tile vaulting in the 21st century ». *Informes de la Construcción* 68 (544): 1-9.



- Mairs, J. 2016. « Norman Foster reveals vaulted Droneport prototype at Venice Architecture Biennale ». *Dezeen*, May 27.
- Muttoni, Aurelio. 2015. *L'art des structures: une introduction au fonctionnement des structures en architecture*. PPUR Presses polytechniques.
- Ramage, Michael. 2007. « Guastavino's vault construction revisited ». *Construction History* 22: 47-60.
- Ramage, Michael H., John A. Ochsendorf, et Peter Rich. 2010. « Sustainable Shells: New African vaults built with soil-cement tiles ». *Journal of the International Association for Shell and Spatial Structures* 51 (4): 255-61.
- Ramage, Michael, Timothy J. Hall, Ana Gatóo, et M. Wesam Al Asali. 2018. « Rwanda Cricket Stadium: Seismically Stabilized Tile Vaults ». In *Proceedings of IASS Annual Symposia*, 2018:1-8. International Association for Shell and Spatial Structures (IASS).
- Schling, Eike. 2018. « Repetitive Structures ». Ph.D. Thesis, Technical University of Munich. <https://doi.org/10.14459/2018MD1449869>.
- Tedeschi, Arturo. 2014. *AAD, Algorithms-aided design: parametric strategies using Grasshopper*. Le penseur publisher.
- Toussaint, Julien. s. d. « Procédés Low-Tech de Liaison du Bambou Structurel », 26.
- Wanda J. Lewis. 2020. « *Spatial Structures; Movers and Shakers* » - with Wanda J. Lewis. <https://www.youtube.com/watch?v=KGwC-IhNzS8&t=1s>.
- Wang Xiang, Chun Pong So, Liming Zhang, Zhewen Chen, et Philip F. Yuan. s. d. « Rethinking Efficient Shell Structures With 3D-printed Formwork ».
- Yuan, Philip F., et Philippe Block. 2019. *Robotic force printing: A joint workshop of MIT/ETH/Tongji*. Tongji University Press.

## 13 Table of figures

Figure 1 : Mapungubwe National Park Interpretive Center (2008).....	1
Figure 2: The Crossway, Hawks, 2009.....	3
Figure 3: Sustainable urban dwelling unit (SUDU), Ethiopia 2010, (Block et al. 2020).....	3
Figure 4 : Rwanda Cricket Stadium, Kigali 2017, (M. Ramage et al. 2018).....	3
Figure 5 : Prototype free-form tile vault, BRG, 2011, (López López, Van Mele, et Block 2016).....	4
Figure 6 : Brick-topia, Barcelona, 2013, (López López, Domènech Rodríguez, et Fernández 2014).....	4
Figure 7 : Workshop at MADA Melbourne, 2013 (López López, Van Mele, et Block 2016).....	5
Figure 8 : Drone port, Venice Biennale 2016, (Mairs 2016).....	5
Figure 9 : La Volta Porosa, Cambridge MIT, 2016.....	6
Figure 10 : Ice Bloom 2017.....	7
Figure 11 : scheme of the algorithm.....	9
Figure 12 : Curves on a surface.....	11
Figure 13 : Finding a geodesic curve on a mesh.....	12
Figure 14 : Grasshopper code with Kangaroo2 to find a geodesic curve on a mesh.....	12
Figure 15 : geometric relation in a deflected beam (image from (Lienhard 2014)).....	13
Figure 16 : grasshopper code of the simulation of a bending rod with kangaroo2.....	14
Figure 17 : (Green) Simulation of a bending rod with kangaroo 2, (red) initial state : flat rod.....	15
Figure 18 : Grasshopper code for a prebended rod.....	15
Figure 19 : (Green) Simulation of the deviation of a prebended rod, (Red) initial state.....	15
Figure 20 : comparison between catenary curves (red) and bended curves (green), for $f/L$ ratios from top to bottom of 0.9, 0.7, 0.5, 0.3, 0.2, 0.1 for the catenary curve.....	16
Figure 21 : Bending rod with karamba (green), and kangaroo2 (red), from a prescribed displacement.....	17
Figure 22 : radius of curvature at the middle points of the segments.....	17
Figure 23 : prebending with Karamba.....	18
Figure 24 : Bending moment values.....	18
Figure 25 : prebending with Karamba. (red) initial curve. (green) equilibrium curve with roller at right side and the solver : (a) with the dynamic relaxation solver, (b) with the 1st order solver.....	18
Figure 26 : modelling of the rods with K2Engineering.....	19
Figure 27 : Prebending with k2Engineering ,max bending moment = 25.5N.m (Rods : green to red = 0 to max deviation), (Moment : green to red = 0 to max moment).....	20
Figure 28 : analytical check of the bending moment calculated by K2E.....	20
Figure 29 : Prebending. Pinned support left and roller right (Rods : green to red = 0 to max deviation), (Moment : green to red = 0 to max moment).....	20
Figure 30 : prebending with. Pinned support left, an roller support right + cable, force in cable = 24N (Rods : green to red = 0 to max deviation), (Moment : green to red = 0 to max moment), (cable, blue = tension, green = neutral).....	21
Figure 31 : External load : 20N/node, prebending with. Pinned support left, an roller support right + cable colour legend : idem Figure 30.....	21
Figure 32 : rod with stiffening cable (colour legend : idem Figure 30).....	21
Figure 33 : geodesic lines on a compression only surface.....	22
Figure 34 : direction layers of the rods.....	22
Figure 35 : finding the intersection nodes with tolerance and rebuilding the curves (example with direction layer u).....	23
Figure 36 : adding points to create the polyline rods in order to increase the resolution and to model properly the bending stiffness of the rod (example with direction layer u).....	23
Figure 37 : alternative strategy to model the gridshell (that we don't recommend). (a) Vertical rods with the position of the nodes, and target guidework, (b) additional intermediate points for modelling the bending behaviour, and target guidework, (c) bended rods and target guidework.....	24
Figure 38 : reorientation of the slats and prebending.....	24
Figure 39 : nodes modelled as zero-length springs.....	25
Figure 40 : "index to beam" to model slats as rigid group of beams, and independent from other slats. Also shows how to create the second layer of stiffening slats.....	25
Figure 41 : Gridshell modelled with Karamba and with some elements that are made of 2 layers of slats connected by shear blocks.....	25

Figure 42 : general overview of the grasshopper code for the modelling with K2Engineering of the falsework for the scaled drone port .....	26
Figure 43 : Left : Form diagram (green), force diagram (blue), right : RV2 shell.....	27
Figure 44 : Dimensions of the shell.....	27
Figure 45 : mesh to surface.....	28
Figure 46 : Optimisation algorithm.....	28
Figure 47 : Optimized guidework with Galapagos .....	29
Figure 48 : Manual choice of the target guidework, (a) 3D view, (b) top view .....	30
Figure 49 : naming of the direction layers of the rods.....	30
Figure 50 : Modelling of the rods.....	30
Figure 51 : Construction of the bottom boundaries Colour legend : (Rods : green to red = 0 to max deviation), (cable, blue = tension, green = neutral) .....	31
Figure 52 : Guidework deviation, with the 2 additional boundary cables Colour legend : (Rods : green to red = 0 to max deviation), (cable, blue = tension, green = neutral) .....	31
Figure 53 : Guidework deviation, with 3 additional cables Colour legend : (Rods : green to red = 0 to max deviation), (cable, blue = tension, green = neutral) (Bending moment : green to red = 0 to max bending moment).....	32
Figure 54 : Guidework deviation, with 5 additional cables Colour legend : idem Figure 53.....	32
Figure 55 : Guidework deviation and displacement, with 5 additional cables and self-weight load Colour legend : (Rods : green to red = 0 to max deviation), (cable, blue = tension, green = neutral) .....	33
Figure 56 : brick load on the falsework for the construction of the first arch .....	34
Figure 57 : Falsework deviation and displacement, with 5 additional cables and self-weight load and 0.1kN/m brick load applied like in Figure 56. Colour legend : (Rods : green to red = 0 to max deviation), (cable, blue = tension, green = neutral).....	34
Figure 58 : Falsework deviation and displacement, with 6 additional cables and self-weight load and 0.1kN/m brick load applied like in Figure 56. Colour legend : (Rods : green to red = 0 to max deviation), (cable, blue = tension, green = neutral).....	34
Figure 59 : step by step load increment Colour legend : (Rods : green to red = 0 to max deviation), (cable, blue = tension, green = neutral) .....	35
Figure 60 : Construction of the drone port in Venice, 2016 .....	36
Figure 61 : Rhino model of the drone port shell and of its falsework (given by Philippe Block).....	37
Figure 62 : target false work (a) top view, (b) front elevation, (c) side elevation.....	37
Figure 63 : perspective render of the target scaled 50% falsework.....	37
Figure 64 : Rod groups : (green) Primary rods : 15mm diameter rods (red) Secondary rods : 8mm diameter rods (red points) anchors.....	38
Figure 65 : Deviation of principal rods alone colour legend : (rods : green to red = 0 to max deviation).....	39
Figure 66 : (green) Catenary curve, (red) Compression shell.....	39
Figure 67 : Deviation of the gridshell (without extra cables) colour legend : (rods : green to red = 0 to max deviation).....	40
Figure 68 : Deviation of the gridshell with 2 extra cables colour legend : (rods : green to red = 0 to max deviation) (cables : bleu = tension, green = neutral) .....	40
Figure 69 : Load of the bricks without considering that a part of the load is taken by the arch in construction .....	41
Figure 70 : repartition of the load of the brick $F$ : load of the brick $F_p$ : load on the brick below $F_n$ : load on the gridshell.....	41
Figure 71 : Approximation of half the boundary arch in 4 segments to define 4 load cases "Fn" from 4 inclination angles of the segments. ....	41
Figure 72 : Final modelling of the brick load on the falsework.....	42
Figure 73 : Carlos Martin working on the Droneport, (« A'A » 2016).....	44
Figure 74 : Physical model rods lengths and diameter .....	46
Figure 75 : All rods used for the construction .....	47
Figure 76 : schematic section of the construction of the longer rods with a connecting tube .....	47
Figure 77 : photos of the tube connection for the fabrication of the longer rods .....	47
Figure 78 : Plastic connectors.....	48
Figure 79 : connector with steel ring.....	48
Figure 80 : Low-tech connections for bamboo (Toussaint, s. d.) (a) Node with rope, (b) node with plastic from bottle, (c) node with plastic from bottle and rubber from old air chamber .....	49
Figure 81 : Chosen connection solution with reusable tie-wraps and rubber membrane .....	49
Figure 82 : Photo of the nodes realised, (a) Crossing node, (b) Boundary node.....	49

Figure 83 : (a) Slipping of the boundary nodes, (b) Addition of a bolt to act as an anchor .....	50
Figure 84 : design of anchor plates .....	50
Figure 85 : Reaction forces in the anchoring plates .....	51
Figure 86 : Positioning then anchoring of the plates .....	51
Figure 87 : Rod anchors, (a) Schematic section, (b)Photo .....	52
Figure 88 : testing of the resistance of the rod at its anchoring location (a) loading perpendicular to fibers (0,47 kN) (b) loading parallel to fibers (0,47 kN) .....	52
Figure 89 : Final anchoring of the gridshell .....	52
Figure 90 : Photo of the gridshell .....	53
Figure 91 : Construction steps of the gridshell (a) Frist two diagonal rods so that the structure stands by itself during construction (b) Completion of the first layer of diagonal rods attached from below the other diagonal (c) Completion of the second layer of diagonal rods attached above the other diagonal layer (d) Placing the 8mm diameter rods of the U layer above the diagonal rods, then attaching the boundary rods of the V layer. (e) Addition of the stiffening cables (f) Finished gridshell and construction team (from left to right : Maryllis, Léopold, Arnaud, Aurélie) .....	54
Figure 92 : View of the gridshell (a) front, (b) side, (c) top. ....	55
Figure 93 : Error in the node position of the boundary rods (a) We see that the 8mm rod is too much bended compared to the numerical model (b) Solution decide onsite to relocate the node position of the boundary rods. ....	56
Figure 94 : Node position on the straight rods (red) with “Evaluate Curve”, which is a wrong way to proceed (green) with “length parameter” and “evaluate length”, which is the correct way to position the nodes .....	57
Figure 95 : Node positioning on the rods (cm) (red points) Wrong way with “Evaluate curve” component (green points) Correct way with “length parameter” and “evaluate length” .....	58
Figure 96 : Comparison between the constructed gridshell (white) and the theoretical model (orange) .....	58
Figure 97 : Hooke’s hanging chain, drawing by Poleni (Block, DeJong, et Ochsendorf 2006) .....	63
Figure 98: Catenary. Dulles airport Virginia. ....	64
Figure 99 : Parabola. Golden gate bridge. ....	64
Figure 100 : Graphical analysis of a funicular shape by Varignon, Nouvelle mécanique ou statique (1725) ..	64
Figure 101 : Vaults of Güell Park, Antoni Gaudi & .....	65
Figure 102 : Minimum (A2-B2) and Maximum(A1-B1) thrust of a semi-circular arch under its own weight. Form diagrams (left) and force diagrams (right).....	65
Figure 103: analysis of St Peter’s dome by Poleni .....	66
Figure 104 : Collapse of a circular arch under a point load (Heyman 1997) .....	66
Figure 105: Salginatobel bridge, Robert Maillart, 1930 .....	67
Figure 106: Physical hanging model by A. Gaudi .....	69
Figure 107: crypt of Colonia Güell, A.Gaudi .....	69
Figure 108: stiffened form-finding model for a compression concrete shell to cover the stands of the open air theatre at Grötzingen, H.Isler (Gass 2016).....	69
Figure 109: Open air theatre at Grötzingen, H.Isler .....	69
Figure 110 : Soap bubble model, F.Otto .....	69
Figure 111 : Roofing of the Munich Olympic park, F.Otto .....	69
Figure 112 : (a) Relationship between the thrust network $\mathbf{G}$ , its planar projection the form diagram $\mathbf{\Gamma}$ , and the reciprocal force diagram $\mathbf{\Gamma}^*$ , and (b) the reciprocal relation between $\mathbf{\Gamma}$ and $\mathbf{\Gamma}^*$ (BLOCK et Ochsendorf 2007) .....	70
Figure 113 : RhinoVault2 model of the Armadillo Vault .....	71
Figure 114 : (blue) catenary shape, (green) Kangaroo2 curve with default “length” component (red) parabola .....	73
Figure 115 : (blue) “real” hanging net (unchanged spring length) (green) default kangaroo2 hanging net with spring target length as initial length (red) mesh with pre-stress (target edge length = 0), and node loads .....	73
Figure 116: Particle spring method applied on a triangular mesh (red) with kangaroo 2 usual “length” component : some springs are in compression (blue) with k2E : edges are cables i.e. no elements take compression. ....	73
Figure 117 : rods lengths (cm) and distance between nodes (cm) for the physical model (scaled droneport falsework).....	74
Figure 118 : Corrected node position after analysis of the physical model errors.....	75







